Identification and characterization of Syndapin I, Vacuolar protein sorting 35 and Neurobeachin as new interaction partners of the glycine receptor

Dissertation

zur Erlangung des Doktorgrades

der Naturwissenschaften

vorgelegt beim Fachbereich Biochemie, Chemie und Pharmazie

der Johann Wolfgang Goethe -Universität

in Frankfurt am Main

von Isabel del Pino Pariente

aus Valencia (Spanien)

Frankfurt 2010

(D30)

Die vorliegende Arbeit wurde in der Abteilung Neurochemie am Max-Planck-Institut für Hirnforschung in Frankfurt am Main unter Anleitung von Prof. Dr. Heinrich Betz durchgeführt und vom Fachbereich Biochemie, Chemie und Pharmazie der Johann Wolfgang Goethe - Universität in Frankfurt am Main als Dissertation angenommen.

Dekan:	Prof. Dr. Dieter Steinhilber
Gutachter:	Prof. Dr. Ernst Bamberg
	Prof. Dr. Heinrich Betz

Datum der Disputation:

Table of contents

Abbreviations

Aa(s)	amino acid(s)
A	adenosine
AMPA	α-amino-3-hydroxyl-5-methyl-4-isoxazolepropionic acid
AMPAR	α-amino-3-hydroxyl-5-methyl-4-isoxazolepropionic acid receptor
AP	alcaline phosphatase
APS	ammonium persulfate
ATP	adenosine triphosphate
bp	base pair
BES	N,N-Bis(2-hydroxyethyl)-2-Aminoethansulfonic acid
BSA	bovine serum albumin
C	cytidine
°C	degrees Celsius
cDNA	complementary DNA
CIP	calf intestine phosphatase
CNS	central nervous system
Cont	control
CEFPICT	Complete EDTA-free protease inhibitor cocktail tablet
d	distilled
Da	Dalton
DIV	days *in vitro*
DMEM	Dulbecco's modified Eagle's medium
DMSO	dimethylsulfoxid
DNA	desoxyribonucleic acid
dNTP	deoxyribonucleotide-5'-triphosphate
dsRED	red fluorescent protein from *Discosoma sp.*
DTT	dithiothreitol
E	day after embryo formation
E.coli	*Escherichia coli*
EDTA	ethylenediamine tetra acetic acid
e.g.	*exempli gratia*
ER	endoplasmic reticulum
FCS	fetal calf serum
g	gram
G	guanosine

GABA	γ-aminobutyric acid
$GABA_AR$	γ-aminobutyric acid receptor type A
GBM	Gephyrin binding motif
GFP	green fluorescent protein
Gly	glycine
GlyR	glycine receptor
$GlyR\beta_{49}$	49 amino acids (from position 378 to 426) of the intracellular loop located between transmembrane domains 3 and 4 of the GlyRβ subunit
$GlyR\beta_{78}$	78 amino acids (from position 378 to 455) of the intracellular loop located between transmembrane domains 3 and 4 of the GlyRβ subunit
GSH	glutathione
GST	glutathione-S-transferase
GTP	guanosine triphosphate
HEK	human embryonic kidney
HPLC	high performance liquid chromatography
h	hour
HRP	horseradish peroxidase
IPTG	isopropyl-β-thiogalactopyranoside
k	kilo
KO	knock out
l	liter
LB	Luria Bertani
LGIC	ligand gated ion channel
mAb	monoclonal antibody
m	milli
μ	micro
M	molar
MEM	minimum essential medium
min	minute
mRNA	messenger RNA
MW	molecular weight
n	nano or number
n.s.	non significant
NMDA	N-methyl-D-aspartic acid
NMDAR	N-methyl-D-aspartic acid receptor
NMJ	neuromuscular junction
NTP	nucleoside triphosphate
OD	optical density

p	pico
PAGE	polyacrylamide gel electrophoresis
PBS	phosphate buffered saline
PCR	polymerase chain reaction
PFA	paraformaldehyde
pH	*potentium Hydrogenii*
PKA	protein kinase A
PRD	proline-rich domain
PSD	postsynaptic density
PVDF	polyvinylidene fluoride
rAAV	recombinant adeno-associated virus
RNA	ribonucleic acid
shRNA	small hairpin RNA
rpm	revolutions per minute
RT	room temperature
s	second
SBM	SH3 binding motif
SDS	sodium dodecyl sulfate
SDS-PAGE	SDS-polyacrylamide gel electrophoresis
T	thymidine
TAE	tris-acetate-EDTA buffer
TBS	tris buffered saline
TE	Tris-EDTA-buffer
TEMED	N,N,N',N'-tetramethylethylendiamine
TGN	trans Golgi network
TMD	transmembrane domain
Tris	tris-hydroxymethyl-aminomethane
U	unit
UV	ultraviolet
V	Volt
v/v	volume per volume
VIAAT	vesicular inhibitory amino acid transporter
Vps	vacuolar protein sorting
WB	western blot
WT	wild type
w/v	weight per volume

1 SUMMARY

The glycine receptor (GlyR) is the major inhibitory neurotransmitter receptor in spinal cord and brainstem. Heteropentameric GlyRs are clustered and anchored at inhibitory postsynaptic sites by the binding of the large intracellular loop between transmembrane domains 3 and 4 of the GlyRβ subunit (GlyRβ-loop) to the cytoplasmic scaffolding protein gephyrin. GlyRs are also co-transported with gephyrin along microtubules in the anterograde and retrograde direction due to the binding of gephyrin to microtubule-associated motor proteins. Additionally, GlyRs undergo lateral diffusion in the plasma membrane from extrasynaptic to synaptic sites and vice versa. Since its discovery, gephyrin has remained for many years the only binding partner interacting directly with the GlyRβ subunit.

In an attempt to elucidate further mechanisms involved in GlyR function and regulation at inhibitory postsynaptic sites, a proteomic screen for putative binding partners to the GlyRβ loop was performed. Three proteins were identified as putative interactors. In this thesis, the interaction between these putative binding proteins and the GlyRβ subunit was analyzed and characterized. Binding studies with glutathione-S-transferase fusion proteins revealed that all putative binding proteins, Syndapin (Sdp), Vacuolar Protein Sorting 35 (Vps35) and Neurobeachin (Nbea), interact specifically with the GlyRβ loop.

The Sdp family of proteins are F-BAR and SH3 domain containing proteins. Inmmunocytochemical experiments showed that SdpI as well as the isoforms SdpII-S and SdpII-L colocalize with the full-length GlyRβ subunit in a mammalian cell expression system. In cultured spinal cord neurons, a partial colocalization of endogenous SdpI with several excitatory and inhibitory synaptic markers was demonstrated. Mapping experiments using deletion mutants narrowed the SdpI binding site down to 22 amino acids. Peptide competition experiments confirmed the specificity of the interaction between SdpI and this sequence of the GlyRβ subunit. Point mutation analysis revealed a SH3-proline rich domain dependent interaction between SdpI and the GlyRβ subunit, respectively. In addition, binding studies in mammalian cells showed that both splice variants of SdpII as well as SdpI interact with the GlyR scaffolding protein gephyrin. Although the SdpI and gephyrin binding sites do not overlap, protein competition studies revealed that interaction of the E-domain of gephyrin with the GlyRβ loop interferes with SdpI binding. Since SdpI is a dynamin binding protein involved in vesicle endocytosis and recycling pathways, a possible function of SdpI in the regulation of GlyR synaptic distribution was

investigated. Co-immunoprecipitation experiments confirmed a SdpI-GlyR association in the vesicle-enriched fraction of rat spinal cord tissue. Immunocytochemical studies of SdpI knock out mice showed that the clustering and distribution of GlyRs in the brain stem is unchanged. However, acute down-regulation of SdpI in rat spinal cord neurons by viral shRNA expression led to a reduction in the number and size of GlyR clusters, an effect that could be rescued upon shRNA-resistant SdpI overexpression. Further immunocytochemical analysis of the localization of gephyrin, the γ2 subunit of the type A γ-aminobutyric acid receptor ($GABA_AR\gamma2$ subunit) and the vesicular inhibitory amino acid transporter (VIAAT) under SdpI knock-down conditions showed that both the number and average size of the γ2-subunit containing $GABA_A$ receptor clusters were significantly reduced in spinal cord neurons. In contrast to GlyR and $GABA_AR\gamma2$ immunoreactivity, the number and average size of gephyrin and VIAAT clusters were barely reduced upon SdpI downregulation. These results suggest that SdpI has a role in GlyR trafficking that can be compensated by other syndapin isoforms or other trafficking pathways. Furthermore, SdpI might be required for the clusters of GlyRs and γ2-subunit containing $GABA_ARs$ in spinal cord and brainstem.

Vps35 is the core protein of the retromer complex, which mediates the endosome to Golgi apparatus retrieval of different types of receptors in mammals and yeast. Here, protein-protein interaction assays revealed for the first time that Vps35 interacts directly with the GlyRβ loop as well as with gephyrin. The generation of specific Vps35 antibodies allowed to determine the distribution of this protein in the central nervous system. Immunocytochemical analyses revealed the presence of Vps35 in the somata and neurites of spinal cord neurons, suggesting a possible interaction of Vps35 with the GlyR under physiological conditions.

Nbea is a BEACH domain containing, neuron-specific protein. Binding studies revealed a direct interaction between two regions of Nbea and the GlyRβ loop. Immunocytochemical experiments confirmed a somatic and synaptic distribution of Nbea in primary cultures. In spinal cord neurons, a partial colocalization of Nbea with excitatory and inhibitory synaptic markers suggests a possible interaction of Nbea with the GlyR at inhibitory synaptic sites.

2 INTRODUCTION

Neurons are cells specialized in reception, integration and delivery of information. They communicate with other neurons by two types of functional cellular contacts: electrical and chemical synapses. At electrical synapses, information transfer between two neurons takes place though gap junctions composed of many connexons. Connexons are oligomeric integral membrane protein assemblies that cross the membranes of both cells and connect their cytoplasms. The gap junctions provide a conducting pathway by which the depolarizing current of one neuron directly flows into the next and, if this surpasses the threshold, leads to its depolarization. Chemical synapses are specialized contact sites formed between neurons or between neurons and muscle or gland cells. They are characterized by membrane specializations, which contain highly specific sets of proteins that allow neurotransmission. Neurotransmission is the unidirectional transfer of information from a presynaptic neuron to a postsynaptic cell mediated by a neurotransmitter. Neurotransmitter transporters fill vesicles with neurotransmitters at the presynaptic terminal of neurons and in glial cells. Many different molecules function as neurotransmitter, e.g. monoamines, peptides and amino acids. In the vertebrate CNS, the main neurotransmitters are glutamate, γ-aminobutyric acid (GABA), glycine (Gly), dopamine, serotonine, histamine and epinephrine. Neurotransmitter release into the synaptic cleft through fusion of the neurotransmitter containing vesicles with the plasma membrane of the presynaptic neuron leads to the activation of neurotransmitter receptors localized in the plasma membrane of the postsynaptic cell. There are two classes of neurotransmitter receptors: metabotropic and ionotropic ones. Metabotropic neurotransmitter receptors are transmembrane proteins coupled to guanine nucleotide-binding proteins (G-proteins) and therefore named G-protein coupled receptors (GPCRs). Agonist binding to GPCRs activates G-proteins, which dissociate into Gα and G$\beta\gamma$ subunits. These subunits modulate ion channels or neurotransmitter receptors directly or through second messenger pathways, thereby inducing a depolarization or hyperpolarization of the plasma membrane. Ionotropic neurotransmitter receptors are transmembrane proteins that form ion-permeable channels, and therefore are named ligand-gated ion channels (LGICs). Activation of a LGICs leads to an influx of ions into the postsynaptic neuron. The activation of excitatory LGICs leads to an influx of Na^+ and Ca^{2+} into the neuron that depolarizes the cell and may result in an action potential. On the contrary, activation of inhibitory LGICs leads to an increase in chloride conductance that hyperpolarizes the cell, thus inhibiting neuronal firing.

2.1 Inhibitory neurotransmitters in the central nervous system

Glycine and GABA are the two major inhibitory neurotransmitters in the central nervous system. At mature inhibitory synapses, glycine activates glycine receptors (GlyRs) whereas at excitatory synapses, glycine is a co-agonist of glutamate required for the activation of N-methyl-D-aspartate (NMDA) receptors (Kleckner and Dingledine, 1988). GABA binds to two distinct types of receptors, ligand-gated ionotropic type A GABA ($GABA_A$) and type C GABA ($GABA_C$) receptors and G-protein-coupled metabotropic type B GABA ($GABA_B$) receptors (Hevers and Lüddens, 1998), thus mediating both fast and slow inhibition of excitability at central synapses.

A different situation is present in neurons during neonatal stages. Due to a different chloride gradient, synaptically relased glycine and GABA depolarize the neuronal membrane pre- and perinatally. Upon further development, the switch to the mature phenotype is mediated by the expression of a K^+-Cl^- cotransporter (KCC) 2. This transporter is responsible for the reduction of the internal Cl^- concentration, thereby shifting the Cl^- equilibrium potential to more negative values and converting the activation of the glycine and GABA receptors from excitatory to inhibitory (Tapia, 1998; Stil et al., 2009).

2.2 Ligand-gated ion channels

Ligand-gated ion channels (LGIC) mediate synaptic communication in the nervous system. In mammals, there are three families of LGICs: the Cys-loop, the glutamate and the P2X receptor channel families. In each case the binding of transmitter to the receptor leads to the opening of a pore, through which ions flow down their electrochemical gradient. Neurotransmitter receptors that belong to the Cys-loop LGIC superfamily include nicotinic acetylcholine, serotonine, $GABA_{A/C}$ and glycine receptors (GlyR). All receptors of this superfamily are composed of five homologous subunits (Fig. 2.1). These subunits share characteristic structural features: a large extracellular amino-terminal domain that harbours the agonist binding site and a Cys-loop, four transmembrane domains (listed as TM1-TM4), with the transmembrane domain TM2 contributing to the central water-filled pore, a large intracellular loop between TM3 and TM4 and a short extracellular C-terminal tail (Fig. 2.1.A).

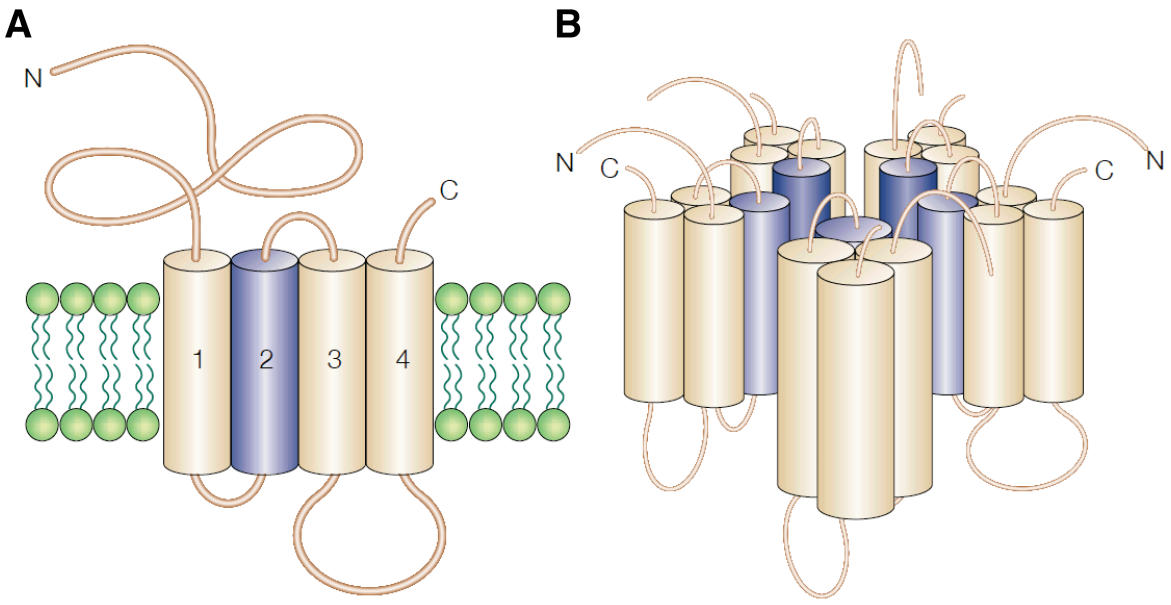

Fig. 2.1. Structure of ligand gated ion channels. A. Membrane threading pattern common to all cysteine-loop receptor-subunits is charachterized by four hydrophobic transmembrane domains (TMDs), a large N-terminus, a short C-terminus and a large intracellular loop between TMD 3 and 4. **B**. Proposed structure of a LGIC. Five subunits assemble to form and pentameric ion channel. Transmembrane domain 2 from different LGIC subunits forms the channel pore (color code is the same as in **A**) (modified from Moss and Smart, 2001).

2.3 Glycine receptors (GlyRs)

The GlyR is a membrane-embedded protein that contains an intern Cl^- selective pore. Glycine binding to the N-terminal region activates and leads to the opening of the Cl^- channel, whereas the competitive antagonist strychnine blocks receptor activation (Young and Snyder, 1973; Betz and Becker, 1988).

2.3.1 Molecular structure and diversity of GlyRs

Five different genes (GLRA1-4 and GLRB) encode for the five subunits of the GlyR, α(1-4) and β. Two subunits were discovered in 1982 when the first purification of the GlyR by H. Betz and colleagues unveiled three distinct aminostrychnine-binding proteins of molecular masses 48, 58 and 93 kDa. The 48 and 58 kDa proteins corresponded to the α1 and β subunits respectively (Pfeiffer et al., 1982). Subsequently, novel α subunits, namely α2, α3 and α4 (Grenningloh et al., 1990; Kuhse et al., 1990; Matzenbach et al., 1994) and splice variants thereof were identified by homology screening. The splice variant GlyRα1^{ins} generated by alternative splicing of the GlyRα1 pre-mRNA was identified in rat spinal cord, but not in other brain regions (Malosio et al. 1991). For rat GlyRα2, two splice variants GlyRα2A and GlyRα2B, which differ by two amino

acid substitutions, were described (Kuhse et al., 1991). Also two splice variants of the human GlyRα3 subunit have been found: α3L and α3K, the latter lacking 15 amino acids in the large intracellular loop (Nikolic et al. 1998). Up to date, only one splice variant of GlyRα4 has been discovered, a zebrafish GlyRα4^{ins} harbouring a 15 amino acid insert in the ligand-binding domain (Devignot et al. 2003). For GlyRβ, two intronic polymorphisms in the GLRB gene had been described previously (Milani et al. 2003). Recently, a new splice variant of the mouse GlyRβ subunit lacking TM1 and TM2 has been found by CM. Becker and his colleagues (Oertel et al., 2007).

The GlyRα1 and GlyRβ subunits share 47% homology, whereas the GlyRα subunits display > 90% homology to each other (Grenningloh et al., 1987; Grenningloh et al., 1990). In LGICs, the large intracellular loop between TM3 and TM4 transmembrane domains is the most poorly conserved domain with respect to both length and aa sequence. In case of the GlyR, the splice variants of the α1 and the α3 subunit differ by inserts, of 8 and 15 aas, respectively, in this region, and the GlyRβ subunit possesses an intracellular loop of 120 aas, which is remarkably larger than the intracellular loop of the GlyRα1 subunit which spans only 86 acids. Thus, the variability in aa sequences of the TM3-4 loops in the GlyRα and GlyRβ subunits as well as their intracellular localization present this domain as a key mediator of specific GlyR subunit interactions with cytoplasmic elements.

2.3.2 GlyR assembly

The assembly of LGICs is a multi-step process that requires proper folding, post-translational modifications and inter-subunit interactions to result in a correct quaternary structure, and is thought to take place in the endoplasmic reticulum (ER) (Green and Millar 1995). The transport of new synthesized receptors to the plasma membrane depends on correct assembly of the subunits with a defined stoichiometry. The subunit composition of GlyRs was originally determined by cross-linking approaches, in which the largest cross-linked product found had a size corresponding to five times the mean size of an individual subunit. Thus, it was concluded that GlyRs are composed of five subunits (Langosch et al., 1988). GlyRs exist as homopentamers and heteropentamers. Heterologous expression in HEK293 cells and in *Xenopus* oocytes revealed that all GlyRα subunits are able to oligomerize and to form functional homopentameric receptors (Schmieden et al., 1989; Griffon et al., 1999). By co-expression of α1 and α2, it was shown that the different GlyRα subunits can also form heteropentameric

receptors (Kuhse et al., 1993). However, the GlyRβ subunit expressed alone produces no glycine-gated currents and requires co-expression with other GlyRα subunits to form functional heteromeric GlyRs (Bormann et al., 1993; Grenningloh et al., 1990). Homopentameric and heteropentameric GlyRs composed of α subunits only can be easily detected and distinguished from each other by their different agonist dose-response profiles. Insensitivity to picrotoxin is a pharmacological hallmark of αβ heteromeric receptors. Whereas homomeric glycine receptors are inhibited by 10 *μ*M picrotoxin, the glycine-gated currents in cells co-expressing α and β subunits require much higher concentrations of the alkaloid for silencing (Pribilla et al., 1992). Whereas stoichiometry in heteromeric receptors formed out of different α subunits is variable (Kuhse et al., 1993), α1β heteromeric receptors assemble at a fixed subunit stoichiometry of 2α3β (Grudzinska et al., 2005).

For GlyR subunit assembly, the N-terminal extracellular domain plays a very important role. Homo-oligomerization of GlyRα1 subunits needs an 8 aa sequence in the N-terminal domain and N-glycosilation occurring before subunit assembly (Griffon N et al., 1999). Assembly boxes in the extracellular N-terminal domain of α and β subunits are crucial for the homo-oligomeric channel formation or stoichiometric assembly of GlyR *in vivo* (Kuhse et al. 1993). In addition, the formation of an intramembrane four-helical bundle by TM1-4 is crucial for stoichiometric subunit assembly (Haeger et al., 2010).

2.3.3 Localization of glycine receptors in the central nervous system

The first studies of GlyR subunit localization in the central nervous system used *in situ* hybridization to reveal the presence of GlyRα1 transcripts mainly in spinal cord and brain stem nuclei and, although at lower levels, also in the superior and inferior colliculi, thalamus and hypothalamus; no signals were found in cortical regions. Transcripts of GlyRα3 showed the same but less prominent distribution as GlyRα1, with maximal expression levels for both subunits occurring around postnatal day 15 (Malosio et al., 1991). Transcripts of the GlyRα2 subunit are highly expressed prenatally throughout most of the CNS and decrease postnatally until postnatal day 20 (Akagi et al., 1991), whereas expression of GlyRα4 is very low but detectable in some regions, e.g. the spinal cord (Harvey et al., 2000). The expression of the GLRB gene starts in the embryo, increases after birth and persists into adulthood throughout most brain regions (Fujita et al., 1991).

The formation of functional GlyRs reflects the receptors' subunit composition. Antibodies against different GlyR subunits were generated to investigate protein expression and distribution of GlyR subunits (Pffeifer et al., 1984; Schröder et al., 1991). The present data on GlyR subunit protein and mRNA expression patterns supports a developmental switch from non-synaptic α2-homopentameric GlyRs at embryonic stages to synaptically localized heteropentameric α1β GlyRs in the adult CNS (Becker et al., 1988).

The major inmunocytochemical results obtained for the human and rat CNS agree with autoradiographic studies, in which GlyRs were prominently seen in the ventral and dorsal horns of the spinal cord and in brainstem (Triller 1985; Baer 2003). However, different immunocytochemical and electrophysiologucal studies have evidenced the presence of GlyR in various subpopulations of the human forebrain, e.g. substancia nigra, hippocampus and striatum, as well as in the rat cerebellum and retina (Wässle et al., 1998; Waldvogel et al., 2007; Dumoulin et al., 2001; Chattipakorn et a., 2002). Some of the GlyR immunoreactivity has been found to colozalize with $GABA_A$Rs at synapses where GABA and glycine are co-released; accordingly, mixed GABA/glycinergic synapses are present in spinal cord, brain stem and cerebellum (van den Pol and Gorcs, 1988; Jonas et al., 1998; Kotak et al., 1999; Dumoulin et al., 2001). Furthermore, electrophysiological studies have provided evidences for a presynaptic localization of GlyRs in spinal cord, retinal bipolar cells and the dentate gyrus (Jeong et al., 2003; Lee et al., 2009; Mϕrkve and Hartveit, 2009; Kubota et al., 2010). In the latter, GlyR expression declines during development.

2.3.4 Clustering of glycine receptors at postsynaptic sites

Postsynaptic membranes in the nervous system are specialized structures highly enriched in neurotransmitter receptors. The enrichment or "clustering" of neurotransmitter receptors at postsynaptic sites is crucial for efficient signal transduction and integration in neurons. Receptor clustering at postsynaptic sites requires interactions with scaffolding proteins that oligomerize beneath the postsynaptic membrane. At excitatory synapses, NMDA-receptors (NMDAR) cluster via their interaction with the synaptic scaffolding protein PSD95/synapse associated protein (SAP) 90 and its family members SAP102 and PSD93 (Niethammer et al., 1996; O´Brien et al., 1998). At glycinergic synapses, the 93 kDa protein co-purifying with the α and β subunits of the GlyR and named gephyrin (meaning "bridge" in Greek) serves as receptor scaffold (Betz et al., 1991). Gephyrin is a tubulin-binding protein, which has a function at inhibitory synapses homologous to that of the actin-binding and nAchR clustering protein, rapsyn, at the

neuromuscular junction (Bloch et al., 1987). Gephryin as well as rapsyn are thought to serve as linker elements between the receptors and the cytoskeleton (Phillips et al., 1991; Kirsch et al., 1992; Prior et al., 1992; Ramarao et al., 2001). The loss of GlyR clusters in spinal cord neurons treated with antisense oligonucleotide and in gephyrin KO mice (Kirsch et al., 1993; Feng et al., 1998) shows that gephyrin is essential for GlyR cluster formation at synaptic sites. Gephyrin binding by the GlyR is mediated by a hydrophobic sequence of 18 aas located in the large cytoplasmic loop of the β subunit (Meyer et al., 1995).

2.3.5 GlyR neuronal trafficking and diffusion

The mechanisms underlying GlyR intracellular transport and the dynamics of GlyR lateral diffusion have been investigated during the past ten years. A prerequisite for GlyR synaptic clustering is the functionality of the GlyRs, as demonstrated by strychnine block, which induces the internalization of GlyRs from synaptic sites (Kirsch and Betz, 1998). On the same line, increased activity and/or depolarization in neurons had the same effect on GlyR clustering as strychnine blockade indicating that synaptic GlyR trafficking is activity-dependent (Maas et al, 2009). Time-lapse imaging showed that gephyrin and GlyR are co-transported on vesicles and the co-purification of gephyrin and GlyR from synaptic vesicles indicated that gephyrin serves as an adaptor in GlyR transport in addition to its function as a synaptic scaffolding protein. Importantly, GlyR and gephyrin influence reciprocally the synaptic clustering/oligomerization, respectively, in a feedback regulation process, since the down-regulation of gephyrin inhibits GlyR clustering, and the blockade of GlyR activates negatively affects the synaptic localization of gephyrin (Kirsch et al., 1998; Maas et al., 2009).

Gephyrin-mediated GlyR vesicular transport requires motor proteins (see Fig. 2.2) The dynein light chains 1 and 2 (Dlc1/2), are subunits of the dynein multi-protein complex mediating transport towards the minus ends of MT. Binding of gephyrin to Dlc1 is not required for gephyrin/GlyR clustering, but necessary for gephyrin transport in the retrograde direction (Fuhrmann et al., 2002, Maas et al., 2006). In contrast, the anterograde transport of gephyrin-GlyR complexes is mediated by isoform 5 of the kinesin protein family (KIF5) (Maas et al., 2009).

Neuronal activity has direct effects on the cytoskeleteton and its associated proteins. GlyR-blockade has been newly found to induce changes in posttranslational modifications of tubulin and microtubule associated proteins (MAP). It increases tubulin polyglutamylation and MAP2 phosphorylation, whereas the mobility of KIF5 and mRFP-gephyrin is decreased (Maas et al.,

2009). In agreement with these results, the phosphorylation-dependent binding of MAP2 to MT is known to negatively influence KIF5 transport (López et al., 1993; von Massow et al., 1989). In conclusion, the anterograde and retrograde transport of GlyRs appears to be gephyrin-dependent by requiring, on one hand, gephyrin to function as adaptor protein for GlyR binding to motor proteins and, on the other hand, the regulation of post-translational modifications of MTs and MAP2 by synaptic activity.

The first evidence for GlyR lateral diffusion was obtained by single particle tracking with antibody-coated latex-beads and by immunocytochemical analysis of GlyRα1 subunit insertion into the plasma membrane over time (Meier et al., 2001; Rosenberg et al., 2001). These studies demonstrated that newly synthesized GlyRs are inserted into the plasma membrane at extrasynaptic locations, and that individual GlyRs diffuse freely within the plasma membrane. Quantum dot tracking approaches allowed single GlyR trajectories to be monitored at synaptic, perisynaptic and extrasynaptic sites in living neurons. Analysis of the resulting single GlyR trajectories revealed that GlyRs dynamically exchange between synaptic and extrasynaptic membrane compartments whilst passing through an intermediate perisynaptic state (Dahan et al., 2003).

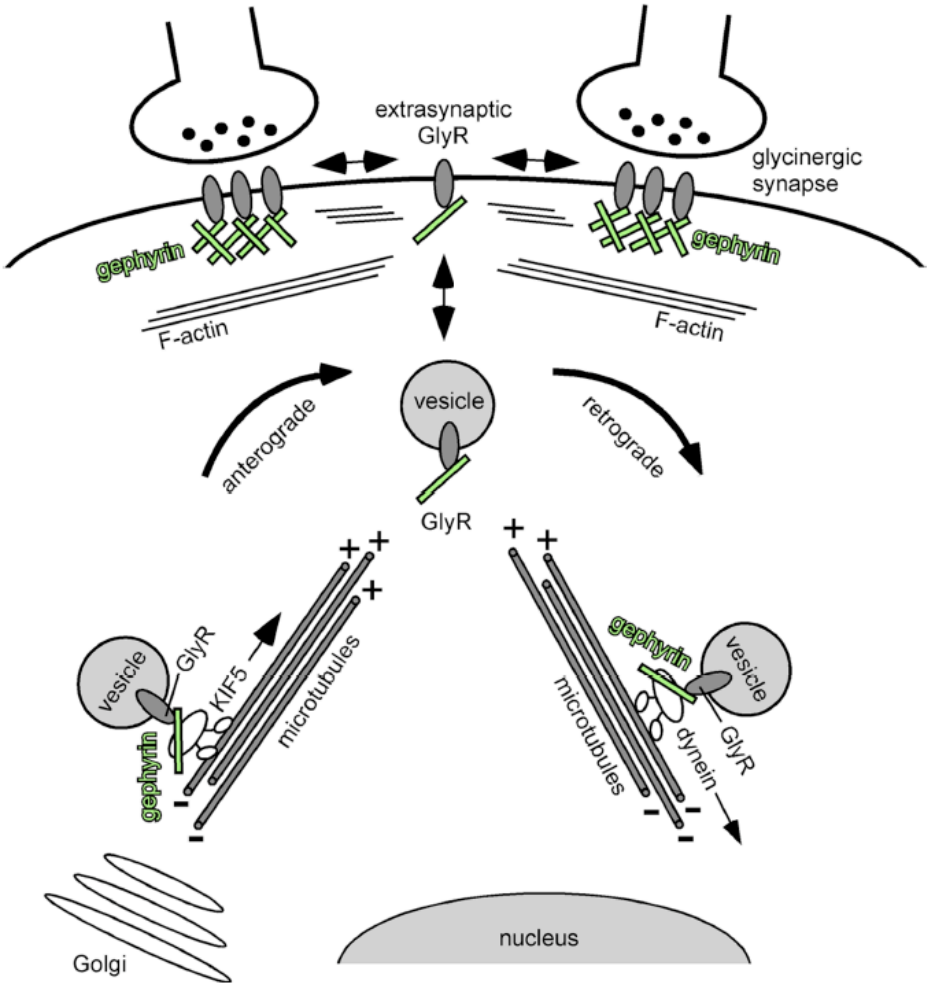

Fig. 2.2. GlyR-gephyrin intracellular co-transport along microtubules. After synthesis and assembly, GlyRs leave the Golgi apparatus and are actively transported along cytoskeletal elements to the plasma membrane. KIF5 is a motor protein that moves anterogradely towards the plus ends of microtubules and connects to GlyRs via gephyrin. After insertion into the plasma membrane, GlyRs are clustered at synaptic sites by gephyrin. Endo- and exocytosis occurs at extrasynaptic sites. Once GlyR are endocytosed, Dlc1, a motor protein travelling towards the minus end of microtubles, mediates the retrograde transport of GlyR-gephyrin complexes (modified from Dumoulin et al., 2010).

2.4 Objectives of the present study

As described in 2.3.5, the intracellular tranport of GlyRs is gephyrin- and motor protein-dependent for both anterograde and retrograde transport along microtubules (Maas et al., 2006; Maas et al., 2009). Furthermore, a model for GlyR lateral diffusion and synaptic/extrasynaptic exchange involving multiple states of GlyR/gephyrin association has been postulated (Ehrensperger et al., 2007). Although the GlyRβ subunit is a key determinant of GlyR synaptic localization, gephyrin has been the only GlyRβ binding-protein known (Betz et al., 1991). In order to shed further light on GlyR transport and distribution mechanisms, in this thesis, the interaction of novel GlyR binding proteins was investigated. Putative binding proteins were isolated in a proteomic screen from rat brain homogenate using the intracellular loop of the GlyRβ subunit as bait and identified by mass-spectrometry (Paarmann et al., 2006). The main aspects of these new GlyRβ binding proteins, synaptic dynamin binding protein (Sdp), vacuolar protein sorting ps35 (Vps35) and neurobeachin (Nbea), are introduced below (see 2.4.1, 2.4.2, 2.4.3). The interactions of these proteins with the GlyRβ subunit and gephyrin were examined and deletion approaches were used to map the SdpI binding site. Peptide competition approaches were performed to investigate the specificity of the SdpI-GlyR interaction. Point mutations introduced in the SH3 binding domain of the GlyRβ subunit were tested in order to characterize the interaction. The production of specific antibodies and immunocytochemical experiments allowed to determine the neuronal localization of these proteins.

All proteins identified here as GlyRβ binding partners have been implicated in different trafficking steps between membrane compartments. On this basis, the functional role SdpI in GlyR trafficking and synaptic distribution was investigated. To this end, co-immunoprecipitation experiments were performed to demonstrate an interaction of endogenous GlyRs and SdpI. Additionally, SdpI deficient mice (SdpI-/-) and SdpI knockdown approaches were used to examine the physiological consequences of SdpI deficiency on GlyR distribution in spinal cord neurons.

2.4.1 Syndapin

Syndapin I (SdpI) (synaptic dynamin-associated protein I) was initially identified in a screen for proteins interacting in rat brain cytosol with the proline-rich domain of dynamin (Qualmann et al., 1999). Two other isoforms of SdpI were subsequently identified in human and murine cDNA libraries: syndapin II (SdpII) (Qualmann and Kelly, 2000) and syndapin III (SdpIII) (Sumoy et al., 2001), both with high sequence conservation. For SdpII, there are two splice variants known: the long form syndapin II-l (SdpII-l) and the short form syndapin II-s (Sdp II-s) (Qualmann and Kelly, 2000). The SdpI gene has been found in mammals, nematodes and insects but not in plants and single-cell eukaryotes. Moreover, up to five Sdp genes have been identified in fugu and zebra fish (Kessels and Qualmann, 2004).

2.4.1.1 Molecular structure and diversity of the syndapin protein family

All Sdps share a common organization with an F-BAR (Fes/CIP4 homology-Bin/Amphiphysin/Rvsp) domain and an SH3 (src homology 3) domain. The aa sequences of SdpI and both splice variants of SdpII comprise additional NPF motifs (named after their asparagine-proline-phenylalanine repeats), whereas SdpIII contains, a proline-rich domain instead of NPF domains (Fig. 2.3.A).

F-BAR domains constitute a subfamily of the BAR domains, protein modules that stabilize and/or induce membrane curvature. The F-BAR domains are composed of a FCH (Fes and CIP4 homology) domain followed by a coiled-coiled region, which by direct interaction forms dimers and tetramers *in vitro* (Halbach et al., 2007). SdpI requires the α-helical part of the N-terminal-FCH region to form oligomers *in vitro* and *in vivo* (Kessels and Qualmann, 2006). The crystalization of F-BAR dimers revealed a sickle-shaped structure of the domain, with a shallow curvature when seen from the side and a tilde shape when viewed from below (Henne et al., 2007, Fig. 2.3.B). Like classical BAR domains, this BAR-related domain is able to bind to flat or curved lipid bilayers due to an enrichment of positively charged residues at the concave surface, which forms the major membrane interaction interface. This, together with its ability to oligomerize with other F-BAR domains and to form intermolecular interactions, induces membrane-tubule formation and shapes helical coats for their stabilization (Shimada et al., 2007; Frost et al., 2008). In contrast to the class of F-BAR domains that prefer weakly curved membrane tubules (Itoh et al., 2005; Shimada et al., 2007), the F-BAR domain of SdpI

constitutes a scaffold that is optimized for the stabilization of a high degree of membrane curvature (Wang et al., 2009).

The C-terminal SH3 domain is highly conserved among all Sdps and widely known as a proline recognition motif (Feng et al., 1994, Li et al., 2005). This domain is responsible for the interaction of SdpI with several proline-rich domain (PRD) containing-proteins of the endocytic pathway such as dynamin (Sever et al., 2000), the phosphatidylinositol 5-phosphatase synaptojanin (Cremona et al., 1999), synapsin I (Hilfiker et al., 1999) and the neural Wiskott-Aldrich syndrome protein (N-WASP) (Qualmann et al., 1998). The NPF motifs are also implicated in protein-protein interactions and mediate binding of SdpI and SdpII to EHD proteins implicated in endosomal recycling (Braun et al., 2005).

2.4.1.2 Cellular and sub-cellular distribution of the Sdp protein family

In mammals, the expression patterns of the three Sdp isoforms are rather different. Whereas SdpI is expressed exclusively in the CNS, both splice variants of SdpII are expressed ubiquitously in all tissues, and SdpIII is present in skeletal muscle and heart and weakly expressed in brain. Developmental expression of SdpI gene and protein levels is detectable at embryonic day (E) 17 and increases continuously up to the adult stage. Studies in pluripotent cells with the ability to differentiate only to neuron-like cells revealed that SdpI gene expression starts as soon as cells stop proliferating and begin to differentiate into neurons (Plomann et al., 1998). Interestingly, the splice variants of SdpII display different distributions, with SdpII-l being prominent in neuronal and heart tissues and SdpII-s being ubiquitously expressed (Qualmann and Kelly, 2000).

At the sub-cellular level, SdpI distributes along processes surrounding the cell bodies of neurons and is found at excitatory presynaptic terminals and postsynapses as well as at the tubulolamellar postsynaptic membrane system of *D. melanogaster* NMJ (Qualmann et al., 1998; Kumar et al., 2009).

2.4.1.3 Functional relevance of Sdp protein family in the CNS

Since the initial identification of SdpI in 1999, the investigation of Sdp functions in the CNS has become the object of several scientific reports. In the zebrafish (*Danio rerio*), loss of function experiments revealed a key function of SdpIII in cell migration and columnar organization of the notochord. This study presented for the first time evidence for a functional role of SdpIII in developmental differentiation (Edeling et al., 2009). In cultured hippocampal neurons, SdpI

regulates neuromorphogenesis by binding N-WASP, releasing N-WASP autoinhibition and inducing actin nucleation at the cell cortex (Dharmalingam et al., 2009). Additionally, subcellular fractionation experiments recently demonstrated that the F-BAR domain of SdpI and SdpII is necessary for Sdp-binding to phosphatidylserine containing membranes and required for SdpI targetting to the plasma membrane in neurons (Dharmalingam et al., 2009).

The name Sdp, for synaptic dynamin binding protein, points toward the currently best-studied function of Sdp *in vivo*. A dephosphorylation-dependent interaction of the large GTPase dynamin with SdpI is essential for synaptic vesicle endocytosis in neurons under intense stimulation, but is not required for clathrin-mediated endocytosis in non-stimulated cells. When neuronal activity is elevated, neuronal depolarization induces a calcineurin-mediated dephosphorylation of dynamin that triggers SdpI-dynamin protein complex formation and activity-dependent bulk endocytosis (Ferguson et al., 2007; Anggono et al, 2006; Anggono et al., 2007; Clayton et al., 2009). On the same line, SdpII joins dynamin II in vesicle formation from the trans-Golgi network (Kessels et al., 2006). Due to the ability of SdpI to oligomerize through the F-BAR domains and to interact with protein elements affecting actin polymerization (N-WASP) and endocytosis (dynamin), Sdp has been proposed to link vesicle formation and cortical cytoskeleton dynamics (Kessels and Qualmann 2002; Kessels and Qualmann 2006). Furthermore, the interaction of EHD proteins, regulators of the endocytic recycling compartment transport, with SdpI and SdpII via their NPF repeats has been shown to be required for transferrin receptor recycling events (Braun et al., 2005). Similarly, activity-dependent vesicle recycling at presynaptic terminals under intense stimulating conditions requires a dynamin-SdpI-N-WASP intact complex (Andersson et al., 2008). This demonstrates that SdpI has a role as key regulator of compensatory endocytosis, coordinating vesicle formation and actin functions.

In contrast to the established function of Sdp in vesicle endocytosis and recycling at the presynapse, the functional role of Sdps at postsynaptic sites remains still poorly understood. Studies performed at the NMJ of *D. melanogaster* have excluded a role of SdpI in presynaptic vesicle endocytosis but shown that Sdp is predominantly associated to postsynaptic terminals, where it mediates the expansion of the subsynaptic reticulum (Kumar et al., 2008; Kumar et al., 2009). Furthermore, in hippocampal neurons an NPF domain-dependent interaction of SdpI, but not SdpII, with NR3A-containing NMDA receptors is crucial for the removal of NR3A subunit containing NMDA receptors from synaptic sites (Pérez-Otaño et al., 2007).

Another protein which binds SdpI and SdpII is the mammalian son-of-sevenless (mSOS), a guanine exchange factor for the small GTPases Ras and Rac (Wasiak et al., 2001). The recruitment of SdpI/II to mSOS and actin at growth cones together with the ability of SdpI to induce filopodia formation through N-WASP mediated activation of Arp2/3 is consistent with Sdp regulating actin dynamics during filopodia and lamellipodia formation (Qualmann and Kelly, 2000).

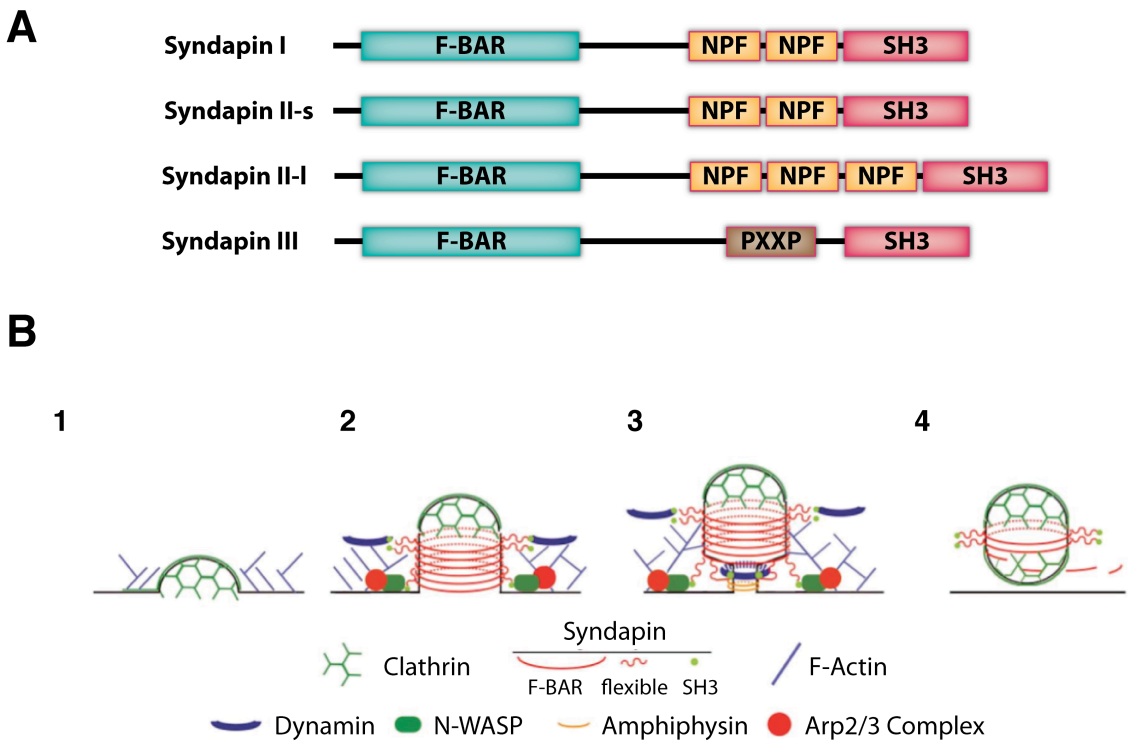

Fig. 2.3. Domain organization of the Sdp protein family and model of vesicle budding, invagination and fission processes. A. Domain organization of Sdp isoforms and both splice variants. F-BAR: Fes/CIP4 homology-Bin/Amphiphysin/Rvsp domain, NPF: asparagine-proline-phenylalanine repeats, SH3: src homology 3 domain, PxxP: proline-rich sequence. **B**. **1**. First adaptor proteins and clathrin coats assemble. **2**. Then the F-BAR domain sense the curvature of the clathin coated bud and oligomerizes, thereby inducing membrane tubulation. F-BAR domain-containing proteins like Sdp recruit dynamin and N-WASP through the SH3 domain. **3**. N-WASP induces Arp2/3-mediated actin polymerization, and BAR-domain containing proteins like amphiphysin bind to the narrowed vesicle-neck and contributes as well to dynamin recruitment. **4**. GTPase activity of dynamin and actin polymerization lead finally to vesicle fission from the plasma membrane (modified by Dennis Koch from Shimada et al. 2007).

2.4.2 Vacuolar protein sorting 35 (Vps35)

Eukaryotic cells contain distinct membraneous organelles, whose identity is defined by their protein composition. The maintenance of sub-compartment identity is achieved through the specific sorting and delivery of proteins to each organelle. In the lysosomal protein delivery pathway, post-translational modifications like the attachment of mannose-6-phosphate groups to N-linked oligosaccharide side chains of lysosomal hydrolases takes place in the Golgi apparatus. In the trans-Golgi network, this native tag is recognized by mannose-6-phosphate receptors (MPRs) in mammals, or N-terminal signal peptides of the carboxipeptidase Y are recognized by vacuolar hydrolases sorting receptors, such as Vps10p in yeast (Hoflack et al., 1987; Johnson et al., 1990), which then leads to the sorting of the hydrolase-receptor complexes to endosomes. There, the hydrolases dissociate from the receptor due to the acidic environment of the endosomes, and both proteins follow then divergent pathways. Hydrolases are delivered to lysosomes, and MPR as well as Vps10p proteins are recycled back to the Golgi apparatus where they mediate further rounds of sorting (Braulke and Bonifacino 2009).

Vacuolar protein sorting (vps) genes were first identified in *Saccharomyces cerevisiae* by a genetic screen for mutants defective in protein trafficking to the lysosome-like vacuole (Paravicini et al., 1992). The first hint for a retrieval function of Vps35, Vps30 and Vps29 in yeast was provided by mutants of these three proteins, which led to a mislocalization of the carboxipeptidase Y receptor Vps10p to the yeast vacuole (Seaman et al., 1997). Moreover, this study also provided the first evidence for a central role of Vps35 as a receptor recognition element (Seaman et al., 1997; Nothwehr et al 2000). A heteropentameric protein complex composed of Vps35, Vps29, Vps26, Vps17 and Vps5 was identified in yeast as a membrane-associated coating complex, which is responsible for receptor retrieval from endosomal and plasma membranes to the Golgi apparatus, and hence was named retromer complex (Seaman et al 1998).

2.4.2.1 Subunit composition of the retromer complex

The retromer complex is organized in two subcomplexes preserved from yeast to mammals: a membrane-targeting heterodimer and a cargo recognition heterotrimer (Horazdovsky et al., 1997; Seaman et al 1998; Fig. 2.4). The membrane heterodimer is composed of proteins of the sorting nexin family: Vps5 and Vps17 in yeast or their mammalian counterparts SNX1/SNX2 and

SNX5/SNX6 (Griffin et al., 2005; Rojas et al., 2007; Wassmer et al., 2007). SNX proteins comprise a BAR domain and a phox homology (PX) domain. BAR domains are banana-like domains with a curved structure different from F-BAR domains. They form dimers and act as membrane curvature sensors, thereby ensuring the localization of SNX at highly curved membrane tubules (Carlton et al 2004; Gallop et al., 2005). PX domains bind to specific phosphoinositides, e.g. phosphatidylinositol 3-phosphate and phosphatidylinositol biphosphate, and thus constitute another membrane binding interface in SNX dimers (Worby et al., 2002; Carlton et al., 2005; Fig. 2.4). The cargo recognition subcomplex is composed of the core protein Vps35 and two regulatory proteins, Vps29 and Vps26. Vps35 directly mediates cargo binding through its interaction with the cytosolic tails of transmembrane proteins. Several of the binding sequences in different transmembrane proteins have been identified and share common features, like their hydrophobicity and the presence of aromatic aas (Seaman et al., 2007; Nielsen et al., 2007). Both Vps29 and Vps26 require Vps35 for their incorporation into the retromer complex, due to binding at the C- and the N-termini of Vps35, respectively (Shi et al., 2006; Hierro et al., 2007).

2.4.2.2 Functional relevance of the retromer complex

The retromer complex, as a novel sorting device for retrograde endosome/plasma membrane to TGN transport, has become the focus of a recent flurry of studies. The latter revealed its participation in a broad range of physiological processes. Its function in intracellular transport is necessary for the retrieval of receptors, e.g. Vps10p, sortilin, SorLA (Mari et al., 2007), the plant seed storage protein receptor AtVSR1/AtELP (Shimada et al., 2006; Fuji et al., 2007) and membrane transporters, such as the iron transporter DMT1-II (Tabuchi et al., 2010). Additional evidence for a role of the retromer complex in protein recycling is its interaction with EHD proteins (Gokool et al., 2007). The retromer complex is also responsible for transcytosis of the polymeric immunoglobulin receptor (pIgR) and its cargo IgA in epithelial cells, i.e. their translocation from the basolateral to the apical cell surface (Verges et al., 2004). Moreover, bacterial toxins like the Shiga toxin B subunit also use a retromer-mediated internalization mechanism to get to the ER and the cytosol (Utskarpen et al., 2007). Finally, the retromer complex mediates endosome to TGN transport of the amyloid precursor protein (APP), β-secretase and/or γ-secretase, and therefore is thought to have a role in Alzheimer's disease (Muhammad et al., 2008).

Since several protein machineries mediating retrograde trafficking between endosomes and the TGN have been identified, their interactions and regulation has only recently received attention. Initial studies proposed a sequential two-step model for retrograde sorting, in which retromer formation would be clathrin dependent (Popoff et al., 2007). Recent reports, however, suggest a model, in which two membrane proteins interacting with SNX1 and Hsc 70, a clathrin uncoating ATPase, affect clathrin dynamics in an antagonistic manner and thereby determines whether either a retromer or a clathrin mediated retrograde sorting process is used (Popoff et al., 2009).

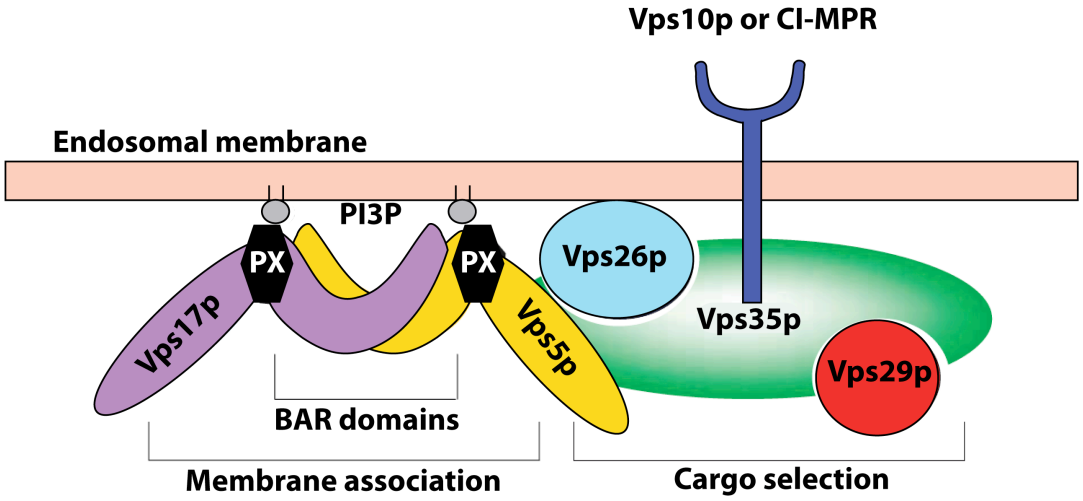

Fig. 2.4. Protein composition of the retromer complex. Schematic depiction of protein interactions in the retromer complex of yeast. Vps35p interacts with Vps26p through its N-terminus and with Vps29p through its C-terminus forming the cargo recognition subcomplex that binds to the receptor (Vps10p in yeast or CI-MPR in mammals). Thus, Vps5p and Vps17p in yeast are members of the SNX family of proteins that constitute the membrane association subcomplex. SNX proteins form dimers through their C-terminal BAR domains and comprise as well PX domains binding to PI3P and PI35BP in membranes. Abbreviations: Vps: vacuolar protein sorting, BAR: Bin-amphiphysin-Rvs domain, PX: phox homology domain, CI-MPR: cation-independent mannose-6-phosphate receptor, PI3P: phosphatidylinositol 3-phosphate, PI35BP: phosphatidylinositol 3,5-biphosphate (modified from Seaman 2005).

2.4.3 Neurobeachin

Ten years ago, in an attempt to screen for new synaptic plasma membrane proteins, a novel protein was identified as the large neuron-specific protein Neurobeachin (Nbea) (Wang et al., 2000). This protein belongs to the BEACH (named after beige mouse and *Chediak-Higashi* syndrome) protein family and to the A-kinase anchor protein (AKAP) family present in unicellular and multicellular eukaryotes (Lozanne, 2003). Since its identification, many studies aimed to disclose the function of this novel protein in the central nervous system.

2.4.3.1 Molecular structure of Nbea

Nbea is a multimeric protein with a molecular weight of 327 kDa. The BEACH protein family members share, apart from the characteristic C-terminal BEACH domain, a Pleckstrin homology (PH) domain and tryptophan-aspartic acid (WD)40 repeats, localized N- and C-terminally of the BEACH domains, respectively, as well as a N-terminal concanavalin-A (ConA)-like lectin domain (Nagle et al., 1996; Jogl et al., 2002; Burgess et al., 2009; Fig. 2.5). Crystal structure analyses have shown a close proximity of the PH and BEACH domains and led to the postulate that both domains function as a single unit in protein-protein interactions (Jogl et al. 2002). On the same line, WD40 repeats are domains involved in protein-protein interactions (Neer et al., 1994). Moreover, the identification of a ConA-like lectin domain in the Nbea sequence implies that this protein could also recognize carbohydrate side chains of their target proteins (Burgess et al., 2009). A particular feature of Nbea is its high-affinity binding site in the B domain for the type II regulatory protein kinase A (PKA RII) (Wang et al., 2000; Fig. 2.5). Due to the association of Nbea with tubulo-vesicular membranes, it may function as AKAP and target PKA to proper locations in the cell.

2.4.3.2 Functional relevance of Nbea in the CNS

BEACH-domain containing proteins are thought to act in cellular trafficking, since mutations in the prototypic BEACH domain protein, LYST, lead to protein sorting defects and giant inclusion bodies (Nagle et al., 1996; Faigle et al 1998). Different studies indicate a predominantly postsynaptic localization of the Nbea protein. Additionally a coat-like GTP-dependent and brefeldin-A sensitive membrane binding activity of Nbea to *trans*-Golgi-near endomembranes of neurons has been observed (Wang et al., 2000). The analysis made on Nbea-deficient mice revealed a complete impairment of spontaneous and evoked excitatory and inhibitory synaptic

neurotransmission. In these studies, a reduction in synaptic protein-content was found, suggesting that Nbea plays a central role in synapse formation and function (Medrihan et al., 2009). However, studies of the NMJ of Nbea -/- mice demonstrated an impairment of only evoked but not spontaneous neurotransmission as well as normal NMJ morphology. Thus, Nbea may have distinct roles at central and neuromuscular synapses (Su et al., 2004).

The precise function of Nbea in the CNS is of medical interest, since genetic studies linked *de novo* translocations of the locus encompassing the Nbea-encoding gene to idiopathic autism (Castermans et al., 2003). Furthermore, the Nbea gene is localized to candidate regions for autism on chromosome 13 and spans the fragile site FRA13A (Barret et al., 1999; Savelyeva et al., 2006). These findings, together with the demonstrated expression of Nbea in the CNS during development and Nbea-dependent inhibitory-excitatory synaptic imbalance, point to the Nbea gene as an important disease gene in autism.

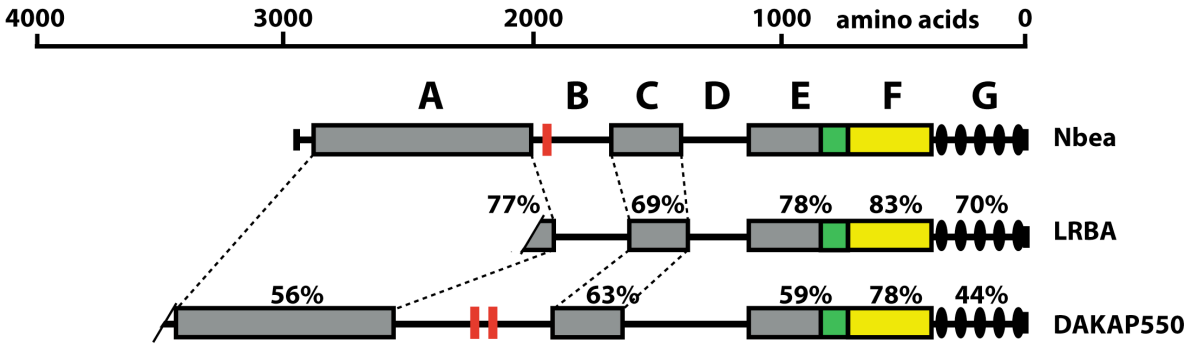

Fig. 2.5. Domain organization of BEACH domain-containing proteins. Domain organization of three BEACH-related proteins starting at the C-temrinus. PH domains are depicted as green boxes followed by BEACH domains and WD40 repeats depicted as yellow boxes and ovals, respectively. Grey boxes indicate conserved sequences, and numbers above show the percentage in aa sequence identity among these BEACH-related proteins. Horizontal lines indicate regions not conserved. Binding sites for the type II regulatory protein kinase A (PKA RII) are marked by red boxes. Oblique lines indicate that the N-terminal sequences of LRBA and DAKAP550 are incomplete. Abbreviations: LRBA: lipopolysaccharide-responsive vesicle trafficking, beach and anchor containing protein; DAKAP550: ortholog of Nbea in *D.melanogaster* (modified from Wang et al., 2000).

3 MATERIALS AND METHODS

3.1 MATERIALS

3.1.1 Chemicals and plastic materials

All chemicals, unless otherwise stated, were ordered from the following companies: Applichem (Darmstadt, Germany), Bio-Rad (Munich, Germany), Biotrend (Cologne, Germany), Calbiochem Merck Biosciences (Schwalbach, Germany), DifcoLaboratories (Detroit, USA), Eppendorf (New York, USA), Fluka (Buchs, Switzerland), GE Healthcare Biosciences (Freiburg, Germany), Gibco-BRL (Karlsruhe, Germany), Invitrogen (Carlsbad, USA), Merck (Darmstadt, Germany), New England Biolabs (Ipswich, USA) Roche Diagnostics (Basel, Switzerland), Roth (Karlsruhe, Gemany), Serva (Heidelberg, Germany) and Sigma-Aldrich (Munich, Germany). All solutions were prepared with Milli-Q water (Millipore, Wartford, USA).

Plastic materials were from the following companies: Falcon (Le Pont De Claix, France), Perbio Sciences (Bonn, Germany), Roth (Karlsruhe, Germany), Greiner (Darmstadt, Germany) and Eppendorf (Hamburg, Germany).

3.1.2 Enzymes

All restriction enzymes, Quick T4 DNA ligase and Deep Vent DNA polymerase used were obtained from New England Biolabs (Frankfurt, Germany). T4 DNA Ligase and Proteinase K were purchased from Roche (Mannheim, Germany), Benzonase from Novagen (Darmstadt, Germany), PANScript DNA polymerase from PAN Biotech (Aidenbach, Germany) and Clonases from Invitrogen (Karlsruhe, Germany).

3.1.3 Kits

Name	Description	Company
BLOCK-iT Pol II miR RNAi Expression Vector Kit	Gateway-adapted expression vector for the expression of microRNA in mammalian cells under control of Pol II promoters	Invitrogen (Carlsbad, USA)
DC Protein Assay Kit	Determination of protein amount	BIO-RAD (Munich)
HiSpeed Plasmid Maxi-Kit	Rapid purification of transfection grade plasmid DNA	QIAGEN (Hilden)
QIAGEN Plasmid-Midi-Kit	Purification of DNA	QIAGEN (Hilden)
QIAGEN Plasmid-Mini-Kit	Purification of DNA	QIAGEN (Hilden)
QIAquick Gel-Extraction-Kit	Isolation of DNA fragments from agarose gels	QIAGEN (Hilden)
REDExtract-N-AmpTissue PCR-Kit	Rapid extraction and amplification of genomic DNA from mouse tails	SIGMA (USA)
Silver Stain Plus Kit	Silver staining of SDS-polyacrylamide gels	BIO-RAD (Munich)

3.1.4 DNA standard

As a reference marker for DNA, the *SmartLadder*-Marker from Eurogentec (Cologne, Germany) was used following the manufacturer's instructions. This marker contains DNA fragments of the following sizes: 10, 8, 6, 5, 4, 3, 2.5, 2, 1.5, 1, 0.8, 0.6, 0.4 and 0.2 kbp.

3.1.5 Protein standard

As reference for protein gels, the *SeeBlue2*-Marker from Invitrogen (Carlsbad, USA) was used. This marker mix contains the following proteins: myosin (250 kDa), phosphorylase (148 kDa), BSA (98 kDa), glutamate dehydrogenase (64 kDa), alcohol dehydrogenase (50 kDa), carbonic anhydrase (36 kDa), myoglobin (22 kDa) lysozyme (16 kDa), aprotinine (6 kDa) and insuline (β-chain) (4 kDa).

3.1.6 Membranes and films

Nitrocellulose membranes from Schleicher and Schuell GmbH (Dassel, Germany) and PVDF

transfer membrane from GE Healthcare (Little Calfont, UK) with a pore size of 0.45 μm were used for Western blot analysis. Files for autoradiography were purchased from BIOMAX MR (Kodak, Cedex, France) or HyperfilmTM MP (GE Healthcare Limited, Little Calfont, UK).

3.1.7 Oligonucleotides

Oligonucleotides were ordered from Metabion (Mastinsried, Germany), received as lyophilized pellets and dissolved in pure water (Braun Melsungen AG, Melsungen, Germany) to a final concentration of 100 pmol/μl. They were used for PCR reactions, genotyping, sequencing and mutagenesis. In the following list of oligonucleotides, restriction sites and point mutations are indicated by an underline and lower-case, respectively.

Table 1. Primers used for mutagenesis or addition of restriction sites.

Primer	Purpose	Orientation	Sequence
IP50	Generation of point mutation to remove the NdeI restriction site from the Vps35 coding sequence	Forward	5'– GAAACAGTAGCcTATG AATTTATGTCCCAG – 3'
IP51		Reverse	5'– CTGGGACATAAATTCATAgG CTACTGTTTC – 3'
IP48	Addition of a XhoI-NdeI site at the 5' and a BamHI at the 3' end of the Vps35 coding sequence	Forward	5'– CGCCGCTCGAGCATATG CCTACAACACAGCAGTC – 3'
IP49		Reverse	5'– CGGGATCCTTAAAGG ATGAGACCTTCATAG – 3'
IP67	Addition of a NdeI site at the 5' and a BamHI site at the 3' end of the Vps29 coding sequence	Forward	5'– GGAATTCCATATG TTGGTGTTGGTACTAGGAGA – 3'
IP68		Reverse	5'– GCGGATCCGCTTTA CGACTTTTTATACTCA – 3'
IP89	Addition of BglII sites at the 5' and 3' ends of the mRFP coding sequence and sequencing of the GlyRβ-mRFP construct	Forward	5'– GAAGATCTATGGCCT CCTCCGAGGACGTCA – 3'
IP90		Reverse	5'– GAAGATCTGGCGCCGG TGGAGTGGCGGCCC – 3'

Table 2. Primers used for genotyping

Mouse line	Primer	Orientation	Sequence
SdpI	IP77	Forward	5'– AGAGATGTTGAGATGTGTAC – 3'
	IP78	Reverse	5'– AAGGGAGTCTGGATGCAAGG – 3'
	IP79	Forward	5'– ATCTGAGGAGACCCATTCAG – 3'
	IP80	Reverse	5'– CGGTAGAATTGACGAAGTTCC – 3'

Table 3. Primers used for sequencing

Vector	Primer	Orientation	Sequence
pRK5	IP81	Forward	5'– AATTAACCCTCACTAAAGGG – 3'
	IP92	Reverse	5'– CTTTCAGAGGTTATTTCAGGC – 3'
	pCMVfor	Forward	5'– CGCAAATGGGCGGTAGGCGTG – 3'
pDP	pDP	Forward	5'– AGAGTGCTTTCCCGTGTCAG – 3'
pCMV	T7	Forward	5'– TAATACGACTCACTATAGGG– 3'
	T3	Forward	5'– AATTAACCCTCACTAAAGGG– 3'
pQE5	pQEfor	Forward	5'– GTATCACGAGGCCCTTTCGTCT– 3'
	pQErev	Reverse	5'– CATTACTGGATCTATCAACAGGAG – 3'
pGEX	pGEXfor	Forward	5'– ATAGCATGGCCTTTGCAGG – 3'
	pGEXrev	Reverse	5'– GAGCTGCATGTGTCAGAGG – 3'
pEGFP	pEGFP-C1for	Forward	5'– GATCACTCTCGGCATGGAC – 3'
	pEGFP-N1for	Forward	5'– GTCGTAACAACTCCGCCC – 3'
	pEGFP-N1rev	Reverse	5'– GTCCAGCTCGACCAGGATG – 3'
Vps35 _pBlue-script	IP51	Reverse	5' – CTGGGACATAAATTCATAGGCTACTGTT TC – 3'
	IP52	Reverse	5'– CACTGTAGCCACCTGTTGTG – 3'
	IP53	Forward	5'– AACGAGAGAGAGACAAGAACTGA – 3'
	IP55	Forward	5'– CTCAGGACCAGGTAGATTCC – 3'
pAAV	6Pfor	Forward	5'– AGGAGTCGTGTCGTGCCTGAG– 3'
	6Prev	Reverse	5'– AGCAGCGTATCCACATAGCG – 3'

3.1.8 Organisms

3.1.8.1 Bacteria

Name	Genotype	Source
***E. coli* XL1-Blue**	*recA1 endA1 gyrA96 thi-1 hsdR17 supE44 relA1 lac* [F´ *proAB lacI*^{q}*ZΔM15* Tn*10* (Tet^r)]	Stratagene (La Jolla, USA)
***E. coli* BL21 codon plus**	*E. coli* B F–*omp*T *hsd*S($r_B^-m_B^-$)*dcm*$^+$ Tet^r gal λ(DE3)*end*A Hte [*arg*U *pro*L *Cam*^{r}] [*arg*U *ile*Y *leu*W Strep/Spec^r]	Stratagene (La Jolla, USA)
***E. coli* Turbo cells**	F´ *pro*A$^+$B$^+$ *lacI*^{q} Δ *lacZ* M15/ *fhu*A2 Δ(*lac-pro*AB) *gln*V *gal* R(*zgb*-210::Tn10)Tet^S *end*A1 *thi*-1	New England Biolabs

	Δ(*hs*^{d}S-*mc*^{r}B)5	
***E. coli* Sure2 cells**	e14^{-}(*Mcr*A^{-}) Δ(*mcr*CB-*hsd*SMR-*mrr*)171*end*A1 *sup*E44 *thi*-1 *gyr*A96 *rel*A1 *lac rec*B *rec*J *sbc*C *umu*C::Tn5 (Kan^{r})uvrC [F´ *pro*AB *lac*I^{q}ZΔM15 Tn10 (Tet^{r}) Amy *Cam*^{r}]	Stratagene (La Jolla, USA)
***E. coli* Top10 cells**	*F´ mcrA Δ(mrr-hsdRMS-mcrBC) ϕ80lacZΔM15 ΔlacX74 nupG recA1 araD139 Δ(ara-leu)7697 galE15 galK16 rpsL(Str^{R}) end A1 λ*	Invitrogen (Carlsbad, USA)

3.1.8.2 Animals

The house mouse *Mus musculus* is the principal model organism used to investigate gene function in mammals. The SdpI deficient mice used in this work had been generated using the Cre/loxP system in Dr. Britta Qualmann´s group at the University of Jena (Germany). Cre induced recombination led to the excision of exon 1 of the SdpI gene encoding the start codon, thus eliminating SdpI expression in all brain regions (Koch D., PhD thesis). SdpI-deficient mouse line was maintained in the animal house of the Max-Planck-Institute for Brain Research (Frankfurt, Germany) by backcrossing of SdpI heterogyzous mice with C57BL/6J mice.

For the preparation of rat primary neurons, pregnant Wistar rats were purchased from Charles River Laboratories Inc. (Kisslegg, Germany).

3.1.9 Cell lines

Name	Donor organism	Source
HEK 293T (Human embryonic kidney cells expressing the SV40 large T-antigen)	Human	ATCC (Manassas, USA) #CRL_1573
COS-7 (African Green Monkey SV40-transformed kidney fibroblast)	Monkey	Stratagene (La Jolla, USA)

3.1.10 Antibodies

3.1.10.1 Primary antibodies for Western blot and immunostaining

Name	Species	Dilution		Source/Reference
		WB	ICC/IHC	
B1	Mouse	1:1000	1:1000	PROGEN (Heidelberg, Germany)
myc	Rabbit	1:1000	1:1000	Santa Cruz Biotechnology (Heidelberg, Germany)
GlyR (mAb4a)	Mouse		1:250	Synaptic Systems (Göttingen, Germany)(Pfeiffer et al., 1984)
Gephyrin	Mouse		1:400	Synaptic Systems (Göttingen,

(mAb7)				Germany)(Pfeiffer et al., 1984)
SdpI	Rabbit	1:1000	1:500	Synaptic Systems (Göttingen, Germany)
anti-calnexin	Mouse		1:1000	BD Biosciences (Heidelberg, Germany)
Anti-His_6	Mouse	1:2000		Novagen (Darmstadt, Germany)
Anti-GST	Goat	1:5000		GE Healthcare (Freiburg, Germany)
Anti-Nbea	Rabbit		1:250	Generated by Dr. M. Kilimann group (Wang et. al, 2000)
Anti-PSD-95	Mouse		1:200	Affinity bioreagents (CO, USA)
Anti-SdpI	Rabbit	1:1000	1:1000	Generation in Magdeburg by Dr. B. Qualmann group (Qualmann et. al. 1999)
Gephyrin	Mouse	1:1000		BD Biosciences (Heidelberg, Germany)
Anti-VIAAT	Rabbit		1:4000	Synaptic Systems (Göttingen, Germany)
Anti-VIAAT	Mouse		1:1000	Synaptic Systems (Göttingen, Germany)
Anti-Vps35	Rabbit	1:1000	1:1000	Generated in this work
GFP	Rabbit	1:1000		Clontech (Heidelberg, Germany)
TGN38	Mouse	1:250		BD Biosciences (Heidelberg, Germany)
Anti-GAD67	Mouse		1:2500	Chemicon international (CA,USA)
Anti-$GABA_AR\gamma2$	Guinea pig		1:2000	Generated by Dr. J.M. Fritschy (Fritschy and Mohler, 1995)

3.1.10.2 Fluorescent secondary antibodies for immunostaining

Name	Dilution	Source/Reference
Alexa 488-anti-mouse	1:1000	Molecular Probes (Eugene, USA)
Alexa 546-anti-mouse	1:1000	Molecular Probes (Eugene, USA)
Alexa 488-anti-rabbit	1:1000	Molecular Probes (Eugene, USA)
Alexa 546-anti-rabbit	1:1000	Molecular Probes (Eugene, USA)
Alexa 635-anti-rabbit	1:500	Molecular Probes (Eugene, USA)
Alexa 635-anti-mouse	1:500	Molecular Probes (Eugene, USA)
Alexa 546-anti-guinea-pig	1:1000	Molecular Probes (Eugene, USA)

3.1.10.3 Peroxidase-linked secondary antibodies for Western blot

Name	Dilution	Source/Reference
HRP-anti-mouse	1:5000	Promega (Madison, USA)
HRP-anti-rabbit	1:5000	Promega (Madison, USA)
HRP-anti-goat	1:5000	Promega (Madison, USA)
HRP-anti-mouse	1:10000	Sigma (Saint Louis,Missouri, USA)
HRP-anti-rabbit	1:30000	Cell signalling Technology (Frankfurt, Germnay)

HRP-anti-goat	1:10000	Dianova (Hamburg, Germany)

3.1.11 Solutions and media

3.1.11.1 Antibiotics

Antibiotic	Stock solution	Final concentration
Ampicilline	100 mg/ml	100 µg/ml
Kanamycine	50 mg/ml	50 µg/ml
Spectinomycine	10 mg/ml	50 µg/ml
Tetracycline	10 mg/ml	10 µg/ml

3.1.11.2 Solutions and media for cell biology

Name	Composition
BBS, 2X	50 mM N,N-bis(2-hydroxyethyl)-2-aminoethanesulfonic acid (BES), 280 mM NaCl, 1.5 mM Na_2HPO_4, pH 6.95
Culture medium for COS-7 cells	10% (v/v) FCS, 50 U/ml penicillin, 50 µg/ml streptomycin, 2 mM L-glutamine in DMEM (Invitrogen, Kalsruhe)
Culture medium for HEK 293T cells	10% (v/v) FCS, 50 U/ml penicillin, 50 µg/ml streptomycin, 2 mM L-glutamine in MEM (Invitrogen, Kalsruhe)
Hybridoma freezing medium	10% (v/v) dimethylsulfoxide (DMSO) in culture medium
Digestion solution for primary culture	10 µg/ml DNase, 0.5 mg/ml papain, 10 mM glucose in PBS, pH 7.5
Neurobasal medium for primary culture	2% (v/v) B27 supplements (Invitrogen, Kalsruhe), 25 µg/ml sodium pyruvate, 50 U/ml penicillin, 50 µg/ml streptomycin, 2 mM L-glutamine in Neurobasal medium (Invitrogen, Kalsruhe)
Preparation medium for primary cultures	10% (v/v) FCS, 23 mM sodium pyruvate, 50 U/ml penicillin, 50 µg/ml, streptomycin, 2 mM L-glutamine in DMEM

3.1.11.3 Solutions for immunostaining

Name	Composition
Blocking solution	10% (v/v) goat serum in PBS, pH 7.5
Fixative solution	10% (w/v) PFA in PBS, pH 7.5
Permeabilization solution for immunocytochemistry	0.5% (v/v) IgePal, 4% (v/v) goat serum in PBS, pH 7.5
Permeabilization solution for immunohistochemistry	0.5% (v/v) Triton X-100, 4% (v/v) goat serum in PBS, pH 7.5

Quenching solution	25 mM glycine in PBS, pH 7.5
Na-Citrate buffer for immunohistochemistry	10 mM sodium citrate, 0.05% (v/v) Tween 20, pH 8.0

3.1.11.4 Solutions and media for molecular biology

Name	Composition
LB medium	1% (w/v) pepton 140, 0.5% (w/v) yeast extract, 1% (w/v) NaCl, pH 7.4
LB-Agar	LB medium with 1.8% (w/v) agar
Lysis buffer for mouse tails	50 mM Tris, 100 mM EDTA, 100 mM NaCl, 1% (w/v) SDS, pH 8.0
TE buffer	10 mM Tris pH 8.0, 1mM EDTA
DNA-Gel loading buffer 10X	30% (v/v) glycerol, 0.25% (w/v) xylene cyanol FF, 0.25% (w/v) bromphenol blue in TE buffer, pH 8.0
TAE electrophoresis buffer 1X	2 mM $Na_2EDTA \cdot 2H_2O$, 40 mM Tris-acetate, pH 8.5
Medium A for production of chemocompetent cells	10 mM $MgSO_4$, 0.2% (w/v) glucose in LB medium, pH 7.0
Medium B for generation of chemocompetent cells	36% (v/v) glycerol, 12% (w/v) PEG (MW 7500), 12 mM $MgSO_4$, in LB medium, pH 7.0
NZY* Broth medium	1% (w/v) NZ amine, 0.5% (w/v) yeast extract, 0.5% (w/v) NaCl, 12.5 mM $MgCl_2$, 12.5 mM $MgSO_4$, 20 mM glucose, pH 7.5

3.1.11.5 Solutions for protein biochemistry

Name	Composition
Blocking solution (Western blot with monoclonal antibodies)	1% (w/v) milk powder in TBS (see below)
Blocking solution (Western blot with polyclonal antibodies)	5% (w/v) milk powder in TBS (see below)
Coomassie-staining solution	0.1% (w/v) Coomassie G (Serva), 50% (v/v) methanol, 10% (v/v) acetic acid
Coomassie-destaining solution	7% (v/v) methanol, 7% (v/v) acetic acid
Dnak removal buffer	2 mM ATP, 10 mM $MgSO_4$, 50 mM Tris-Cl pH 7.4
Elution buffer for Ni-NTA beads	300 mM NaCl, 250 mM imidazol, 50 mM Tris pH 8.0
Fixative enhancer solution (Silver staining)	50% (v/v) methanol, 10% (v/v) acetic acid, 10% (v/v) fixative enhancer concentrate (Bio-Rad) and 30% H_2O
Im-Ac buffer	20 mM Hepes, 100 mM KCl, 5 mM EGTA, 5 mM $MgCl_2$, 0.5% (v/v) Trition X-100, 1 CEFPICT in 50 ml H_2O, pH 7.2
Lysis buffer for bacteria (GST	1 Complete EDTA free protease inhibitor cocktail

fusion proteins)	(CEFPICT) tablet in 50 ml PBS, pH 7.5
Lysis buffer for Bacteria (His_6-Fusion proteins)	500 mM NaCl, 50 mM Tris-Cl, 5 mM β-mercaptoethanol, 20 mM imidazol, 1 CEFPICT in 50 ml H_2O, pH 7.4
HEK 293T cell homogenate buffer	100 mM NaCl, 25 mM Tris-Cl, 1 CEFPICT in 50 ml H_2O, pH 7.4
Homogenate buffer (rAAV purification)	150 mM NaCl, 50 mM Tris-Cl pH 8.0
PBS 1X	137 mM NaCl, 2.7 mM KCl, 4.3 mM $Na_2HPO_4 \cdot 7H_2O$, 1.4 mM KH_2PO_4, pH 7.5
PBS-MK	1 mM $MgCl_2$, 2.5 mM KCl, in 1X PBS pH 7.5
PBS-T	1% (v/v) Tween 20 in PBS pH 7.5
Ponceau-staining solution	3% (w/v) TCA, 2% (w/v) Ponceau S
Protein sample buffer (GST pulldown)	192 μM glycine, 0.1% (w/v) SDS, 25 mM Tris-Cl pH 7.5
SDS loading buffer 6X	36% (w/v) glycerol, 0.012 % (w/v) bromphenolblue, 6% (v/v) β-mercaptoethanol, 10% (w/v) SDS, 350 mM Tris-Cl pH 6.8
SDS Stacking buffer (3, 4 or 5%)	3,4 or 5% (v/v) acrylamide, 0.1 % (w/v) SDS, 130 mM Tris-Cl pH 6.8
SDS Resolving buffer (8, 10 or 12%)	8,10 or 12% (v/v) acrylamide, 0.1% (w/v) SDS, 390 mM Tris pH 8.8
10X SDS-PAGE running buffer	2 M glycine, 1% (w/v) SDS, 0.25 M Tris pH 8.3
TBS	150 mM NaCl, 10 mM Tris-Cl pH 7.5
TBS-T	0.1 % (v/v) Tween 20 in TBS pH 7.5
TBS-TT	50 mM NaCl, 0.2% (v/v) Triton X-100, 0.05% (v/v) Tween 20, 20 mM Tris-Cl pH 7.5
Transfer buffer for Western Blot	10% (v/v) methanol in 1X SDS-PAGE running buffer
Washing buffer for GST pulldown	0.5% (v/v) Triton X-100 in PBS pH 7.5
Washing buffer for His_6-proteins	500 mM NaCl, 5 mM β-mercaptoethanol, 20 mM imidazol, 50 mM Tris-Cl pH 7.4
Washing buffer for Affi-Gel matrix	500 mM NaCl, 10 mM Tris-Cl pH 7.5

3.1.12 Vectors

Name	Source/Reference
pBK-CMV	Stratagene (La Jolla, CA, USA)
pBluescriptSK+	Stratagene (Heidelberg, Germany)
pEGFP-C3	Clontech (Heidelberg, Germany)
pGEX-4T-1	GE Healthcare Biosciences (Freiburg, Germany)
pGEX-5x-1,2,3	GE Healthcare Biosciences (Freiburg, Germany)
pGEX-RB	Optimized pGEX vector (Brundiers et al. 1999)
pET-15b	Novagen (Darmstadt, Germany)

pQE-30	Stratagene (La Jolla, CA, USA)
pAAV-6P-SEWB	Sebastian Kügler (Göttingen, Germany)
pAAV_6P_noTB_attR_WB	Sebastian Kügler (Göttingen, Germany)
pDP1 and pDP2	Jürgen Kleinschmidt (Heidelberg, Germany)

3.1.13 Plasmid constructs

Name	Insert	Receiving vector	Restriction sites	Source/Reference
Myc-SdpI-pRK5	-	-	-	Kessels *et al*., 2006
SdpII-l-pCMV-Tag3B	-	-	-	Kessels *et al*., 2006
SdpII-s-pCMV-Tag3B	-	-	-	Kessels *et al*., 2006
Myc-SdpI-6P-SEWB	Myc-SdpI	6P-SEWB	NheI-HindIII	In this work
Myc-SdpI-siR-6P-SEWB	Myc-SdpI-siR	6P-SEWB	NheI-HindIII	In this work
SdpI$_{SH3\text{-}P434L}$-pBluescriptSK+	SdpI$_{SH3\text{-}P434L}$	pBluescript SK+	BamHI-EcoRI	by Dr. Paarmann
SdpI$_{SH3}$-pGEX-4T-1	SdpI$_{SH3}$	pGEX-4T-1	Sty-EcoRI	by Dr. Paarmann
SdpI$_{SH3}$-pBluescriptSK+	SdpI$_{SH3}$	pBluescript SK+	BamHI-EcoRI	In this work
SdpI$_{\Delta SH3}$-pRSETA	SdpI$_{\Delta SH3}$	pRSETA	BamHI-EcoRI	by Dr. Paarmann
SdpI$_{P434L}$-pRSETA	Sdp$_{P434L}$	pRSETA	BamHI-EcoRI	by Dr. Paarmann
SdpII-l-pRSETA	SyndapinII-l	pRSETA	BamHI-EcoRI	by Dr. Paarmann
SdpII-s-pRSETA	SyndapinII-s	pRSETA	BamHI-EcoRI	by Dr. Paarmann
GlyRβ$_{378\text{-}426}$-pGEX-5x-1	-	-	-	Meyer G. et al. 1995
GlyRβ-GFP-pRK5				Maas et al. 2006
GlyRβ-mRFP-pRK5	mRFP	GlyRβ-pRK5	BglII	In this work
GlyRβ$_{\Delta UTR}$-mRFP-pRK5	mRFP	GlyRβ-pRK5	BglII	In this work
GlyRβ$_{KKAA}$-mRFP1-pRK5	GlyRβ$_{KKAA}$	pRK5	EcoRI-HindIII	by Dr. Schmitt
GlyRβ$_{PPAA}$-mRFP1-pRK5	GlyRβ$_{PPAA}$	pRK5	EcoRI-HindIII	by Dr. Schmitt
DSRed2-C1	-	-	-	Clontech (Germany)
GE45-pRSET	-	-	-	Sola et al. 2004
Gephyrin-peGFP-C2	-	-	-	Fuhmann et al. 2002
Gephyrin-pmRFP1	-	-	-	Maas et al. 2006
Gephyrin-pGEX-5x-1	-	-	-	Fuhmann et al. 2002
pEGFP-N1/CbII	-	-	-	by Dr. Papadopolous
CollybistinII$_{2\text{-}240}$-pRSETA	CollybistinII$_{2\text{-}240}$	pRSETA	NheI-HindIII	by Dr. Paarmann
Myc-Dlc1-pcDNA3	-	-	-	Fuhmann et al. 2002
NbeaA-peGFP-N1	-	-	-	Dr. Kilimann

				(Uppsala)
NbeaBCD-peGFP-C1	-	-	-	Dr. Kilimann (Uppsala)
NbeaEFG-peGFP-C1	-	-	-	Dr. Kilimann (Uppsala)
Vps29-pGEX-RB	Vps29	pGEX-RB	NdeI - BamHI	In this work
Vps29-pCMV-SPORT6	-	-	-	RZPD
Vps35-pBluescriptSK+	Vps35	pBluescript SK+	XhoI - BamHI	In this work
Vps35-pCMV-SPORT6	-	-	-	RZPD
Vps35-peGFP-C3	Vps35	peGFP-C3	NdeI - BamHI	In this work
Vps35-pET-15b	Vps35	pET-15b	NdeI - BamHI	In this work
Vps35-pGEX-RB	Vps35	pGEX-RB	XhoI - BamHI	In this work

RZPD: Deutsches Ressourcenzentrum für Genomforschung GmbH.

3.2 MOLECULAR BIOLOGY METHODS

3.2.1 Alcohol precipitation of nucleic acids

Two volumes of ice-cold 100% ethanol were added to the DNA solution mix that was left on ice for 15 min. The sample mix was then centrifuged for 15 min at 13.000 rpm in a table centrifuge at room temperature (RT). The DNA pellet was washed with 70% (v/v) ethanol at RT, centrifuged again for 5 min, air-dried in a vacuum centrifuge for 5 to 10 min and resuspended in water.

3.2.2 Isolation and purification of plasmid DNA from *E. coli* XL1-Blue

DNA plasmid extractions were performed using QIAGEN (Hilden, Germany) plasmid purification kits according to the manufacturer's protocol. The procedure is based on alkaline lysis of the bacterial cell wall (Barber et al., 1971) and consists of removal of the cell debris while keeping the supernatant containing the nucleic acids, followed by the degradation of RNA by RNase and binding of plasmid DNA to a silica-gel matrix. Washing with medium-salt solution removes RNA, proteins and low-molecular-weight impurities, and then DNA is eluted in a high-salt buffer.

3.2.2.1 Small scale plasmid purification

5 ml LB medium containing the appropriate antibiotic was inoculated with transformed *E. coli* XL1-Blue and incubated overnight at 37ºC and 250 rpm. Cells were then pelleted at 5000 x g for 15 min, and plasmid purification was performed by using the *QIAGEN Plasmid Mini-kit* (QIAGEN, Hilden, Germany) following the manufacturer's instructions. DNA was resuspended in 50 μl dH_2O and stored at -20ºC.

3.2.2.2 Large scale plasmid purification

Bacteria were grown and harvested as cited above (3.2.2.1) but with 100 or 250 ml medium. Plasmid purification was performed by using the *QIAGEN Plasmid Midi-kit* or *HiSpeed Plasmid Maxi-kit* (QIAGEN, Hilden, Germany) following the manufacturer's instructions. In the case of plasmid Midi-preparation, 1/5 volume of 10 M ammonium acetate (pH 5.0-5.2) was added to the DNA solution to equalize ion concentrations and an alcohol-precipitation was performed (see 3.2.1). DNA was resuspended in water to a final concentration of 1 *µ*g/*µ*l and stored at -20ºC.

3.2.3 Determination of DNA concentration by spectrophotometry

The concentration of a DNA solution was analyzed using a spectrophotometer Nanodrop ND-100 (Thermo Fisher Scientific, Waltham, USA) following the manufacturer's instructions. The concentration of DNA plasmids was determined at 260 nm and adjusted to 1*µ*g/*µ*l (1 $OD_{260\ nm}$ = 50 *µ*g/*µ*l for double stranded DNA). In addition, the 260 nm/280 nm ratio was measured to check protein contamination in the sample. This ratio should fall within a range of 1.7 to 1.8. If the ratio is larger than 1.8, it indicates RNA contamination.

3.2.4 DNA sequencing

The sequencing, separation and detection of DNA products were performed by MWG Biotech Inc. (Ebersberg, Germany). Reactions were performed with a non-radioactive dideoxy chain termination / cycle sequencing method (Sanger *et al.*, 1977).

3.2.5 Polymerase chain reaction (PCR)

PCR, *in vitro* DNA amplification, invented by Kary B. Mulliscan is a technique to exponentially amplify *in vitro* a small quantity of a specific nucleotide sequence. This amplification is performed in the presence of template sequence, two oligonucleotide primers that hybridize to opposite strands and flank the region of interest in the target DNA, a thermostable DNA polymerase and a mixture containing the four desoxyribonucleotide triphosphates (dNTP). The reaction is cycled involving template denaturation, primer annealing, and the extension of the annealed primers by DNA polymerase. The annealing temperature is set depending on the melting temperature (Tm) of the primers, 5°C below the lowest melting temperature of the primers to be used. The melting temperature (Tm) is calculated on the basis of base composition following the simple rule: Tm = 4 x (#C + #G) + 2 x (#A + #T). The length of the amplified fragment and the elongation kinetics of chosen polymerase (1 kb per min for the DNA polymerases used in this thesis) determine the

elongation duration.

Preparative PCR reaction:

Component	Amount
Template DNA	500 ng
Sense primer (100 pmol/µl)	0.5 µl
Antisense primer (100 pmol/µl)	0.5 µl
dNTP mix (2.5 mM each)	2.5 µl
DNA polymerase	0.5 µl
ThermoPol Reaction Buffer (10 X)	5 µl
H_2O	Add up to 50 µl

Criteria for choice of DNA polymerase:

- Deep Vent: 3' to 5' proofreading exonuclease activity, high fidelity, used for preparative PCR.
- Taq: high yield, no proofreading activity, used for analytical PCR.

Program for preparative PCR:

Phase	Temperature	Time	Cycles
Initial denaturating	95ºC	5 min	1
Denaturing	95ºC	30 sec	20
Annealing	50ºC	30 sec	
Elongation	72ºC	1min/kb DNA	
Final elongation	72ºC	3 min	1

PCR products were purified by agarose gel electrophoresis (see 3.2.6.3) and eluted (see 3.2.6.4), further elongated with other PCR products and then cloned into the desired vector. For elongation with other PCR products, the PCR reaction was performed as detailed above, but the reaction contained both purified amplicons, the sense primer of the amplicon to be elongated upstream and the antisense primer of the amplicon to be elongated downstream.

3.2.6 Cloning procedures

Primer design and all major cloning steps were first simulated using MacVector 8.0 software (Accelrys Inc. Sand Diego, USA). Restriction sites necessary for cloning of the DNA fragments into respective plasmids, as well as epitope sequences were introduced in the cDNAs by PCR

using the corresponding primers. All basic cloning procedures were essentially performed according to the protocols described in *Molecular Cloning Laboratory Manual*, 3rd edition (Sambrook, J. et al., 1989).

3.2.6.1 Site-directed mutagenesis

In order to introduce desired point mutations in a DNA sequence, site-directed mutagenesis was employed using the PCR technique. For this purpose, 3´ and 5´primers containing a different base in the center of the primer sequence were designed with at least 10-15 bases at both the 5'- and 3'- ends of the primer with 100% sequence complementarity. Primer length was about 30 bp, with a G+C content of about 50%, and was adjusted depending on the G+C content, melting temperature (as in 3.2.5) or web-based prediction (Promega). Mutagenic oligonucleotides incorporate at least one base change, but can be designed also to generate multiple substitutions, insertions or deletions. When using such primers in a PCR reaction, the amplicon will contain the desired point mutation.

3.2.6.2 DNA restriction by endonucleases

For the sequence-specific digestion of doubled stranded DNA, restriction enzymes and the corresponding buffer from the companies Roche (Mannheim, Germany) or NEB (Ipswich, USA) were employed. Buffers and temperatures for the reaction were chosen according to manufacturer's instructions. Per 1 µg of DNA, 2-5 U of restriction enzyme were used. Since high concentrations of glycerol inhibit enzyme activity, all glycerol-containing enzyme suspensions were diluted at least 10 times. DNA digestion with two different restriction enzymes was performed simultaneously whenever possible. Otherwise, when serial DNA restriction was required, the DNA was precipitated after the first digestion with Sureclean (Bioline GmbH, Luckenwalde, Germany) following the manufacturer´s instructions. Incubations were carried out according to conditions suitable for the corresponding enzyme: 37°C during 4-6 h for PCR cloning, 2 h for non-PCR cloning or 30 min for electrophoretic analysis.

Standard reaction mix:

Component	Amount (for analysis)	Amount (for cloning)
Plasmid DNA	0.5 µg	5 µg
Buffer 10 X	1 µl	2 µl
BSA 10 X	1 µl	2 µl
Enzyme 1 (10 U/µl)	0.5 µl	1 µl
Enzyme 2 (10 U/µl)	0.5 µl	1 µl
H_2O	Add up to 10 µl	Add up to 20 µl

3.2.6.3 Separation of oligonucleotides by agarose gel electrophoresis

A horizontal agarose gel electrophoresis system was used for the separation of double- stranded DNA in both analytical and preparative studies (plasmids solutions, PCR products). Depending on the expected sizes of the DNA fragments, gels with different concentrations of agarose (0.5-2% (w/v); Biozym, Hess. Oldendorf) in TAE buffer were prepared. DNA samples were mixed with 1/10 of loading buffer 10X, loaded onto the gel in parallel with 10 μl of DNA *SmartLadder* marker (Eurogentec, Cologne, Germany) and run in TAE buffer for 30 min at 120 V. For the detection and visualization of DNA by UV illumination (254 nm), gels were stained with 1μg/ml ethidium bromide solution. Images were taken using the Gel Documentation 2000 System (Bio-Rad, Hercules, USA).

3.2.6.4 Isolation of DNA fragments from agarose gels

To isolate DNA fragments from a sample after restriction digestion or PCR amplification, the samples were subjected to gel electrophoresis (see 3.2.6.3). Under 302 nm illumination, fragments of desired size were cut out of the gel using a sterile scalpel and placed in 1.5 ml micro-centrifuge tubes. DNA was purified with the *QIAquick Gel Extraction Kit* (QIAGEN, Germany) based on the principle of spin-column technology which exploits the selective binding properties of a silica-gel membrane. The purified samples were vacuum-dried and resuspended in 10 μl H_20.

3.2.6.5 Dephosphorylation of DNA ends

In order to avoid re-ligation of a linearized vector, the free ends of the vector were dephosphorylated after restriction digestion. 3 U of calf intestinal alkaline phosphatase were added to the restriction reaction per 1 μg of DNA and incubated at 37ºC for 60 min. The reaction was stopped by incubation at 56ºC for 10 min, and the product was analysed and purified by gel electrophoresis (see 3.2.6.3).

3.2.6.6 Ligation of DNA fragments

To generate new constructs by sticky end ligation of a DNA-insert into a dephosphorylated vector, gel-purified fragments were quantified on agarose gels by comparing their staining intensity with weight marker bands of the standard *SmartLadder*. Fragments were used for the ligation reaction according to the following standard protocol:

Component	Amount
Vector fragment	50 ng

Insert fragment	x
T4 DNA ligase (1U/µl)	0.5 µl
Quick Ligation Buffer (2 X)	5 µl
10 mM ATP	0.5 µl
H_2O	Add up to 10 µl

x : calculated amount for vector: insert molar ratio, generally 1:3

As a negative control, the same reaction was run in the absence of insert. Ligation reactions were performed at 25ºC for 30 min.

3.2.6.7 Direct purification of PCR products

After amplification by PCR, DNA fragments were isolated from the reaction mixture via reversible binding to a silica matrix using the *QIAquick PCR Purification Kit* (QIAGEN, Hilden, Germany) and following the manufacturer's instructions.

3.2.6.8 Transformation of chemo-competent cells

A frozen 50-100 µl aliquot of chemo-competent *E. coli* was thawed on ice for 5 min. To the bacterial solution, 5-10 µl of the ligation reaction or 10-100 ng of plasmid DNA was added. The mixture was stirred and incubated on ice for 30 min. The cells were then subjected to a heat-shock pulse at 42ºC for 20 seconds for *E. coli* BL21 cells and 30 seconds for other *E. coli* strains, then chilled on ice for 1-2 min and diluted in SOC medium for the transformation of *E. coli* Turbo cells (NEB, Ipswich, USA), and into LB for other *E. coli* strains. *E. coli* Turbo cells were directly plated on agar plates. Other *E. coli* strains were incubated at 37ºC under rotation for 60 min to allow bacterial growth. The bacterial suspension was then pelleted in a table centrifuge at 400 x g for 10 min. The bacterial pellet was resuspended in 200 µl LB medium to spread the bacteria on agar plates containing the appropriate antibiotic concentration. Plates were incubated overnight at 37ºC.

3.2.6.9 Transformation of electro-competent cells

A frozen aliquot of electro-competent *E. coli* XL1-Blue bacteria was thawed on ice for 5 min and kept on ice. The DNA ligation product (3 - 5 ng DNA) or 100 ng of plasmid-DNA were then added to 50 µl of the electro-competent *E. coli* cells. The mixture was transferred to a cuvette prechilled on ice, and subjected to electroporation with a Gene Pulser II (Bio-Rad, Munich, Germany) at a voltage of 2.5 kV, a pulse controller- low resistance of 200 Ω, and a capacitance of 25 µF. Immediately after the pulse, 1 ml of LB medium was added to the cells, and the bacterial suspension was transferred to a sterile tube. The transformed *E. coli* were incubated for 40 min under shaking at 37ºC, and spread on agar plates containing the appropriate antibiotic

concentration for clone selection. Plates were incubated overnight at 37ºC.

3.2.7 Preparation of glycerol stocks

For long-term storage of transformed XL1-Blue or Turbo *E. coli*, 800 µl of grown bacterial culture were added to 200 µl of autoclaved glycerol under sterile conditions. After vortexing, the cells were mixed and stored at -80°C.

3.2.8 Preparation of chemo-competent bacterial cells

Chemo-competent bacteria were prepared according to the method of Nishimura et al. (1990). *E. coli* XL1-Blue cells were spread on agar-plates containing 10 µg/ml tetracycline and incubated overnight at 37ºC. A single colony was inoculated in a pre-culture of 10 ml LB medium, which was incubated overnight at 37ºC. A culture of 50 ml of medium A (see 3.1.11.4) was inoculated with 0.5 ml of the overnight grown pre-culture and incubated at 37ºC until the mid logarithmic phase ($OD_{600\ nm}$ = 0.3-0.5). The presence of 10 mM Mg^{2+} in the medium stimulates transformation efficiency, and the increased growth rate due to the extra carbon source glucose enhances transformation efficiency. The cells were then kept on ice for 10 min, pelleted at 1500 x g for 10 min at 4° C, resuspended gently in 0.5 ml of ice-cooled medium A, and then 2.5 ml of ice-cooled storage solution, medium B, sterilized by filtration (see 3.1.10.4), was added and mixed well without vortexing. The resulting competent cells were divided in aliquots of 0.1 ml each in Eppendorf tubes, rapidly frozen in liquid nitrogen and stored at –80°C until use for up to 6 months.

3.2.9 Genotyping of SdpI -/- mice

The SdpI -/- mouse line was generated during the thesis project of Dr. D. Koch in Jena (Germany) and at our disposal on a collaborative basis.

3.2.9.1 Extraction of genomic DNA from mouse tail tissue

Approximately 5 mm of tail tissue from newborn mice were digested overnight in a solution containing 500 µl of lysis buffer (see 3.1.11.4) and 3.2 µl of Proteinase K at 55ºC under 1400 rpm shaking. Then the tubes were vortexed briefly and centrifuged at 13000 rpm for 5 min in a table centrifuge. 450 µl of the supernatant were transferred to a new tube, and 500 µl of 2-propanol added. Tubes were shaken and centrifuged again for 10 min at 13000 rpm to precipitate genomic DNA. The resulting pellets were washed with 250 µl of 70% (v/v) ethanol,

dried in vacuum centrifuge for 5 min and resuspended in 100 µl of TE buffer (see 3.1.11.4).

3.2.9.2 Rapid extraction of genomic DNA from embryonic tissue

During the preparation of KO and WT spinal cord cultures, fast genotyping of embryonic tissue was required. For this, the *REDExtract-N-AmpTissue PCR-Kit* (Sigma, USA) was used following the manufacturer's instructions. For the analysis of mouse tails, two different PCR reactions were performed: one WT-lox PCR (IP77 forward primer and IP78 reverse primer) to detect the WT allele and one KO-lox PCR (IP79 forward primer and IP80 reverse primer) to identify the KO allele.

The following components were included in each PCR-reaction mixture (25 µl total volume):

Component	Amount
NH_4^+ reaction buffer + 1.5 mM $MgCl_2$	3.25 µl
dNTP mix (10 mM each)	0.5 µl
PANScript (5 U/µl)	0.125 µl
Primer mix (5 µM each)	5.0 µl
Tail DNA	0.5 µl
H_2O	15.625 µl

Both the WT and KO PCR reactions were performed with the following amplification program:

Phase	Temperature	Time	Cycles
Initial denaturating	95ºC	5 min	1
Denaturing	95ºC	30 sec	35
Annealing and elongation	60ºC	30 sec	
Final elongation	72ºC	3 min	1

To the PCR samples, 1/10 volume of 10 X DNA-loading buffer was added. 20 µl of each DNA sample were loaded onto an agarose gel and analyzed by gel electrophoresis (see 3.2.6.3). Expected sizes of amplified DNA fragments were 355 bp for WT and 227 bp for KO, respectively.

3.3 PROTEIN BIOCHEMISTRY METHODS

3.3.1 Colorimetric determination of protein concentration

For determining protein contents, the *DC Protein Assay Kit* from Bio-Rad (Munich, Germany) was used. Assays were performed following the manufacturer's instructions in 96-well plates. For each protein sample, three replicates of sample solution and protein standard (BSA) solution were analyzed. Absorption at 750 nm was measured using a *Fluostar Galaxy* spectrophotometer (BMG Labtech, Offenburg, Germany).

3.3.2 Discontinuous Polyacrylamide Gel Electrophoresis (PAGE)

In a discontinuous PAGE system (Laemmli, 1970), protein complexes migrating through a stacking gel of low density (3-5% polyacrylamide) are concentrated in a very thin zone on the surface of a resolving gel. By migrating through the resolving gel of higher density (8-12% polyacrylamide), proteins are then separated according to their molecular mass. Before proteins are loaded into this discontinuous pH-gel system, they are dissociated by heating the samples in the presence of the strong anionic detergent such as sodium dodecyl sulfate (SDS) in combination of a reducing agent β-mercaptoethanol or dithiothreitol (DTT). The denatured polypeptides bind SDS and become negatively charged. Because the amount of SDS bound is almost always proportional to the molecular weight and largely independent of the aa sequence, the migration of polypeptides through the SDS-gel is solely determined by their size.
Here, the polymerized gel was mounted in a vertical mini-electrophoresis chamber (MiniProtean 3, Bio-Rad; Munich, Germany), and reservoirs were filled with 1X SDS-PAGE running buffer. Before loading, 1/6 volume of SDS loading buffer was added to the protein samples, which were then heated at either 48ºC for the analysis of membrane proteins, or at 95ºC for the analysis of soluble proteins, for 10 min. The electrophoresis was carried out at 25 mA per gel, until the bromphenol blue dye in the sample buffer had reached the bottom of the gel. Protein bands were either visualized by Coomassie staining (see 3.3.3), or silver staining (see 3.3.4), or were transferred to a membrane by Western blotting for immunodetection (see 3.3.5).

3.3.3 Coomassie staining of protein gels

Proteins separated by SDS-PAGE were simultaneously fixed and stained with Coomassie

staining solution (Wilson, 1983). Coomassie Brilliant Blue R/G 250 is a triphenylmethane dye that binds nonspecifically to proteins and forms strong but not covalent complexes with positively charged aa. This method has a detection limit of 50-100 ng of protein per band.
In order to visualize proteins on gels, gels were stained by incubating with Coomassie staining solution for 10 min on a shaker at 50 rpm. The staining solution was replaced by destaining solution and kept overnight on the shaker at 50 rpm to wash away unspecifically bound dye. The gels were then inspected under bright light, and pictures were taken either with a digital camera or the gel documentation 2000 system (Bio-Rad; Munich, Germany).

3.3.4 Silver staining of protein gels

When staining a SDS polyacrylamide gel with a solution of silver nitrate, ions of silver bind to the side chains of aa and are afterwards reduced, thus giving a brown-black colour to the protein bands. This method has a detection limit lower than the Coomassie staining, of about 0.1-1 ng of protein per band. Silver staining of SDS polyacrylamide gels was performed using the Silver Stain Plus-Kit from Bio-Rad (Munich, Germany) following the manufacturer's instructions.

3.3.5 Western blot analysis

Western blotting is extremely useful for the identification and quantification of a specific protein in complex mixtures of proteins that are not radiolabeled. In this technique, electrophoretically separated protein samples (see 3.3.2) are transferred from a gel to a solid membrane support and probed with antibodies that react specifically with a particular antigenic epitope. Proteins can be detected down to femtomole quantities, well below the detection limit for most other staining methods.

3.3.5.1 Membrane transfer

Following SDS-PAGE the separated proteins were transferred to a membrane by electrotransfer using a Mini Trans-Blot electrophoretic chamber (Bio-Rad; Munich, Germany). PVDF membranes were pre-rinsed in pure methanol for 2 min and equilibrated in transfer buffer for 10 min. Nitrocellulose membranes were pre-rinsed in transfer buffer for 2 min. Subsequently, membranes were stapled at the cathode side of the transfer-cassette in the following order: Whatman paper, protein gel, nitrocellulose membrane/ PVDF filter and again Whatman paper. The transfer was carried out in transfer buffer (see 3.1.11.5) at 10 V overnight, or at 100 V for 1h 30 min, on ice. After transfer, membranes were taken out and processed for immune detection

with specific antibodies.

3.3.5.2 Immune detection with specific antibodies

The specific identification of protein bands was done by indirect immune detection. To avoid unspecific binding of the primary antibody, the membrane was incubated with blocking solution (see 3.1.11.5) for at least 45 min at RT under shaking. The membrane was then incubated, depending of the primary antibody to be used, overnight at 4ºC, or for 1 h 30 min at 25ºC, with blocking solution containing a proper dilution of the primary antibody. Subsequently, the membrane was washed twice with TBS-TT/TBS-T for 10 min to remove unbound primary antibody, and once with TBS for 10 min to remove detergent. Then the membrane was incubated with blocking solution containing a dilution of secondary antibody conjugated to HRP for 1 h at (RT). After washing at least four times for 10 min with TBS-TT, visualization of the protein bands was performed by chemiluminecence. The membrane was incubated with *enhanced chemiluminescence* (ECL) solution (Super Signal West Pico, Perbio Science GmbH; Bonn Germany) following the manufacturer's instructions for 5 min at RT. HRP is an enzyme that catalyzes the oxidation of the luminol-based substrate, leading to an excitation of the chemiluminescent substrate that generates light at the site of reaction which is visualized through exposure to an X-ray film. The membrane was exposed to X-ray films (3.1.6) for variable times. An AGFA X-OMAT 2000 processor (Kodak, Atlanta, USA) was used to develop the exposed films.

3.3.5.3 Scanning of bands

Developed films were scanned using Epson Perfection 4780 Photo (Epson, Long beach, USA). Images were obtained and optimized using Epson and Adobe Photoshop software. The images were analyzed subsequently for determining binding, expression, antibody specificity, etc. Parameters like band size or band intensity for the protein of interest were determined using the ImageJ image analysis software (NIH, USA). Each experiment was performed three times. Data are presented as means ± standard error (S.E.M.) Statistical significance was evaluated with a two tailed Student's *t*-test.

3.3.6 Expression of recombinant proteins in *E. coli* BL21

For the expression of recombinant proteins in bacteria, the desired plasmid construct was transformed by heat-shock into *E. coli* BL21 DE3 (see 3.2.6.8.). The bacteria were spread on an

agar plate with the respective antibiotic and incubated overnight at 37ºC. With a single colony, a pre-culture of 20 ml LB medium containing the proper antibiotic was inoculated and incubated overnight at 37ºC under shaking. The next day, 5 ml of the pre-culture medium were used to inoculate 200 ml LB medium containing antibiotic, which then was left shaking at 250 rpm and 37ºC. When the culture reached the exponential growth phase (OD_{600nm} between 0.7-0.9), an aliquot equivalent to 1 OD was separately stored at
-20ºC for SDS-PAGE analysis. The culture was then cooled down to 25ºC. This gives newly formed proteins more time to fold correctly and thus increases the protein yield. Protein expression was induced by the addition of IPTG (Isopropyl-β-D-thiogalactopyranoside) to a final concentration of 0.2 mM. IPTG compound is used as a molecular mimic of allolactose, a lactose metabolite that triggers transcription of the lac operon in the plasmid. The culture was left at 25ºC with shaking at 250 rpm overnight. The OD_{600} of the induced culture was measured the next day, and a culture equivalent to 1 OD_{600} was separately stored for analysis as previously described. Then, the bacterial culture was centrifuged at 5000 x g for 20 min, and the pellet was either frozen at -20ºC for further analysis or resuspended in PBS for direct use. For examining protein expression, aliquots of the culture prior to and after induction were separated by SDS-PAGE and stained with Commassie (see 3.3.3) or further analyzed by Western blotting (see 3.3.5).

3.3.7 Affinity purification of GST- and His_6- fusion proteins

In order to reduce protease activity, all steps were carried out on ice, with cold buffer and using cold centrifuges. Recombinant GST- or His_6- fusion proteins were expressed from pGEX-5x-1, pGEX-RB, pGEX-4T-1, pQE-30, pQE-32, pRSET-A or pET-15b in *E. coli* BL21 DE3 (see 3.3.6). All procedures were performed in the cold room whenever possible.

3.3.7.1 Lysis of bacteria by sonication

Bacterial pellets (see 3.3.6) were resuspended in 1 ml of lysis buffer. Lysis of the bacterial membrane was achieved by applying several sonication pulses of 1 min with a Branson Sonifier (Kyonggi-do, Korea) at an output level of 4 and with a 50% duty cycle on ice. To the sonified suspension, 20 % (v/v) Triton X-100 was added to a final concentration of 1% (v/v), and tubes were placed on an overhead shaker at 4ºC for 30 min for solubilization of membrane proteins. For the removal of cell debris, the resulting lysate was centrifuged at 10000 x g for 30 min. The supernatant was aliquoted in 100 µl aliquots, shock frozen in liquid nitrogen and stored at -70ºC.

3.3.7.2 Purification of His_6- fusion proteins

The purification of recombinant proteins tagged with six consecutive histidine residues at the N-terminus was performed using a nickel-nitrilotriacetic acid (Ni^{2+}-NTA) metal-affinity chromatography agarose matrix from Qiagen (Hilden, Germany). The Ni^{2+}-NTA/His-tag purification system is based on the high-affinity binding of 6 neighboring histidines to immobilized metal ions such as Ni^{2+}. The metal ion is bound to a sepharose matrix by NTA, which is a chelator with four sites available for interaction with metal ions and thus minimizes leaking of the metal from the solid support. Proteins containing the His_6 tag are bound to the matrix through their interaction with the Ni^{2+} cations, whereas unbound proteins are washed through. The bound His-tagged protein can then be recovered by elution with imidazole.

Per 10 ml bacterial lysate, 600 µl of Ni^{2+}-NTA agarose matrix were used. The matrix was washed first with PBS and then incubated on an overhead shaker with the bacterial lysate for 2 h at 4ºC. Afterwards, unbound proteins were washed out by washing twice with PBS, and contaminant proteins like the DnaK chaperones were removed from binding proteins by washing with 10 bead volumes of DnaK removal buffer, once under overhead rotation for 10 min at 37ºC and once shortly at 4ºC. Furthermore, the protein suspension was washed once with PBS and twice with washing buffer for His_6-tagged proteins. Elution of the bound His_6-fusion proteins from the matrix was performed in five elution steps. For each step, 70 µl of the elution buffer for Ni-NTA beads were used per 100 µl Ni-NTA agarose beads. The eluates were mixed, and reducing and toxic components like β-mercaptoethanol and imidazol were removed from the protein suspension by dialysis against the respective elution buffer lacking β-mercaptoethanol and imidazol. Dialysis was with 200-500 times the volume of the sample at 4ºC overnight, with dialysis buffer changes after 2 and 4 hours. The protein in the dialysed solution was then concentrated to 0.4-0.5 µg/ml by centrifugation using an Amicon filter, with an appropriate molecular weight cut off following the manufacturer's instructions (Millipore, Wartford, USA). Protein samples were shock-frozen in liquid nitrogen and stored at -80ºC until further use.

3.3.7.3 Purification of GST-fusion proteins by glutathione-sepharose affinity chromatography

In the GST-pulldown technique (Kaelin et al., 1991) recombinant proteins fused to glutathione-S-transferase (GST) are purified due to the high affinity binding of GST to glutathione immobilized on sepharose GSH-matrix (GE Healthcare, Freiburg). An amount of 28-35 µl GSH-matrix was washed twice with 1 ml of PBS. Then the glutathione-sepharose matrix was incubated with the bacterial lysate (see 3.3.7.1) for 2 h at 4ºC under overhead shaking. The protein-loaded matrix

was washed once with 1 ml of 0.1% (v/v) Triton X-100 in PBS, once with 1 ml DnaK removal buffer and once with 1 ml 0.1% (v/v) Triton X-100 in PBS.

3.3.8 GST pull-down assay for the analysis of protein-protein interactions

To analyze the interaction between two proteins, one of the binding partners was tagged with GST and immobilized on a GSH-matrix (see 3.3.7.3). The immobilized protein bound to the matrix was then incubated with a protein suspension, lysate from *E. coli* or detergent extract from mammalian cells, for 2 h at 4ºC on an overhead shaker to allow putative binding partners to bind to the GST protein. The incubation was performed in the presence of 1% (v/v) Triton X-100 to prevent unspecific binding. Then the matrix was washed four times with 1 ml of wash buffer; washing included centrifugation at 2000 x g for 2 min at 4ºC and removal of the supernatant. After the last washing step, the supernatant was completely removed, and bound proteins were eluted from the matrix by two incubations with 20 µl of sample buffer followed by shaking at 48ºC and 1400 rpm in a thermo-mixer and centrifugation at 2000 x g at RT. The eluates were then mixed with 7 µl of SDS loading buffer and further analyzed by SDS-PAGE (see 3.3.2) or Western blotting (see 3.3.5).

3.3.9 Co-immunoprecipitation

Solubilization of membrane proteins in the P3 fraction isolated from spinal cord homogenates was performed by the addition of 0.5% (v/v) Triton X-100 and incubation for 30 min at 4ºC under shaking. 50 µl of protein G-agarose (Roche Diagnostics, Mannheim, Germany) was washed twice with Im-Ac buffer. 600 µl of P3 lysate were pre-cleared by incubation with 50 µl of protein G-agarose for 1 h at 4ºC. After the agarose beads had been spun down at 5000 x g for 1 min, 150 µl of the pre-cleared supernatant was incubated with the corresponding antibody diluted 1:10 overnight at 4ºC under shaking. Subsequently, 1 volume of protein G-agarose slurry was washed once with Im-Ac buffer, centrifuged at 5000 x g for 1 min. The bead pellet was resuspended in one volume of Im-Ac buffer to obtain a 50% slurry. 50 µl of this bead slurry was added to the spinal cord detergent extract incubated with antibodies and re-incubated for 4 h at 4ºC. Afterwards, the agarose matrix was washed with 1 ml of Im-Ac buffer for four times. Bound proteins were eluted by the addition of 50 µl of SDS sample buffer (3.1.11.5) and analysed by SDS-PAGE (3.3.2) and Western blotting (3.3.5).

3.3.10 Production of polyclonal antibodies

The production of polyclonal antibodies against Vps35 was carried out through a collaboration with the group of Jaroslav Blahos at the Academy of Sciences of the Czech Republic. Two rabbits were immunized 5 times with purified His_6-tagged Vps35 (see 3.3.7.2) following the schedule given below:

Day	Procedure
0	1st Injection
7	2nd Injection
14	3rd Injection
21	Sera test
28	4th Injection
35	Sera test
42	5th Injection
49	Final bleed

The specificity of the resulting immunesera was analysed by Western blotting and immunocytochemistry. In western blot, immunoreactivity against the following antigens was tested: purified recombinant His_6-Vps35, detergent extract of COS-7 cells expressing eGFP-Vps35 and of untransfected COS-7 cells, and detergent extract of rat spinal cord.

3.3.11 Purification of polyclonal antibodies by antigen affinity chromatography

The previously purified His_6-tagged Vps35 (see 3.3.7.2) was immobilized onto a pre-activated Affi-Gel 15 matrix (Bio-Rad, Munich, Germany). Before coupling the antigen to the gel, the matrix was washed with three bed volumes of dH_2O at 4ºC. Then, 4ml of 0.5 mg/ml His_6-tagged Vps35 protein was added to 2 ml of matrix, which was gently agitated to get a uniform suspension. The mixture was incubated for 5 h at 4ºC on an overhead shaker. The remaining active ester groups were blocked by adding 0.1 ml of 1 M glycine, pH 8.0, per 1 ml of gel for 1 h. The gel was transferred to a glass column and intensely washed first with water, then with 10 bed volumes of 10 mM Tris-Cl, pH 7.5, and subsequently with 10 bed volumes of 100 mM glycine-HCl, pH 2.5, followed by 10 volumes of 10 mM Tris, pH 8.8, until the pH of the column effluent reached a value of 7.5. The polyclonal serum was diluted 1:10 in 10 mM Tris-Cl, pH 7.5, and passed three times through the column to ensure complete binding of the antibody. Afterwards the gel was washed with 20 bed volumes of 10 mM Tris-Cl, pH 7.5, and then with 20 bed volumes of

washing buffer. Antibodies bound to the immobilized antigen by acid-sensitive interactions were eluted by passing 10 bed volumes of 100 mM glycine-HCl, pH 2.5, through the column. The eluates were immediately neutralized by collecting them in tubes containing 1 bed volume of 1 M Tris-Cl, pH 8.0. The pH value should adjust to pH 8.0 and was rapidly checked. If needed, additional 1 M Tris-Cl buffer, pH 8.0, was added to the eluates. Then, columns were washed with 10 mM Tris-Cl, pH 8.8, until the pH reached a value of 8.8. Antibodies bound to the column by base-sensitive interactions were eluted by passing 10 bed volumes of freshly prepared 100 mM triethylamine, pH 11.5, through the column. Eluates were neutralized by collection in a tube containing 1 bed volume of 1 M Tris-Cl, pH 8.0. Subsequently, columns were washed with 10 mM Tris-Cl, pH 8.8, until the pH of the column had reached a value of 8.8. For further use, the columns were stored in 0.01 % merthiolate.

3.4 METHODS FOR VIRAL INFECTION

3.4.1 Calcium phosphate transfection for the production of recombinant adeno-associated virus (rAAV)

In the calcium phosphate transfection method (Graham and Van der Eb, 1973), a sodium phosphate solution (BES) is mixed with a calcium phosphate solution containing a DNA sample. The resulting calcium phosphate-DNA complexes adhere to the cell membrane and enter the cytoplasm by endocytosis.

The calcium phosphate transfection of HEK 293T cells was carried out in 10 cm cell culture dishes. Cells were split into 20 culture dishes one day before transfection. At the time point of the transfection cultures were approx. 50% confluent. For each dish, 10 μg of DNA mix containing 10μg pDP1, 10μg pDP2 and 5 μg of the rAAV encoding the gene of interest were mixed with 375 μl dH_2O and 125 μl 1 M calcium chloride. Rapidly 500 μl of 2 X BES buffer was added to the solution, vortexed for 5 seconds and incubated at RT for 5 min. The mixture was added to 7 ml of pre-heated MEM medium, which was then used to replace the culture medium of one dish. Cells were then incubated overnight at 37ºC and 3% CO_2. After 24 hours, the medium was replaced by fresh medium. The transfected cells were then transferred to a 5% CO_2 incubator and left for another 24 hours in culture. Subsequently, the cells were washed and resuspended with PBS and transferred to a 15 ml falcon tube. After 10 min centrifugation at 1000 x g, supernatant was removed, and the cell pellet was stored at -20ºC until further analysis.

3.4.2 Preparation of HEK 293T detergent extract for rAAV purification

Forty-eight hours after transfection, cells were harvested from the culture dishes after removing the medium by using a cell scraper. Cells from 20 dishes were resuspended in 8 ml homogenate buffer, DNAse treatment was carried out by adding 1.6 µl of Benzonase (300 U/µl) and incubation for 30 min at 37°C. Afterwards the cells were subjected to a "shock freeze" cycle in an ethanol dry-ice bath three times for approximately 10 min and afterwards in a 37°C waterbath. During these incubations, the suspension was slightly shaken every 5-10 min. Subsequently the suspension was spun for 30 min at 4000 x g. The supernatant containing the virus particles was removed from the pellet, and further purification of virus was performed as explained below (see 3.4.3).

3.4.3 rAAV purification through an iodixanol gradient

To obtain different Iodixanol (Opti Prep™ Fresenius Kabi, Norge, Axis-Shield, Oslo, Norway) gradients, solutions were intermixed as is indicated in the following table:

Gradient	54% Iodixanol (working solution)	2 M NaCl	PBS-MK	Final volume
15 %	12 ml	21.6 ml	9.6 ml	43.2 ml
25 %	20 ml	-	23.2 ml	43.2 ml
40 %	32 ml	-	11.2 ml	43.2 ml

Diluted supernatant containing the virus particles (see 3.4.2) was carefully loaded onto 25 x 89 mm centrifuge tubes (Beckmann Instruments, CA, USA) filled with a discontinuous iodixanol gradient. The gradients were composed of 6 ml of 15 %, 4 ml of 25 %, 3 ml of 40 % and 3 ml of 54 % iodixanol. The discontinous gradient was prepared with an underlayering technique in which solutions with higher density are underlayed beneath lighter ones avoiding the generation of air-bubbles. The gradients were spun for 2 h at 50000 rpm (50.1 Ti-rotor) and 18° C. The viral particles are mainly found above the 54% fraction and were collected carefully with a syringe. The viral particle solution was then further concentrated using a filter (Amicon, Millipore, Cork, Ireland) of 100 KDa molecular weight cut-off and washed 2-3 times with 10 ml 1X PBS-MK. After concentrating the solution down to roughly 200 µl, the preparation was aliquoted into 20 µl samples, shock-frozen in liquid nitrogen and kept at -70° C for long-term storage.

3.4.4 rAAV infection in primary cultures

In order to assess the number of completely assembled rAAV that can effectively carry out an

infection, i.e. infectious units per ml (i.u/ml), serial dilutions of purified virus were added to the medium of hippocampal neurons cultured (see 3.5.4) for seven days in vitro (DIV7). Neurons were fixed at DIV10 and the neuronal expression of the reporter gene, GFP, was analyzed. For the down-regulation of SdpI in spinal cord neurons, 10 μl of PBS containing equivalent i.u. of each miR-rAAV were added to spinal cord neuron cultures (see 3.5.5) at DIV6-7. For rescue experiments additional 10 μl containing equivalent i.u. of rAAV encoding the miR-resistant SdpI protein were added simultaneously to miR-rAAV infection for SdpI knockdown. Neurons were further analyzed by immunocytochemistry (see 3.5.9) or Western blotting (see 3.3.5)

3.5 CELL BIOLOGY METHODS

3.5.1 Coating of coverslips and well plates with poly-L-ornithine

To facilitate the attachment of cells on glass and plastic surfaces, sterile and ethanol-washed cover-slips placed in 24-well-plates and 6-well-plates were incubated for at least 2 h with poly-L-ornithine (15 μg/ml in PBS, pH 7.5) (Sigma, USA) at 37ºC and 5% CO_2. Before use, the coating solution was removed, and the wells were washed three times with PBS.

3.5.2 Culture and maintenance of HEK 293T and COS-7 cells

All steps were performed in a sterile hood with sterile solutions and media (MEM or DMEM). Solutions and media were pre-warmed for 30 min prior to use in a water-bath at 37ºC. Twice per week, cells at a confluence of approx. 70-90% were split. For splitting, cells were washed with 4 ml PBS. The adherent cells were harvested by incubation with 1 ml of preheated 0.25 % trypsin-EDTA (Gibco, Invitrogen, Kalsruhe, Germany) for 1 min. Then, cells were resuspended in 5 ml of PBS and 1ml aliquot of the resuspended cells was plated in new 10 cm dishes containing 10 ml of the respective culture medium. Cells were cultured at 37ºC and 5% CO_2. After 30 rounds of splitting, a new batch of each cell line was thawed.

3.5.3 Freezing and thawing of cell lines

Cells growing in a 10 cm dish with a confluence of approx. 80-90% were washed once with PBS, pH 7.5, incubated for 1 min with 1 ml of 0.25 (v/v) % Trypsin-EDTA (Gibco, Invitrogen, Kalsruhe, Germany). Cells were centrifuged at 100 x g for 5 at RT, resuspended in hybridoma freezing medium (see 3.1.11.2) to a final concentration of 10^6-10^7 cells/ml. The cell dilution was transferred in 1 ml aliquots to Cryo-Tubes™ (*Thermo Fischer Scientific*, Langenselbold,

Germany). The tubes were left overnight at -80ºC in a cryocontainer filled with isopropanol. In the cryocontainer, cells were cooled down to -70ºC with a velocity of about 1ºC/min. The frozen cells were then stored in liquid nitrogen.
To revitalize frozen cells, the Cryo-tubes™ were rapidly warmed up in a 37ºC water bath. Then the thawed cell suspension was transferred to several 10 cm dishes containing pre-warmed culture medium, and cells were further incubated at 37ºC as described under 3.5.2.

3.5.4 Preparation of rat hippocampal neuron cultures

For the isolation of hippocampal neurons from mouse or rat embryos as described by Fuhrmann *et al*. (2002), a pregnant female at embryonal day 18 (E18) was anesthetized by inhalation of isofluorane (Deltaselect, Pfullingen, Germany) and killed by cervical dislocation. The embryos were then removed from the uterus, killed by decapitation, and their heads were collected in 10 cm dishes containing PBS + 10 mM glucose on ice. Brains were taken out of the skull and placed for further preparation in a new 10 cm dish containing PBS/glucose. Hemispheres were separated, and the covering meninges were removed such that the inner surface of the hemisphere faced upward. Hippocampi were surgically isolated and immersed in tubes containing PBS/glucose on ice. After setting down, the hippocampi were transferred to a tube containing 200-500 µl of digestion solution for primary culture, and incubated at 37ºC for 20 min. The digested tissue was then washed with 10 ml of preparation medium for primary culture and dissociated by 10-15 times pipetting up and down with a 1 ml pipette (Gilson) in 1 ml of preparation medium. Following cell number determination using a Neubauer counting chamber, neurons were diluted and seeded on poly-L-ornithine coated 24 well plates (see 3.5.1) at a density of 40.000-60.000 neurons per well. After 3-4 hours at 37ºC and 5% CO_2, the medium was replaced by neurobasal medium. At DIV3, the proliferation of non-neuronal, e.g. glial, cells was inhibited by the addition of cytosine-D-arabinofuranoside to a final concentration of 3 µM.

3.5.5 Preparation of spinal cord neuron cultures

For the isolation of spinal cord neurons from mouse or rat embryos as described by Kirsch and Betz (1995), a pregnant female at embryonal day E14 was anesthetized, killed and embryos were removed as described under 3.5.4. After placing the embryos face-down in a dry cell culture dish, the skin of the back was cut along the mid line in anterior-posterior direction. Spinal cords were dissected and collected in a 3 cm culture dish containing PBS supplemented with 33 mM glucose. The meninges covering the spinal cord tissue were carefully removed, and the

spinal cord fragments were then cut into small pieces and dissociated by gentle trituration for three times with a glass pipette. After allowing cell clumps to settle for 2-3 min, the supernatant was carefully collected into a new tube, and the dissociation process was repeated for the remaining cells and tissue clumps. A total 6 ml supernatant containing the dissociated neurons was centrifuged at 100 x g for 10 min. After discarding the supernatant, 1 ml of neurobasal medium was added to the pellet and the suspension was mixed gently. Following cell number determination using a Neubauer counting chamber, neurons were diluted and seeded onto poly-L-ornithine coated 24 well plates (see 3.5.1) at a density of 1.2 x 10^5 neurons/well. Neuron cultures were maintained in the incubator for 14 to 30 days.

3.5.6 Lipofection of HEK 293T and COS-7 cells

Cells were seeded on poly-L-ornithine coated coverslips with culture medium in the absence of antibiotic. The lipofection reagent, Lipofectamine 2000 (Invitrogen, Kalsruhe, Germany), builds cationic lipid vesicles, which form complexes with negatively charged DNA. These complexes enter the cytoplasm by endocytosis. Lipofection was carried out following the manufacturer's instructions.

3.5.7 Preparation of detergent extract from HEK 293T cells

Cells were resuspended in 10 ml PBS, transferred to a 15 ml falcon tube and harvested by centrifugation at 100 x g for 10 min. The supernatant was discarded and the cell pellet was stored at -20ºC. Cell pellet was mixed with 300 μl of HEK 293T cell homogenate buffer per 10 cm dish and slowly thawed. Then cells were resuspended in the HEK 293T cell homogenate buffer by pipetting up and down and homogenized on ice using a hand-held rotor-stator homogenizer (Xenox Motorhandstück 2.35, Carl Roth, Kalsruhe, Germany) for 1 min. For the solubilization of proteins, 20 % Triton X-100 and 1 M DTT were added to final concentrations of 1 % and 5 mM, respectively, and the homogenate was left shaking under overhead rotation for 30 min at 4ºC. Finally, cell debris was removed by centrifugation for 10000 x g for 10 min. The resulting detergent extract was directly used for analysis or stored at -20ºC.

3.5.8 Fractionation of spinal cord neuron homogenate

The spinal cords of adult rats were dissected and homogenized in Im-Ac buffer without Triton X-100. The homogenate was clarified by centrifugation at 1000 x g for 10 min. The postnuclear supernatant (S1) was centrifuged at 10000 x g for 10 min to pellet large membrane organelles

(P2). The remaining supernatant was then centrifuged at 100000 x g to collect small membrane organelles (P3). This P3 fraction was resuspended in Im-Ac buffer for co-immnoprecipitation experiments (3.3.9).

3.5.9 Immunocytochemistry

Cells cultured in 24-well plates on coverslips coated with poly-L-ornithine were washed once with cold PBS and then incubated with 0.5 ml of cold fixative solution for 2 min for GlyR staining, or 5-10 min for staining with other antibodies, at RT. To quench unspecific fluorescence due to the fixation procedure, cells were incubated for 15 min with 25 mM glycine in PBS following two washes with PBS. To permeabilize cell membranes, cells were incubated with 0.5 ml of permeabilization buffer for 30 min at RT. Unspecific antibody binding was blocked by incubating the cells in 0.5 ml of blocking solution for 1 h at RT. Subsequently the fixed cells were incubated with the primary antibody diluted in blocking solution at dilutions as summarized under 3.1.10.1. 100 μl of the dilutied antibody were placed onto a piece of Parafilm (Pechiney, Chicago, USA) in a moist chamber to prevent drying. Coverslips were then located with cells facing down over the antibody solution and incubated for 1 h at RT. Following three washing steps with PBS for 5 min each, cells were incubated with a fluorescently labelled secondary antibody diluted in blocking solution (for dilution, see 3.1.10.2) for 45 min at RT. Followed by three washes with PBS, for staining of cell nuclei, cells were incubated in DAPI solution diluted 1:1000 in blocking solution for 2 min at RT in a dark chamber and again washed twice with PBS. Coverslips were mounted onto microscope glass slides (76 x 26 x 1 mm) (Paul Marienfeld, Lauda-Königshofen, Germany) by placing them upside down on a drop of Aqua Polymount (Polysciences Inc. Warrington, USA). They were allowed to dry and stored at 4°C.

3.5.10 Immunohistochemistry

3.5.10.1 Cryostat brain sectioning

For immunohistochemical analysis, 1 year-old mice were anesthetized by inhalation of isofluoran (Deltaselect, Pfullingen, Germany) and killed by cervical dislocation. Heads were cut off with scissors, brains were carefully removed from the skull and rapidly frozen at -70ºC through contact with a piece of dry ice. The frozen brains were then embedded in Tissue-Tak (Sakura Finetek, Zoeterwoude, The Netherlands), placed on a cryostat holder and left at -18ºC to allow the embedding gel to polymerize. Transversal or sagital slices of 15-30 μm width were cut in a Cryostat (Leica, Jung Frigocut, 2800E). During slicing, the temperature of the chamber reached -

19ºC, whereas the temperature of the tissue remained at -16ºC. Between 4-6 slices were transferred to each coated microscope glass slides (75 x 25 x1 mm, SuperFrost^{R} Plus, Menzel Glaeser, Braunschweig, Germany) and either processed rapidly or stored for further analysis at -80ºC.

3.5.10.2 Immunostaining of brain sections

Tissue slices were dried at RT and fixed for 10 min in cold 4 % (w/v) PFA in PBS. Afterwards, slices were washed three times for 5 min with PBS to completely remove the fixative. To avoid aldehyde- or formalin-derived protein cross-linking and to unmask antigens/epitopes in formalin-fixed tissue sections, a sodium citrate solution was applied. A first wash for 5 min with Na^{+}-citrate buffer at RT was followed by 30 min incubation with Na^{+}-citrate buffer at 95ºC and a last cooling down to RT. After two washes with PBS, membrane permeabilization was achieved through incubation with permeabilization solution for 30 min at RT. Unspecific binding was blocked by incubation with blocking solution for 3 h at RT. Primary antibodies diluted at proper dilution (see 3.1.10.1) in blocking solution were incubated with the slices overnight at 4ºC in a moist chamber. On the next day, unbound antibody was removed by three washes with PBS for 5 min. Incubation with secondary antibodies (see 3.1.10.2) diluted in blocking solution was in a moist chamber for 45 min at RT. Following three washes with PBS, the slides were mounted with Aqua Polymount (Polysciences Inc. Warrington, USA).

3.5.11 Confocal microscopy, image acquisition and analysis

Immunostained neurons and tissue sections were analyzed using a confocal Leica TCS-SP Laser Scanning-Microscope (Leica Microsystems, Bensheim, Germany). Specimens were analyzed in x, y and z-axis in multiple z-layers. Pictures were obtained at 1024x1024 pixel resolution. Serial confocal images were captured at a total magnification of 630x. For immunhistochemistry data collection, six stacks of 0.1 μm each were compressed using a maximum projection algorithm in the Leica TCS software. For analysis of cluster number and size by immunocytochemistry experiments, maximal projections of 8-12 z-stacks of 0.1 μm each were obtained with a Leica-TCS-NT software. For the quantification of punctate immunofluorescence in spinal cord neurons, 50 μm neurite segment emanating from the somas of randomly selected cells was marked. The binarization, thresholding and quantification was implemented using the ImageJ 1.42q software (National Institutes of Health). Synaptic clusters were selected by counting those puncta exceeding 0.4 μm^2.

For colocalization analysis, single z-stack images were obtained using an AxioImager

microscope equipped with an apotome (Zeiss, Goettingen, Germany). For the quantification of colocalizing puncta, the objects in the green channels exceeding a minimal size were counted along neurites. An object was considered to colocalize if more than 0.1 μm^2 of its area colocalized with signal in the red channel. Images were further developed and organized by Adobe Photoshop and Adobe Illustrator software (Adobe, San Jose, USA). Quantifications were performed using ImageJ 1.42q software (National Institutes of Health,USA). A minimum of three distinct experiments of identically processed cultures were analyzed and 10 images were collected from randomly selected dendrites of 10 different neurons. Data are presented as means ± standard error (S.E.M.) Statistical significance was evaluated with a two tailed Student's *t*-test.

4 RESULTS

4.1 Analysis of the interaction between the Sdp protein family and the GlyRβ subunit

In a attempt to identify novel interaction partners of the glycine receptor β subunit (GlyRβ), a GST fusion protein encompassing 78 amino acids (position 378 and 455) of the intracellular loop located between transmembrane domains 3 and 4 of the glycine receptor β subunit ($GlyR\beta_{78}$) was utilized for the isolation of proteins from rat brain detergent extract. One of the proteins bound with an apparent molecular weight of about 52 kDa was identified by matrix-assisted laser desorption/ionisation–time of flight mass (Maldi-ToF) spectrometry (Paarmann et al., 2006) as SdpI. In this thesis, the interaction between SdpI and the GlyRβ subunit was investigated. Glutathione-S-transferase (GST) pull-down experiments using recombinantly expressed Sdp isoforms and $GlyR\beta_{78}$ were performed in order to examine the binding activity of SdpI and SdpII to the large intracellular loop of the GlyRβ subunit and gephyrin *in vitro*. Deletion, peptide competition and point mutation approaches were used to characterize the interaction between SdpI and $GlyR\beta_{78}$. Co-localization experiments in COS-7 cells and spinal cord neurons were used to investigate a possible interaction of SdpI and SdpII with the full-length GlyRβ subunit and gephyrin *in vivo*. Additionally, the possible implication SdpI in GlyR-trafficking mechanisms was investigated. Co-immunoprecipitation experiments using detergent extracts of a spinal cord homogenate fraction enriched in small membraneous organelles were performed to disclose a possible interaction of SdpI with the GlyR in transport vesicles. Taking advantage of a KO mouse-line and rAAV techniques, SdpI depletion studies were performed to analyse the distribution of inhibitory synaptic proteins in brain stem and spinal cord neurons lacking SdpI.

4.1.1 Characterization of the interaction between Sdp protein family members and the GlyRβ subunit

In order to investigate whether SdpI interacts with the GlyRβ subunit, GST pull-down experiments were performed. This *in vitro* protein-protein interaction analysis required the expression of one of the binding-partners as a GST fusion protein in *E. coli* followed by its immobilization on a glutathione (GSH)-matrix. The immobilized GST-fusion protein was then

incubated with a protein solution containing putative binding partners, which had been also generated in *E. coli* (C41 for SdpI, BL21DE3 for others) with a short N-terminal His_6-tag to allow immnune detection. Proteins binding to the immobilized GST-fusion protein should sediment with the beads. The analysis of bound co-sedimented proteins was carried out by SDS-PAGE and Western blotting using an antibody that specifically recognized the respective protein. To validate the specificity of the interaction, GST and GST fusion constructs of unrelated proteins were utilized as negative controls. As a positive control, either 50% of the input was loaded onto a SDS-gel, or GST fusion constructs of known binding partners were used in the pull-down experiment.

4.1.1.1 *In vitro* interaction between recombinant proteins: GST fusion proteins of the GlyRβ loop and His_6-tagged Sdps

The interaction between the 78 amino acids of the large intracellular loop of the GlyRβ subunit ($GlyR\beta_{78}$) and SdpI was confirmed by GST pull-down experiments. GST fusion proteins of $GlyR\beta_{78}$ and $GlyR\beta_{49}$ as well as GST alone were incubated with a bacterial lysate containing His_6-tagged SdpI (His-SdpI). After SDS-PAGE, the Coomassie stained gel showed a prominent band around 55 kDa in GST-$GlyR\beta_{78}$ pull-downs, but not with GST-$GlyR\beta_{49}$ or GST alone (Fig. 4.1.A). Bands around 80 kDa in the second lane corresponded to the *E.coli* DnaK protein, a common contamination when dealing with GST fusion proteins. Western blot analysis with an anti-His_6 antibody confirmed that the band at 55 kDa, indicated in red in Fig. 4.1.A, represented the recombinant His_6-SdpI protein (see Fig. 4.1.B).

To further examine whether GlyRβ is binding to Sdps, GST pull-down assays were performed using the His_6-tagged constructs of SdpI and both splice variants of SdpII. As shown for SdpI, SdpII-L and SdpII-S co-precipitated with GST-$GlyR\beta_{78}$ but not with GST-$GlyR\beta_{49}$ or GST alone (see Fig. 4.1.C). These results confirm that SdpI and both splice variants of SdpII bind to the GlyRβ subunit *in vitro*. Furthermore, the intensities of the Sdp protein bands eluted from GST-$GlyR\beta_{78}$ are indicative of strong interactions between SdpI, or SdpII-L and SdpII-S and the GlyRβ subunit *in vitro*.

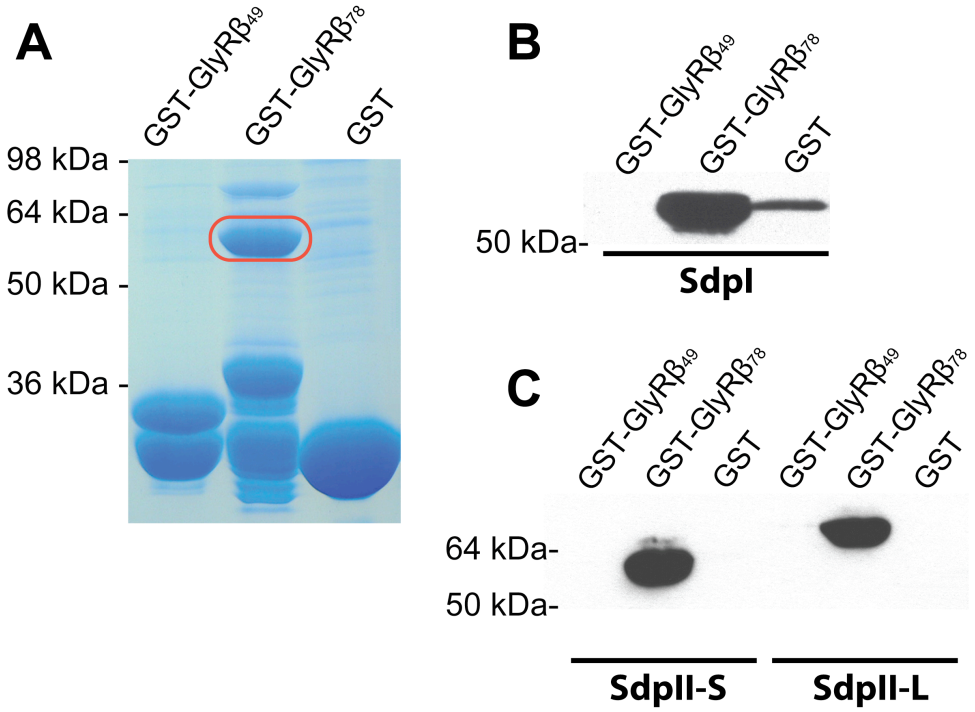

Fig. 4.1. *In vitro* interaction of Sdp isoforms with the intracellular loop of the GlyRβ subunit. A. GST pull-down of recombinantly expressed His_6-tagged SdpI from lysates of bacteria expressing: left lane, GST-GlyRβ_{49}; middle lane, GST-GlyRβ_{78}; right lane, GST. A prominent band present in the middle lane but not in the two control lanes with a molecular weight around 60 kDa is circled in red. Lower molecular weight bands are GST fusion proteins. Double bands for GST-GlyRβ_{49} and GST-GlyRβ_{78} result from partial cleavage between GST and fusion partner. **B**. Corresponding anti-His_6 immunodetection of protein samples shown in **A**. The prominent band in the second lane represents His_6-tagged SdpI running above 50 kDa. Some weak unspecific binding to GST was observed in the right lane. **C**. Anti-His_6 immunodetection of the GST pull-down of His_6-tagged SdpII-S (first three lanes) and His_6-tagged SdpII-L (last three lanes) with GST-GlyRβ constructs. Both splice variants of SdpII interact with the GST-GlyRβ_{78} construct but not with the negative controls GST-GlyRβ_{49} and GST. Experiments done by Dr. Ingo Paarmann.

4.1.1.2 Mapping of the SdpI binding site on GlyRβ_{78}.

The GlyRβ intracellular loop fragment used to isolate SdpI from rat brain lysate contains a gephyrin binding motif (GBM) and a SH3 binding motif (SBM). The binding site of SdpI on GlyRβ was first mapped using a deletion approach. Several GST fusion constructs of GlyRβ_{78} were generated and probed for binding to a His_6-tagged SdpI protein by GST pull-down. Removal of the first 49 amino acids including the GBM did not affect SdpI binding (see Fig. 4.2). The construct lacking the last 15 amino acids of the GlyRβ_{78} including part of the SBM exhibited a slightly reduced binding, whereas GlyRβ_{49} lacking the complete SBM was not able to bind His-SdpI at all (Fig. 4.1 and Fig. 4.2). The sequence mediating SdpI binding to the GlyRβ loop thus could be narrowed down to 22 aa (GlyR$\beta_{427-448}$ construct), which included the SBM. These

mapping experiments suggested that the SH3 binding motif is essential for the interaction between SdpI and the GlyR intracellular loop.

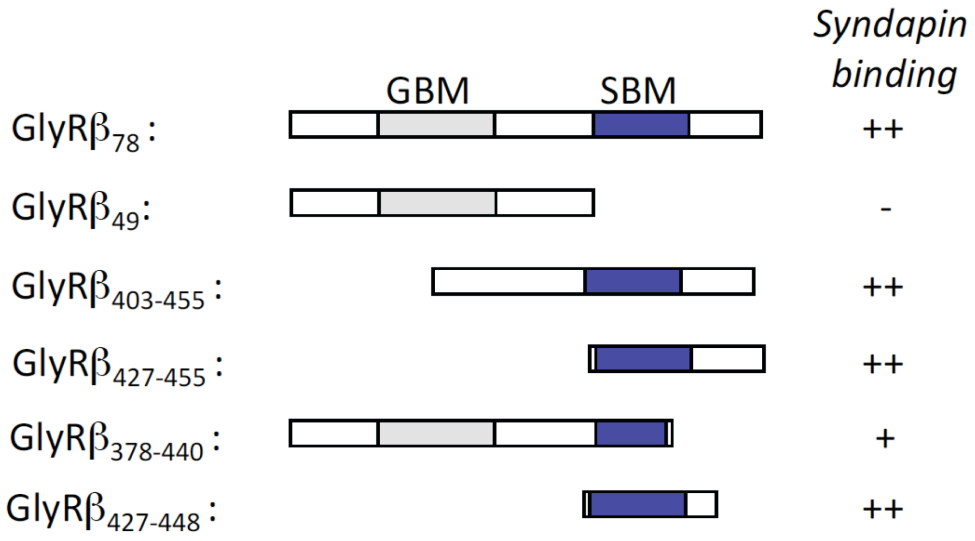

Fig. 4.2. Mapping of the SdpI binding site in GlyRβ$_{78}$. SdpI binding to several GST-tagged fragments of the GlyRβ$_{78}$ was analysed. Taking the binding of SdpI to GST-GlyRβ$_{78}$ and GST-GlyRβ$_{49}$ as maximal and minimal references for SdpI-binding, respectively, the intensities of the SdpI bands bound to the different fragments as revealed by Western blot were compared qualitatively. ++: Strong binding of SdpI. +: Weak binding of SdpI. -: no binding of SdpI. GBM: gephyrin binding motif depicted in grey. SBM: SH3 binding motif depicted in blue. Experiments done by Dr. Ingo Paarmann.

In conclusion we found that 22 amino acids from positions 427 to 448 containing the entire SBM were sufficient for strong interaction. This result was confirmed using a peptide competition approach. Immobilized GST-GlyRβ$_{78}$ was incubated with His$_6$-SdpI and different concentrations of either a TAT peptide containing the 22 binding residues identified in our mapping experiments (TAT-GlyRβ$_{22}$) or a TAT scrambled peptide containing the same aa in random order (TAT-scrambled) (see Fig. 4.3.A.). As a positive control, GlyRβ$_{78}$ was incubated with His$_6$-SdpI in the absence of peptide. Upon detecting the bound His$_6$-SdpI by Western blotting, it became obvious that incubation with the TAT-GlyRβ$_{22}$ peptide, but not the TAT-scrambled peptide reduced SdpI binding to GST-GlyRβ$_{78}$ (Fig. 4.3.B). When quantifying the SdpI band densities found by Western blotting using the ImageJ software, a marked reduction in SdpI band intensity was observed upon the addition of 100, 10 and 1 μM of TAT-GlyRβ$_{22}$. Intensity values were 10.9 ± 7.3%, 14.1 ± 11.9% and 70.6 ± 10.3% of control, respectively (n=3, $p < 0.001$, $p < 0.01$ and $p <$

0.05, respectively) (Fig. 4.3.C). However, when 100, 10 and 1 μM of TAT-scrambled peptide were added, no significant reduction of SdpI band intensity was found (intensity values: 44.6 ± 24.9%, 55.1 ± 23.8% and 76.1 ± 15.8% of control, respectively; n=3, $p > 0.05$) (Fig. 4.3.C). These results confirm that the region encompassing the amino acids 427 to 448 of the large intracellular loop of the GlyRβ subunit is responsible for SdpI binding. Furthermore, they show that the interaction between GlyRβ and SdpI is indeed specific.

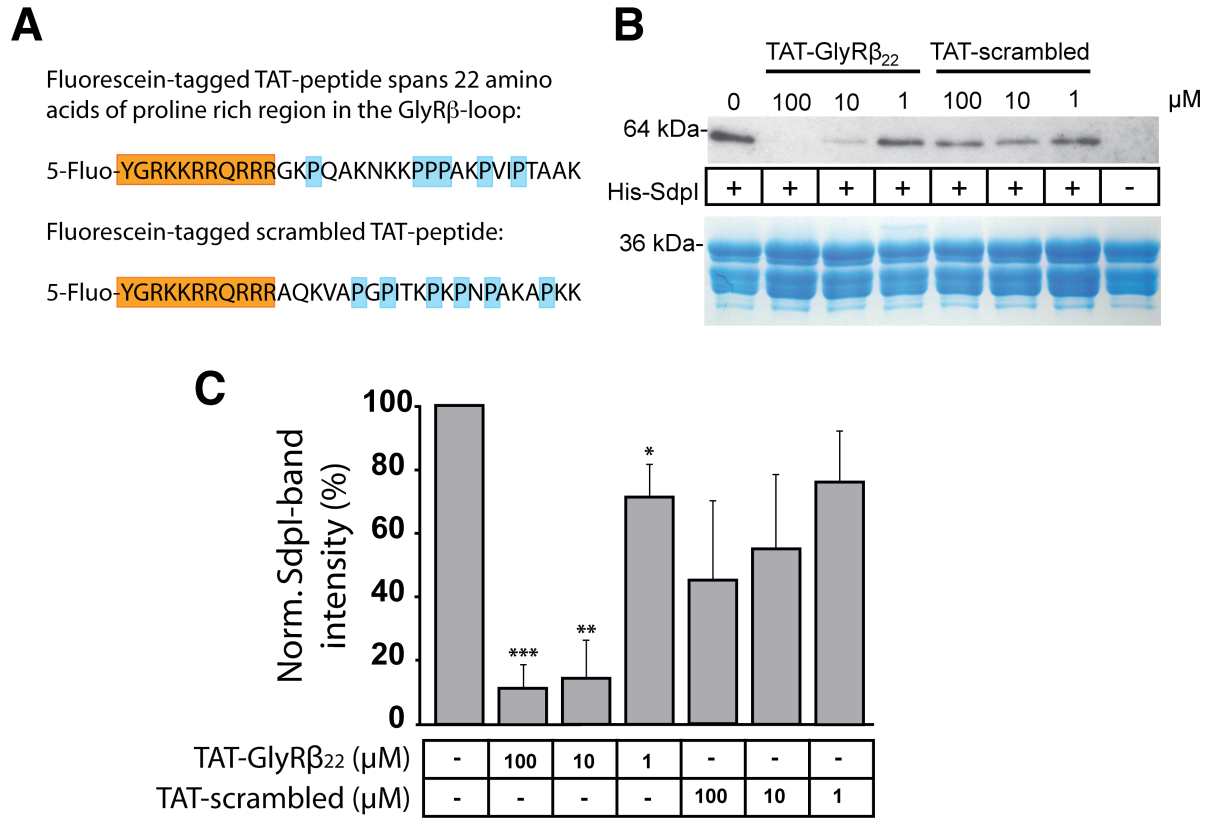

Fig. 4.3. Sequence-specific interaction between SdpI and amino acids 427-448 of the intracellular loop of the GlyRβ subunit. A. Depiction of peptide sequences. TAT sequence for internalization is highlighted in red, whereas proline residues are depicted in blue. **B**. Peptide competition experiment. Pull-down with GST-GlyRβ_{78} and His_6-SdpI was performed in the presence of GlyRβ_{22} peptide or scrambled peptide. Coomassie stained gel confirmed the presence of GST-GlyRβ_{78} protein eluted from the beads. Western blot shows reduced SdpI binding when GlyRβ_{22} peptide was added to the sample (lanes 2 and 3). SdpI binding did not differ as compared to control (lane 1) when scrambled peptide was added to the sample (lanes 5, 6 and 7). **C**. Quantification of relative SdpI-band intensities from peptide competition experiment shown in **B**. Values represent means ± SEM (n=3). Significant differences as compared to control (no peptide): *, $p < 0.05$; **, $p < 0.01$; ***, $p < 0.001$.

4.1.1.3 Identification of GlyRβ point mutants interfering with SdpI binding

The mapping and peptide competition experiments described above (4.1.1.2) revealed that the GlyR$\beta_{427-448}$ sequence was sufficient for SdpI binding. This region contains a complex SH3 binding motif (SBM). Additional mapping experiments showed that an intact SH3 domain of SdpI is essential for strong interaction (data not shown). Therefore, we assumed that the GlyRβ subunit binds to SdpI through a SH3-SBM interaction. From previous studies, it was known that SH3 domains bind to proline-rich regions and generally favour peptides which bear a PxxP core motif (where x represents any amino acid) (Li, 2005), and that the residues flanking this core motif define the selectivity of a given SH3 domain (Sparks et al., 1996).

Inspection of the amino acid sequence of the GlyRβ_{78} construct used for the pull-down of SdpI disclosed the presence of the common R/KxxPxxP SH3 ligand-binding motif (residues K435, P438 and P441). In this motif, the R/K side chains would not only provide additional binding energy through electrostatic interactions but also orient the ligand with respect to the binding groove of the SH3 domain (Li, 2005). Therefore, in order to further delineate the SdpI binding site and to establish the importance of the SH3 binding motif for GlyRβ-SdpI binding, we designed double point mutations to disrupt this motif (Fig. 4.4.A). On the basis of the GST-GlyRβ_{78} fusion protein, two mutants were created in which the proline residues P438 and P441 (GST-GlyR$\beta_{78\text{-}PPAA}$) as well as the lysine residues K434 and K435 (GST-GlyR$\beta_{78\text{-}KKAA}$) were mutated to alanines. SDS-PAGE analysis showed that both mutant constructs produced fusion proteins of the same apparent molecular weight as the wild-type protein (Fig. 4.4.C). When these GST-GlyRβ_{78} mutants were expressed in *E. coli* and examined for SdpI interaction by GST pull-down, SdpI binding was found to be completely lost with both GST-GlyR$\beta_{78\text{-}PPAA}$ and GST-GlyR$\beta_{78\text{-}KKAA}$, with SdpI band intensities being reduced to 3.0 ± 1.5% and 6.3 ± 4.7% of control, respectively ($n=3$, $p < 0.001$). These values are similar to the SdpI band intensity value obtained upon incubation of SdpI with GST-GlyRβ_{49} (4.3 ± 3.8% of control)(Fig. 4.2.B and E). Notably, gephyrin co-precipitated with GST-GlyRβ_{49} and the GST-GlyRβ_{78} wild-type and mutant forms, but not with GST alone (Fig. 4.4.D).

Together, these results show that the KxxPxxP motif is responsible for SdpI binding to the GlyRβ subunit, but not involved in gephyrin binding. Furthermore, these results agree with the peptide competition data and further support the hypothesis of an SH3 domain mediated interaction of SdpI with the GlyRβ subunit.

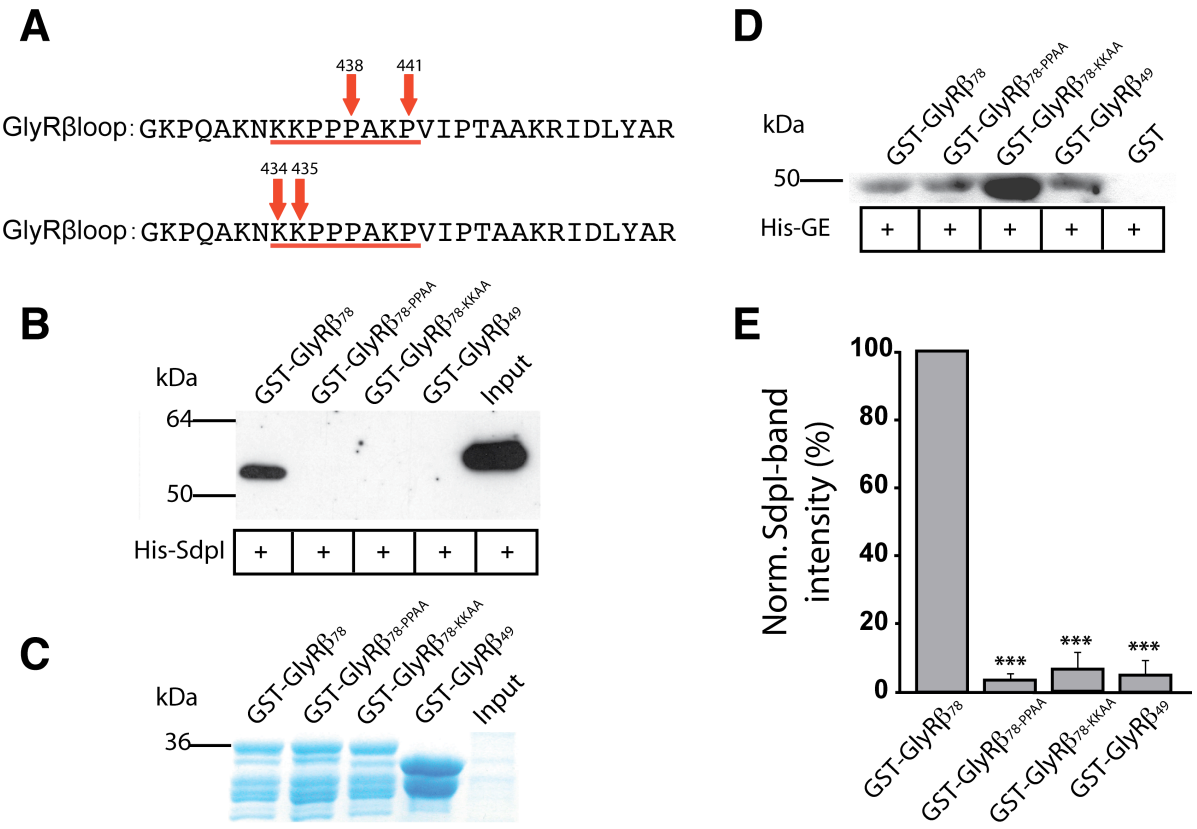

Fig. 4.4. Point mutations interfering with SdpI binding in GST pull-down experiments. A. Positions of point mutations. Proline-rich motifs are underlined in red. Arrows point to the proline and lysine residues within the large intracellular loop of GlyRβ that were mutated to alanines. **B**. GST fusion proteins of GlyRβ$_{78}$ and GlyRβ$_{49}$ as well as the mutated forms GlyRβ$_{78\text{-PPAA}}$ and GlyRβ$_{78\text{-KKAA}}$ were immobilized to a GSH-matrix and incubated with bacterial lysate containing His$_6$-tagged SdpI. Anti-His$_6$ western blot shows that the fusion protein GST-GlyRβ$_{78}$ (lane1), but not GST-GlyRβ$_{49}$ (lane 2) or the mutants GST-GlyRβ$_{78\text{-PPAA}}$ and GST-GlyRβ$_{78\text{-KKAA}}$ (lanes 3 and 4), co-precipitated with recombinant His$_6$-syndapin I. Input: 50% of the His$_6$-Sdp-I-containing lysate loaded per sample. **C**. Coomassie stained gel shows GST fusion proteins. **D**. Immundetection of His$_6$-tagged E-domain binding to GST-GlyRβ$_{78}$, GST-GlyRβ$_{49}$, GST-GlyRβ$_{78\text{-PPAA}}$ and GST-GlyRβ$_{78\text{-KKAA}}$, but not to GST. His-GE: His$_6$-tagged E-domain of gephyrin. **E**. Quantification of relative SdpI-band intensities in the GST pull-down experiments shown in **B**. Values represent means ± SEM (n=3). Significant differences as compared to control (GST-GlyRβ$_{78}$): ***, $p < 0.001$.

4.1.2 Interaction between Sdp proteins and GlyRβ in a mammalian cell expression system

The GST-pulldown experiments described under 4.1.1.1 demonstrated that two isoforms of Sdp, SdpI and SdpII, interact with $GlyR\beta_{78}$ *in vitro*. As new binding partners of GlyRβ, Sdp I and SdpII should form complexes with the GlyRβ subunit *in vivo*. Therefore, colocalization experiments were performed in a mammalian cell line transfected with cDNAs encoding both proteins. After fluorescent labelling with different Alexa dyes and digital recording, overlapping emission signals indicated close proximity of antigens within microscopically defined subcellular structures.

4.1.2.1 Endoplasmic reticulum (ER) retention assay

To clarify whether SdpI and the GlyRβ subunit interact in a mammalian cell expression context, colocalization experiments were performed in COS-7 cells. A plasmid encoding the GlyRβ subunit N-terminally tagged with monomeric red-fluorescent protein (mRFP) was transfected into COS-7 cells for 24 h. Red fluorescence then was found throughout the cytoplasm in speckled form. From previous studies it was already known that GlyRβ expressed in HEK 293 cells cannot exit the endoplasmic reticulum (ER) in the absence of GlyRα subunits (Kirsch et al. 1995). Colocalization experiments with an anti-calnexin antibody (Fig. 4.5), which recognizes an integral protein of the ER, confirmed that mRFP-GlyRβ expressed in COS-7 cells is retained in the ER. This demonstrates that retention of the singly expressed GlyRβ subunit in the ER is a general event.

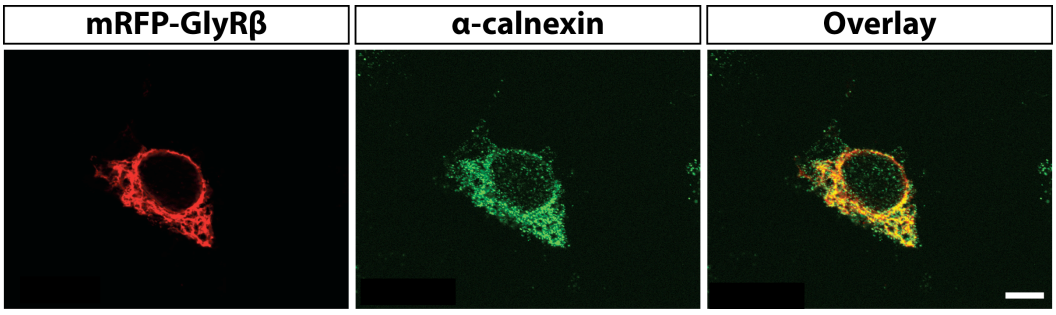

Fig. 4.5. Subcellular distribution of the GlyRβ subunit in COS-7 cells. COS-7 cells were transfected with mRFP-GlyRβ. 24 h after transfection, cells were stained with an anti-calnexin antibody and an Alexa-488 anti-mouse antibody. Note the extensive colocalization as indicated in the overlay in yellow. Scale bar: 10 μm.

4.1.2.2 Gephyrin binding monitored by ER retention

To establish the ER retention assay, mRFP-GlyRβ was co-transfected with N-terminally GFP-tagged gephyrin (GFP-gephyrin), or GFP as control. After 24 hours, cells were fixed and the fluorescence signals of the mRFP and GFP channels were detected using an AxioImager equipped with an Apotome (Zeiss) and AxioVision software (Zeiss).

As previously shown in many studies, there is high-affinity binding between gephyrin and the intracellular loop of the GlyRβ subunit (Meyer et al., 1995; Sola et al. 2004; Schrader et al. 2004). As expected, upon co-expression in COS-7 cells, GFP-gephyrin colocalized in with mRFP-GlyRβ in the ER (Fig. 4.6. overlay in middle pannel). Unexpectedly, gephyrin blob formation as seen in previous studies (Kirsch et al. 1995; Saiyed et al. 2007) upon recombinant expression of gephyrin, was absent when gephyrin was co-expressed with the GlyRβ subunit. Instead of recruiting GlyRβ into gephyrin blobs, in our experiments gephyrin-immunofluorescence was restricted to the ER. In control experiments, little colocalization was seen when GFP alone or a gephyrin mutant harbouring a mutation in the E-domain, GFP-gephyrin$_{mut}$, and therefore being unable to bind to the GlyRβ loop (Sola et al., 2004), were co-expressed with mRFP-GlyRβ (Fig. 4.6, overlays in top and bottom panels).

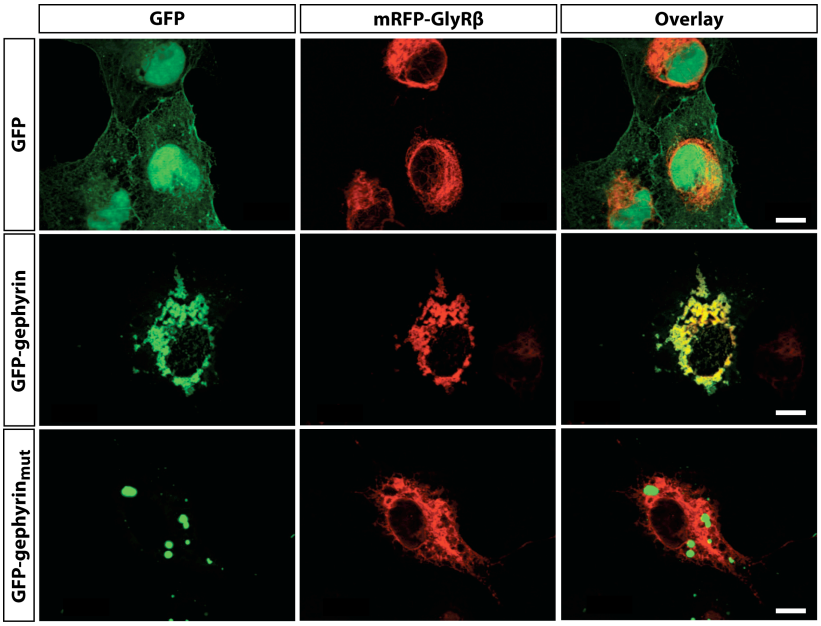

Fig. 4.6. Colocalization of gephyrin with the GlyRβ subunit in COS-7 cells. COS-7 cells were co-transfected with GFP, GFP-gephyrin or GFP-gephyrin$_{mut}$ (gephyrin mutant unable to bind to the GlyR) and mRFP-GlyRβ and fixed 24h after transfection. Upon co-expression with mRFP-GlyRβ, GFP distributed mainly into the nucleus and little colocalization was seen near nucleus-ER contacts (overlay in top panel). Note extensive colocalization of mRFP-GlyRβ with GFP-gephyrin in the ER as indicated in yellow (overlay in middle), but lack of co-localization with GFP-gephyrin$_{mut}$ (overlay in bottom panel). Scale bar: 10μm.

Thus, the gephyrin-GlyRβ colocalization experiments in COS-7 cells show that retention of gephyrin on the ER is due to the interaction with the GlyRβ subunit and exclude that ER retention-signals in gephyrin or other secondary events could be responsible for this colocalization. Moreover, these results suggest that the ER retention assay can indeed be used to study interactions of putative binding proteins of the GlyRβ subunit.

4.1.2.3 Binding of Sdps in the ER retention assay

The colocalization experiments described above revealed that the ER retention assay can be used to study interactions with GlyRβ (see 4.1.2.2). Therefore, colocalization assays were performed in order to test whether SdpI binds to GlyRβ upon heterologous expression in COS-7 cells. Additionally, the binding activity of the two splice variants of SdpII, SdpII-L and SdpII-S, was examined.

4.1.2.3.1 Colocalization of SdpI with GlyRβ in COS-7 cells.

Full-length mRFP-tagged GlyRβ was co-expressed with myc-tagged SdpI in COS-7 cells for 24 h. As a control, a DsRed-tagged ER-marker was used to stain the ER, and myc-tagged dynein light chain 1 (myc-Dlc1) was used as a non-binding control protein. Myc-tagged proteins were stained with anti-myc and Alexa-488 anti-rabbit antibodies. The fluorescences of mRFP, DsRed and Alexa-488 were monitored as described under 4.1.2.2.

Upon co-expression of myc-SdpI with DsRed-ER, anti-myc immunoreactivity was detected in the cytoplasm, and little colocalization was seen in the ER (see Fig. 4.7.A, top panel). However, when myc-SdpI was co-expressed with mRFP-GlyRβ, myc-SdpI anti-myc immunoreactivity was detected prominently in the ER and to a lesser extent in the cytoplasm (see Fig. 4.7.A, middle panel). In additional control experiments, myc-Dlc1 co-expression with mRFP-GlyRβ resulted in a cytoplasmic and nuclear localization of myc-Dlc1 and little co-localization of myc-Dlc1 with the mRFP-GlyRβ in the ER (see Fig. 4.7.A, lower panel). This indicates that recombinant GlyRβ changes the subcellular distribution of SdpI. Closer inspection of myc-SdpI and mRFP-GlyRβ colocalization was accomplished using the ImageJ software. The colocalization rate was quantified as percentage of ER area in the red channel that colocalized with the myc-tagged protein in the ER in the overlay image.

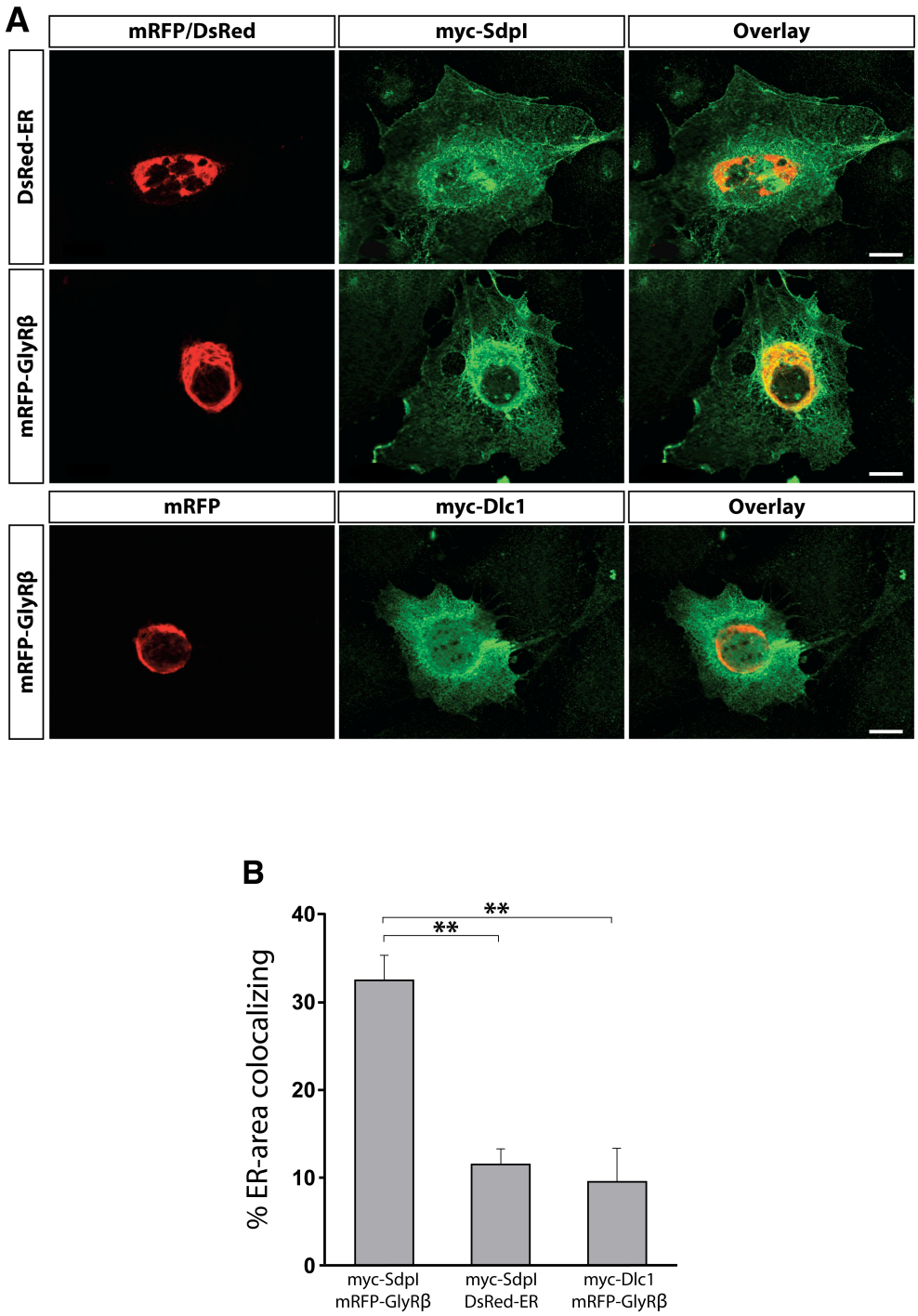

Fig. 4.7. Colocalization of SdpI with the GlyRβ subunit in COS-7 cells. A. Myc-tagged SdpI and Dlc1 were co-transfected with mRFP-GlyRβ and DsRed-ER control marker in COS-7 cells. After 24 h, cells were fixed and incubated with anti-myc antibody and Alexa-488 anti-rabbit. Note extensive co-localization of myc-SdpI in the ER of cells expressing mRFP-GlyRβ as indicated in yellow (middle panel), but only a background co-localization signal when expressed with the DsRed-ER control marker (top panel) or when myc-Dlc1 was co-expressed with mRFP-GlyRβ (bottom panel). Scale bar: 10 μm. **B**. The percentage of ER area colocalizing with myc-protein was quantified in the experiment shown in **A**. Values represent means ± SEM (n=3). Significant differences as compared to mRFP-GlyRβ and myc-SdpI co-expression: **, $p < 0.01$.

The colocalization rate in the ER was significantly higher upon myc-SdpI + mRFP-GlyRβ co-expression (32.3 ± 2.8 %) than upon myc-SdpI + control DsRed-ER-marker (11.4 ± 1.7 %). Similarly, there was a background colocalization in the ER in cells co-expressing Dlc-1, a non-related myc-tagged protein, and mRFP-GlyRβ, which was significantly reduced (9.5 ± 3.8%) as compared to myc-SdpI + mRFP-GlyRβ co-expression (Fig. 4.7.B). Thus, these results confirm that SdpI is a protein interacting with the GlyRβ subunit and demonstrate that both proteins can interact in a mammalian cell expression system.

4.1.2.3.2 Colocalization of SdpII splice variants with GlyRβ in COS-7 cells

From the SdpI isoform SdpII, two splice variants are generated in neuronal tissue: SdpII-S and SdpII-L (2.4.1.1). In order to clarify whether these splice variants also interact with the GlyRβ subunit in a cellular context, co-expression experiments in COS-7 cells were performed using myc-tagged forms of SdpII-S and -L following the protocol described above (4.1.2.3.1).

When expressed alone in COS-7 cells, both myc-SdpII-S and myc-SdpII-L accumulated in the cytosol (data not shown). Upon co-expression with the DsRed-ER marker, myc-tagged SdpII splice variants displayed similar distributions, prominently in the cytosol and little at the plasma membrane. Overlays showed that both splice variants displayed background signals in the ER (Fig. 4.8). In contrast, when expressed with the mRFP-GlyRβ, both splice variants concentrated in the ER and were less intense in the cytosol (Fig. 4.8). Parallel co-expression of myc-Dlc1 with mRFP-GlyRβ in COS-7 cells served as a control for unspecific co-localization. As described above (4.1.2.3.1), myc-Dlc1 co-expressed with mRFP-GlyRβ displayed a cytosolic and nuclear distribution with background accumulation in the ER (data nor shown). These results indicate that, similarly to what is seen with SdpI, recombinant GlyRβ also changes the subcellular distribution of myc-SdpII-S and myc-SdpII-L.

A more accurate analysis of ER colocalization was performed with the ImageJ software as described above (4.1.2.3.1). The area where proteins colocalized in the ER was significantly larger upon co-expression of myc-SdpII-L with mRFP-GlyRβ (33.5 ± 3.8 %) than with the DsRed-ER marker (6.2 ± 2.9 %), or of myc-Dlc1 protein and mRFP-GlyRβ (8.1 ± 4.3 %) (Fig. 4.8). Co-expression of myc-SdpII-S with mRFP-GlyRβ similarly resulted in 29.2 ± 2.9 % colocalization area. Again, this value was significantly higher than that obtained upon co-expression of myc-SdpII-S and the DsRed-ER marker (6.0 ± 0.8 %), or with the myc-Dlc1 construct and

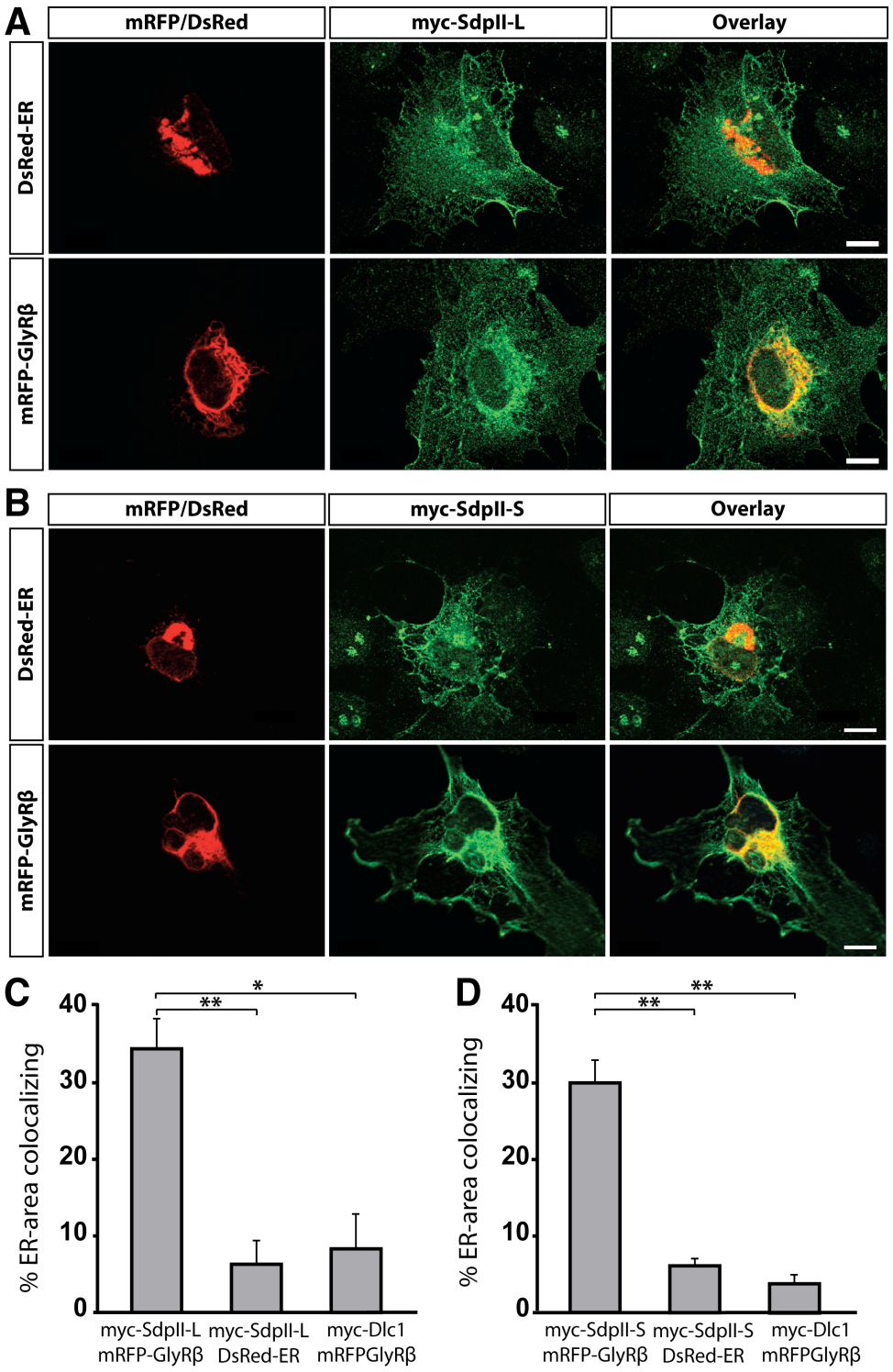

Fig. 4.8. Colocalization of SdpII-L and SdpII-S with GlyRβ in COS-7 cells. A and **B**. Myc-tagged SdpII-L (**A**) and SdpII-S (**B**) and Dlc1 (not shown) were co-transfected with mRFP-GlyRβ and DsRed-ER control marker in COS-7 cells. After 24 h, cells were fixed and stained as in Fig. 4.7. Note the extensive co-localization of myc-SdpII-L and myc-SdpII-S in the ER of cells expressing mRFP-GlyRβ as indicated in yellow, but only background co-localization signal when expressed with the DsRed-ER control marker. Scale bar: 10 μm. **C** and **D**. Quantification of colocalization experiments as shown in **A** and **B,** respectively, was performed as in Fig. 4.7. Values represent means ± SEM (n=3). Significant differences as compared to GlyRβ-Sdp co-expression: *, $p < 0.05$; **, $p < 0.01$.

mRFP-GlyRβ (3.7 ± 1.0 %) (Fig. 4.8.D). Together, these colocalization experiments demonstrate that the interaction with GlyRβ is not restricted to SdpI. Clearly, both splice variants of SdpII interact with GlyRβ in COS-7 cells.

4.1.3 Interaction between Sdp proteins and gephyrin

4.1.3.1 *In vitro* analysis

Gephyrin is a direct binding partner of the GlyRβ subunit and, presently, the only protein reported to directly interact with the glycine receptor (Schmitt et al., 1987). Previous live imaging experiments have demonstrated that glycine receptors and gephyrin are co-transported as a complex along neurites (Maas et al., 2006). In order to test whether SdpI only binds the GlyRβ subunit or also gephyrin, GST pull-down experiments were performed using several GST fusion constructs of gephyrin fragments spanning the E, E+linker and G domains, respectively. Preliminary data had already indicated weak binding of SdpI to the linker region but not the E-domain (I. Paarmann, unpublished observation).

4.1.3.2 SdpI-gephyrin interaction analysis in a mammalian cell expression system

Upon overexpression in heterologous cells, gephyrin forms intracellular aggregates usually named “blobs” (Kirsch and Betz, 1995; Meyer et al., 1995). These gephyrin aggregates recruit binding proteins, and hence subcellular colocalization as detected by fluorescence microscopy serves as a well-established assay to confirm interactions between gephyrin and candidate binding partners (Fuhrmann et al., 2002). Here, evidence for an *in vivo* interaction between gephyrin and SdpI as well as SdpII was obtained in a mammalian cell expression system by using the colocalization assay. To this end, cDNAs encoding myc-tagged SdpI, SdpII-L and SdpII-S were co-transfected with full-length mRFP-tagged gephyrin in COS-7 cells. As positive and negative controls for gephyrin binding, myc-tagged Dlc1 and GFP, respectively, were co-transfected with mRFP-gephyrin. After 24 h, the cells were fixed and stained with anti-myc and Alexa-488 anti-rabbit antibodies. Subsequent colocalization analysis revealed that myc-SdpI, myc-SdpII-L and myc-SdpII-S, like myc-Dlc1 (Furhmann et al., 2002), colocalized with mRFP-gephyrin upon co-expression in COS-7 cells. In contrast, upon co-expression of GFP with mRFP-gephyrin no colocalization was observed (Fig. 4.9).

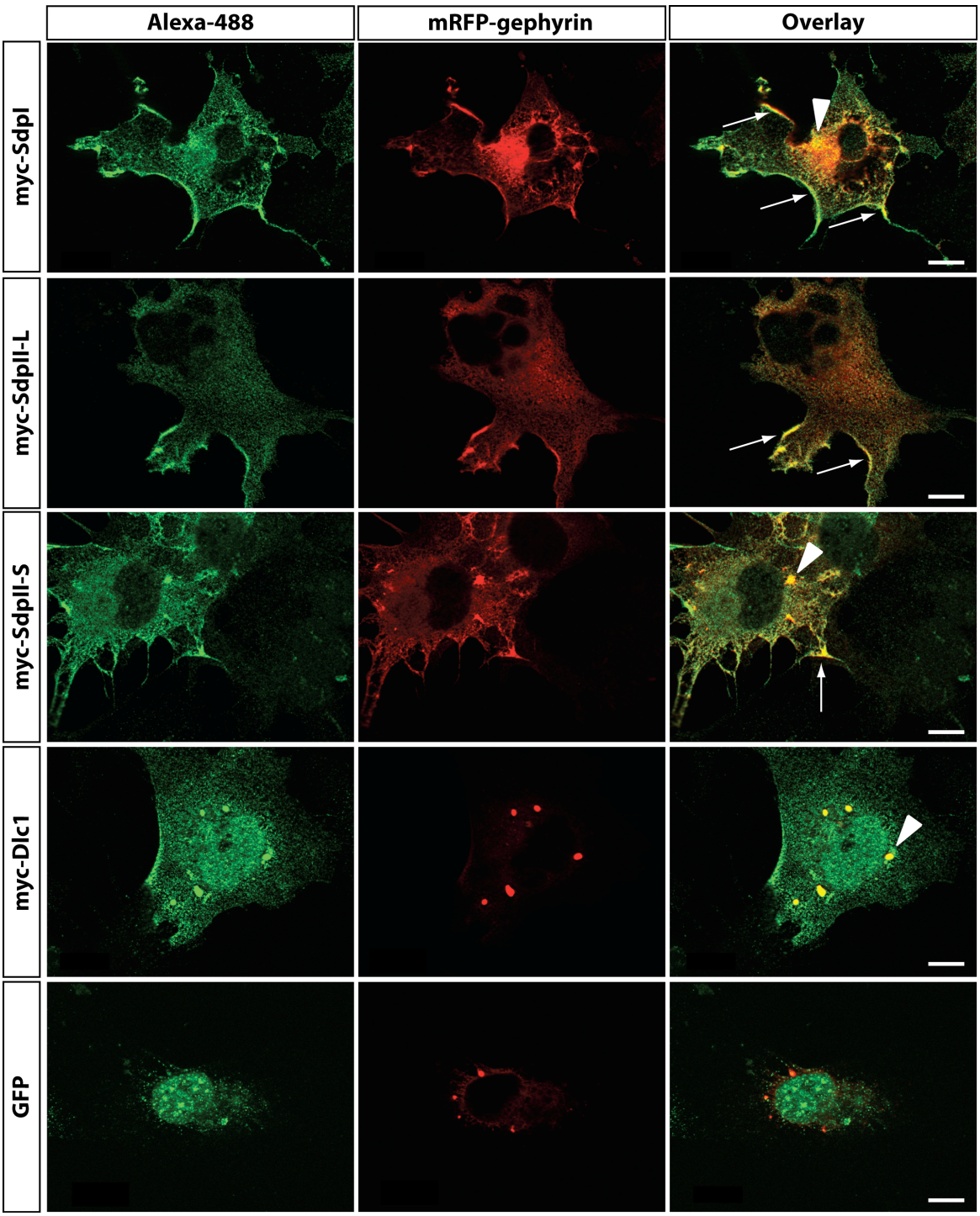

Fig. 4.9. Gephyrin colocalization with SdpI and SdpII in COS-7 cells. cDNAs encoding GFP, myc-tagged SdpI, SdpII-L, SdpII-S and Dlc1, respectively, were co-transfected with mRFP-gephyrin in COS-7 cells. After 24 h, cells were fixed and sequentially incubated with anti-myc and Alexa-488 anti-rabbit antibodies. Myc-tagged SdpI, SdpII-L, SdpII-S and Dlc1 but not GFP colocalized with the cytoplasmic aggregates of gephyrin formed upon co-expression. Note that gephyrin cytoplasmic distribution varied upon co-expression with myc-SdpI, myc-SdpII-L or myc-SdpII-S. Arrows point to membrane associated of colocalization; arrowheads indicate colocalization in cytoplasmic gephyrin aggregates. Scale bar: 10 μm.

These results confirm that the above described *in vitro* interaction between SdpI and gephyrin (4.1.3.1) also occurs in mammalian cells. They also show that both splice variants of SdpII also bind to gephyrin in COS-7 cells. In these colocalization experiments, the extent of overlap of myc-SdpI with mRFP-gephyrin immunoreactivity varied. Specifically, a colocalization of both proteins was frequently seen in the plasma membrane and less frequently in cytoplasmic aggregates of reduced size (see Fig. 4.9). The number of cells showing cytoplasmic gephyrin aggregates was significantly reduced in cells co-expressing myc-SdpI and mRFP-gephyrin (15.6 ± 2.2 %) as compared to cells co-expressing myc-Dlc1, or GFP, and mRFP-gephyrin (35.6 ± 4.4 % and 37.7 ± 3.3 % for myc-Dlc1 and GFP, respectively; 300 cells per sample, n=3, $p < 0.05$). These results indicate that SdpI expression redistributes gephyrin upon co-expression in a heterologous system and suggest that SdpI is a binding protein which contributes to, or induces, gephyrin submembraneous clustering.

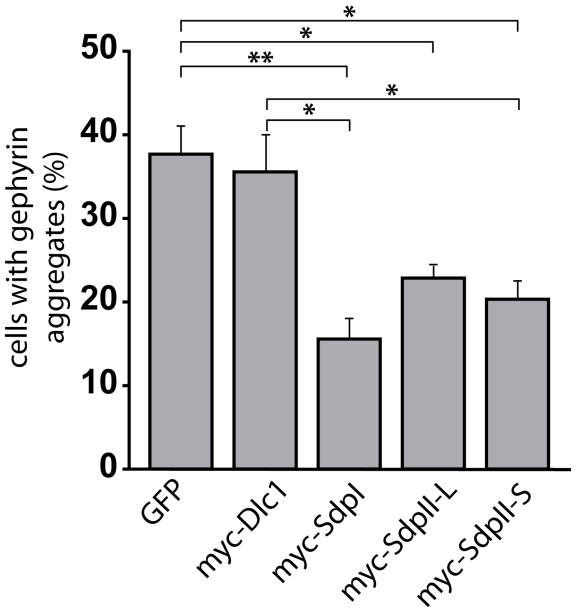

Fig. 4.10. Effect of SdpI and SdpII co-expression in gephyrin blob formation in COS-7 cells. Quantification of cells showing cytoplasmic gephyrin aggregates in the experiment shown in **Fig. 4.9**. The number of COS-7 cells displaying gephyrin aggregates decreased when gephyrin was co-expressed with myc-SdpI, myc-SdpII-L and myc-SdpII-S, but not myc-Dlc1 as compared to GFP co-expression. The number of cells displaying gephyrin aggregates was also reduced in myc-SdpI and myc-SdpII-S co-expressing cells as compared to myc-Dlc1 + mRFP-gephyrin co-expressing cells. Values represent means ± SEM (n=3). Significant differences as compared to GFP and myc-Dlc1 co-expression with mRFP-gephyrin: *, $p < 0.05$; **, $p < 0.01$.

4.1.4 SdpI competes with gephyrin for binding to GlyRβ$_{78}$

As shown above, the gephyrin and SH3 binding sites are both located in the large intracellular loop of the GlyRβ subunit**.** The gephyrin binding motif in the GlyRβ loop comprises amino acids 394-411 (Meyer et al., 1995), whereas the SdpI binding site lies C-terminally of the gephyrin binding-motif, i.e. within residues 427 to 448 (see 4.1.1.2). Since both binding sites are separated by only 16 residues, we investigated whether the interaction of gephyrin with GlyRβ might influence the ability of SdpI to bind the receptor. To address this question, GST pull-down experiments were performed as mentioned under 4.1.1, but increasing amounts of lysates containing the His_6-tagged gephyrin-E-domain (His-GE) were added to the His_6-tagged SdpI-containing lysates (His-SdpI). After Western blot detection with anti-His_6 antibody, His-SdpI and His-gepyrin-E-domain were distinguished by their different molecular weights, 54 kDa and 47 kDa, respectively (Fig. 4.11.A). The addition of 0.1 µl of His-GE lysate already reduced the amount of SdpI protein bound, and increasing concentrations of His-GE proportionally inhibited the binding of His-SdpI to GST-GlyRβ$_{78}$. SdpI band intensities were reduced to 61.3 ± 10.3 %, 42.3 ± 14.2 %, 24.2 ± 6.6 % and 2.1 ± 1.3% of control in the presence of 0.1, 1, 10 and 100 µl of His-GE lysate, respectively (n=4). The addition of 100 µl of the His-GE lysate completely blocked SdpI-binding to GST-GlyRβ$_{78}$ (Fig. 4.11.B). Since SdpI does not bind to the E-domain of gephyrin (see 4.1.3.1), a direct inhibition of gephyrin binding by the SdpI-GlyRβ$_{78}$ interaction can be excluded. Thus, binding of the E-domain of gephyrin appears to be sufficient to sterically impair the interaction of SdpI with the intracellular loop of GlyRβ. However, since the E-domains of gephyrin dimerize during postsynaptic scaffold formation (Sola et al., 2004), the biological role of E-domain interference with SdpI binding remains unclear.

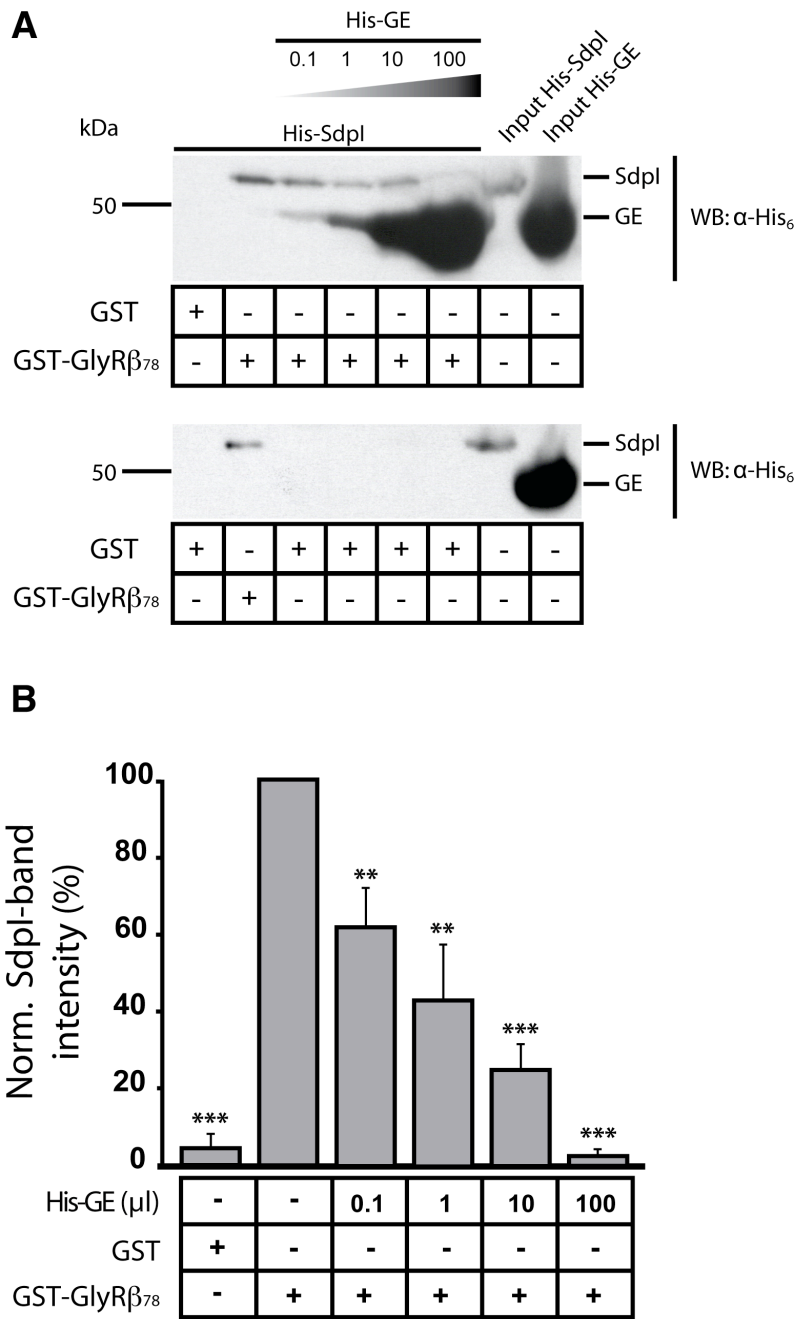

Fig. 4.11. SdpI competes with gephyrin for binding to the GlyRβ subunit. A. Anti-His_6 immune detection of SdpI and GE after pull-down with GST and GST-GlyRβ_{78} fusion proteins. The His-SdpI lysate was incubated with increasing concentrations of His-Gephyrin-E-domain (His-GE) prior to pull-down. The addition of His-GE inhibited His-SdpI binding to GST-GlyRβ_{78} (top panel). No binding of His-GE or His-SdpI to GST was observed (bottom panel). **B.** Quantification of relative His-SdpI band intensities obtained in the GST-pull-down experiments shown in **A.** Addition of 0.1 μl of His-GE lysate significantly reduced His-SdpI binding to GST-GlyRβ_{78}. Subsequent addition of 1 and 10 μl of His-GE lysate increasingly reduced His-SdpI binding to GST-GlyRβ_{78}. The addition of 100 μl of His-GE lysate blocked His-SdpI binding to GST-GlyRβ_{78} to a similar extent as seen with unspecific binding of His-SdpI to GST. Values represent means ± SEM (n=4). Significant differences as compared to control (GST-GlyRβ_{78} + His-SdpI) : **, $p < 0.01$; ***, $p < 0.001$.

4.1.5 Localization of SdpI in spinal cord neurons

SdpI is specifically expressed in neurons, and previous studies have reported its presynaptic localization by fluorescence microscopy, and its peri- and postsynaptic distribution at asymmetric synapses by electron microscopy (Qualmann et al., 1999;Pérez-Otaño et al., 2006). However, the presence of SdpI at inhibitory synapses and its colocalization with inhibitory synaptic markers have not been investigated. Upon subcellular fractionation of rat spinal cord homogenate and Western blotting, SdpI was detected in the fraction containing small membraneous organelles, suggesting an association of SdpI with intracellular membranes of spinal cord neurons (see Fig. 4.20).

To gain further insight into the distribution of Sdp at different stages of neuronal differentiation, double immunostainings were performed with primary rat spinal cord neurons grown for 11-13 and 20-22 DIV, respectively. Neurons were co-stained with the anti-SdpI antibody kindly provided by Dr. B. Qualmann (Qualmann et al., 1999) and several markers of excitatory (PSD95) and inhibitory (VIAAT, GAD67) presynaptic terminals as well as of inhibitory postsynapses (GlyR, gephyrin). After incubation with anti-mouse Alexa-488 and anti-rabbit Alexa-546 secondary antibodies, fluorescence signal distributions along 50 μm of neuronal processes were analysed in an AxioImager microscope equipped with an Apotome grid projector (Zeiss). This revealed that SdpI staining was present in neuronal cell bodies and enriched along neuronal processes in intensely stained punctate structures (see Fig. 4.12.A, middle panel). Importantly, these punctate SdpI-positive structures colocalized to some extent with the immunoreactive spots of excitatory and inhibitory markers (see Fig. 4.12.A).

Since the GlyRβ subunit is a key determinant of the synaptic clustering of GlyRs at inhibitory synapses, a prerequisite for a functional interaction between SdpI and the GlyRβ subunit at synaptic sites is their *in situ* colocalization at inhibitory postsynapses *in vivo*. A partial colocalization was found along neurites double-stained with anti-SdpI and anti-GlyR, anti-gephyrin as well as anti-VIAAT antibodies. To establish the presence of SdpI at inhibitory synapses, colocalization ratios with SdpI puncta were quantified. At 11-13 DIV, SdpI was often detected near GlyR puncta (27 ± 2 % colocalization rate Fig. 4.12.B). This value was significantly lower than the VIAAT colocalization rate (40 ± 3 %, $p < 0.05$) whereas gephyrin colocalization with SdpI (40 ± 9 %) was comparable to that seen for VIAAT.

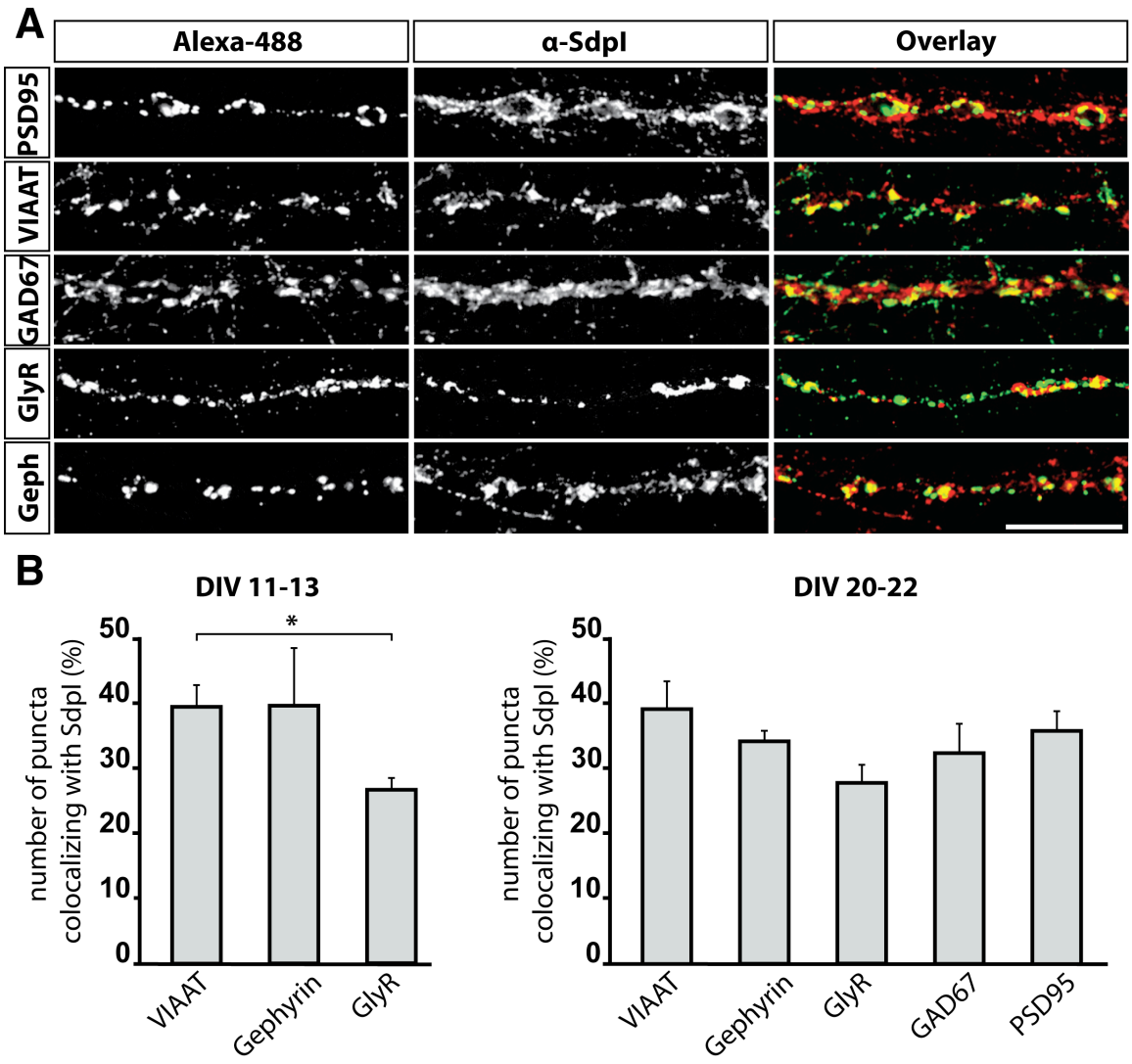

Fig. 4.12. Localization of SdpI in processes of rat spinal cord neurons. A. Spinal cord neurons were fixed and double-stained with SdpI antibody and antibodies against several inhibitory (gephyrin, glyR, VIAAT, GAD67) and excitatory (PSD95) synaptic markers. Note yellow signals indicating clear co-localization of SdpI-stained punctate structures with all synaptic markers used (overlays). Scale bar: 10 μm **B**. Quantification of the experiment shown in **A**. Percentages of immunoreactive spots of each synaptic marker colocalizing with SdpI were quantified. Values represent means ± SEM (n=3). Significant differences as compared to VIAAT staining: *, $p < 0.05$.

From these results we conclude that SdpI is present at inhibitory synapses. Due to the low resolution that conventional fluorescence microscopy offers, pre- and postsynaptic localizations of SdpI at inhibitory synapses cannot be distinguished. Additionally, the difference in SdpI colocalization with GlyRβ and gephyrin suggests that, at this stage of differentiation, SdpI is present at both glycinergic and GABAergic synapses.

To determine whether the SdpI puncta observed had a predominantly excitatory or inhibitory synaptic localization, colocalization rates were determined for different synaptic marker proteins

as above but at a later stage of *in vitro* development (20-22 DIV, Fig. 4.12.A). Interestingly, similar colocalization values were found for excitatory and inhibitory presynaptic and postsynaptic markers (PSD95: 36 ± 3 %, VIAAT: 39 ± 4 %, gephyrin: 34 ± 2 %; n=3) in these experiments. This confirms that SdpI is present at excitatory as well as at inhibitory synapses (Fig. 4.12.B). Also, the percentages of SdpI puncta colocalizing with a presynaptic marker for GABAergic synapses and for GlyR revealed no major difference in relative colocalization rates (32 ± 5 % and 27.8 ± 2.7% for GAD67 and GlyR, respectively, n=3, $p > 0.05$). These results suggest that SdpI might be present at GABAergic, glycinergic and possibly also mixed GABA-glycinergic synapses.

4.1.6 Analysis of SdpI function at inhibitory synapses

Sdps are proteins involved in endocytosis and recycling processes. The *in vitro* binding experiments presented above (see 4.1.1, 4.1.2 and 4.1.3) show that SdpI and SdpII bind to the GlyRβ loop and gephyrin. Based on these results, a possible role of SdpI as GlyR trafficking factor was examined. First, co-immunoprecipitation studies with the cytoplasmic vesicle-rich fraction of rat spinal cord homogenates were performed. Subsequently, the localization of GlyRs in SdpI deficient mice and the effects of SdpI down-regulation in rat spinal cord neurons were analyzed.

4.1.6.1 SdpI and the GlyR form complexes in vesicles

The immunocytochemical experiments described above show that SdpI colocalizes with punctate GlyR immunoreactivity, suggesting that SdpI and GlyR might form complexes *in vivo* (see 4.1.5). To investigate whether SdpI and the GlyR are associated endogenously in neurons, co-immunoprecipitation experiments were performed with spinal cord homogenates. After overnight incubation of a detergent extract prepared from the cytoplasmic vesicle-enriched fraction of a rat spinal cord homogenate with the SdpI antibody and subsequent incubation with protein G beads, the bound protein complexes were analysed by SDS-PAGE and Western blotting. Immunodetection with the mAb4 antibody, which recognizes GlyR subunits, revealed the presence of a band with a molecular weight of around 48 kDa corresponding to that of the α1 subunit of the GlyR in the input, supernatant and the immunoprecipitate obtained with anti-SdpI, but not in the precipitate obtained with an unspecific IgG (Fig. 4.13). This result is consistent with SdpI and the GlyR being associated in intracellular vesicles of spinal cord neurons *in vitro.*

Fig. 4.13. The GlyR co-immunoprecipitates with SdpI from detergent extracts of a vesicle-enriched fraction from spinal cord. Detergent extracts from spinal cord homogenates were pre-cleared with protein G-Sepharose and incubated overnight with the corresponding antibody. Antibody-protein complexes were precipitated by incubation with protein G-Sepharose beads. After repeated washing, bound protein complexes were eluted from the beads and analysed by SDS-PAGE followed by Western blot with anti-GlyR antibodies (mAb4). Note that GlyRα subunits (MW around 48 kDa) co-precipitated upon incubation with SdpI, but not unspecific IgG antibodies. Bands above 50 kDa in the immunopellet containing SdpI antibodies result from an unspecific reaction of the primary or secondary antibodies with the light chain of the SdpI antibody.

4.1.6.2 Analysis of glycine receptor clustering in SdpI deficient neurons

The data presented above suggested that the SdpI-GlyR interaction may take place in cytosolic vesicles, and hence may be important for GlyR trafficking. To investigate whether SdpI is essential for GlyR transport, the synaptic localization of GlyRs was examined in neurons isolated from SdpI KO mice. Spinal cord neurons were prepared from SdpI -/- and wildtype mice and cultured *in vitro* using our standard protocol (see 3.5.5). At 20-22 DIV, the cultures were double-stained with the mAb4 and VIAAT antibodies. Fluorescences were analyzed as described under 3.5.11. The direct inspection of neuronal morphology and neurite formation did not reveal any obvious impairment in the neuronal development of SdpI -/- spinal cord neurons. GlyR clusters colocalized with VIAAT staining in both wildtype and SdpI -/- neurons (Fig. 4.14). To investigate the distribution of GlyR in more detail, the number and average size of GlyR immunoreactive clusters along 50 μm of neuronal processes proximal to the soma were analyzed using the ImageJ software. Automated image analysis revealed that the number of GlyR clusters per 50 μm neurite did not differ between wildtype (41.7 ± 3.0 IR-spots) and SpdI -/- neurons (41.4 ± 5.3 IR-spots; 10 neurons each; n=5; $p > 0.05$), and that the GlyR mean cluster size was not significantly reduced upon SdpI -/- deficiency (76.4 ± 10.3 % of control; 10 neurons each; n=5; $p > 0.05$) (see Fig. 4.14.B). These results indicate that GlyR trafficking and synaptic clustering is not impaired in the absence of SdpI in 20-22DIV spinal cord neurons.

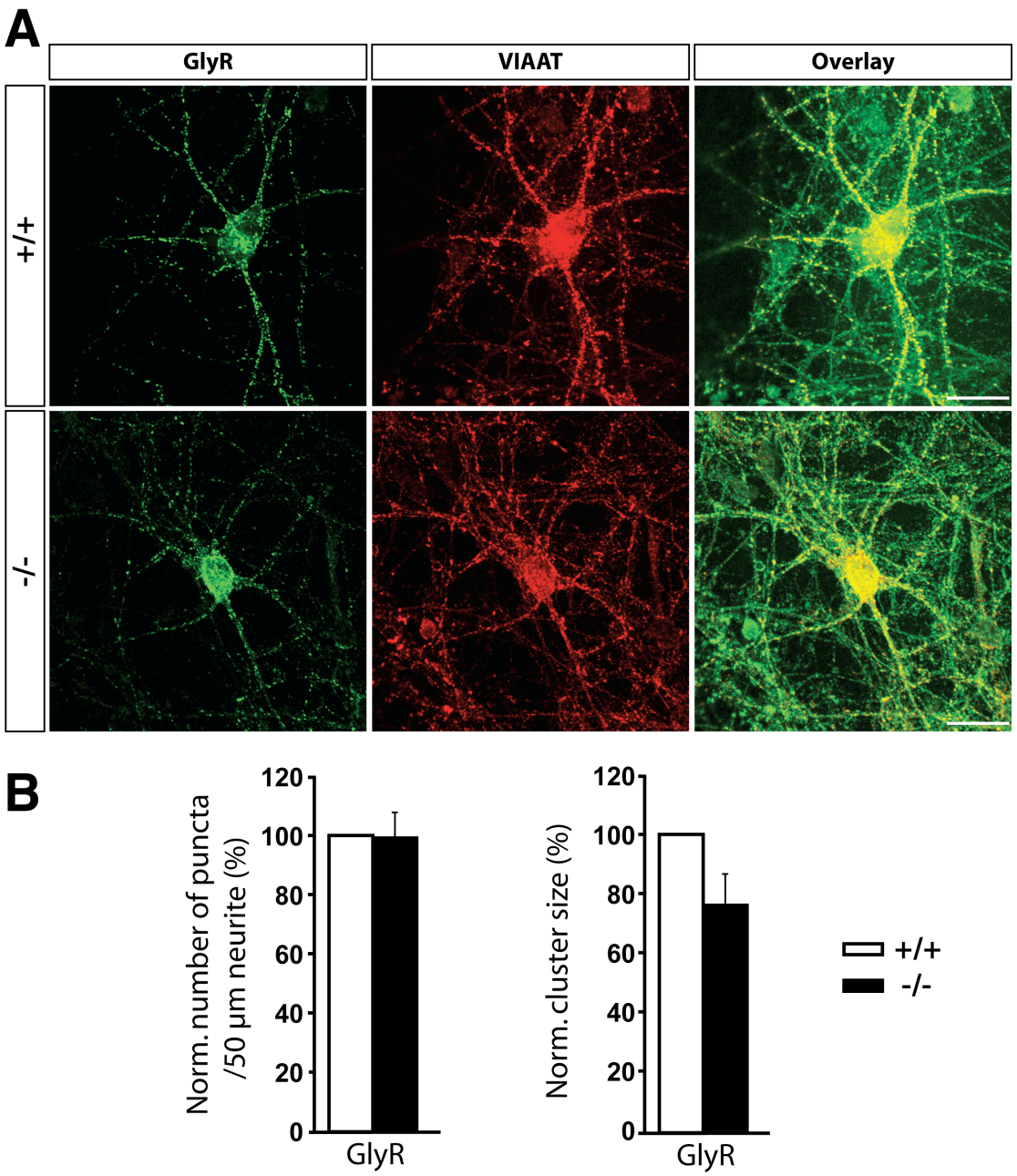

Fig. 4.14. GlyR clusters in cultured +/+ and SdpI-/- spinal cord neurons. A. DIV20-22 spinal cord neurons cultured from +/+ or SdpI-/- mouse embryos were fixed and stained with primary mAb4 and VIAAT antibodies as well as the corresponding secondary antibodies, anti-mouse Alexa-488 and anti-rabbit Alexa 546. Note that regardless of genotype GlyR clusters are present along neurites and co-localize with VIAAT-enriched puctate structures in the overlay (left panel in yellow). Scale bar: 20 μm **B**. Quantification of the experiments shown in **A**. Number of GlyR puncta per 50 μm neurite and average size of GlyR clusters were quantified with the ImageJ software. Values represent means ± SEM (n=5). No significant differences as compared to +/+: $p > 0.05$.

Spinal cord neurons can be maintained in culture only up to four weeks. To investigate a possible contribution of SdpI to GlyR trafficking mechanisms at later developmental stages, the distribution of synaptic GlyR clusters was also analysed in brainstem sections prepared from adult wildtype and SdpI -/- mice. Specifically, cryostat sections from brainstems of wildtype and

littermate SdpI -/- mice were fixed and double-stained (3.5.10.2) with VIAAT and mAb4, or mAb7, antibodies to reveal presynapses as well as GlyR and gephyrin clusters, respectively. Both the GlyR and gephyrin puncta colocalized with VIAAT in wildtype and SdpI -/- mice (data not shown). Also, GlyR cluster numbers per 30 μm^2 field were similar for wildtype (16.7 ± 2.7 IR-spots) and SdpI -/- mice (16.7 ± 1.6 IR-spots). Additionally, quantification of the GlyR mean cluster size showed no significant change in SdpI -/- (98.2 ± 24.3 % of control, n=3, $p > 0.05$) as compared to wildtype mice (see Fig. 4.15.A and B). Similarly, the analysis of gephyrin clusters did not disclose any significant change in cluster density/ 30 μm^2 and mean cluster size in SdpI -/- (92.8 ± 6.5 % and 95.5 ± 8.5 % of control, respectively) as compared to littermate wildtype mice (see Fig. 4.15.A and B). Based on these results we conclude that SdpI is not a limiting factor for GlyR and gephyrin trafficking to inhibitory synaptic sites in both developing and adult SdpI -/- neurons.

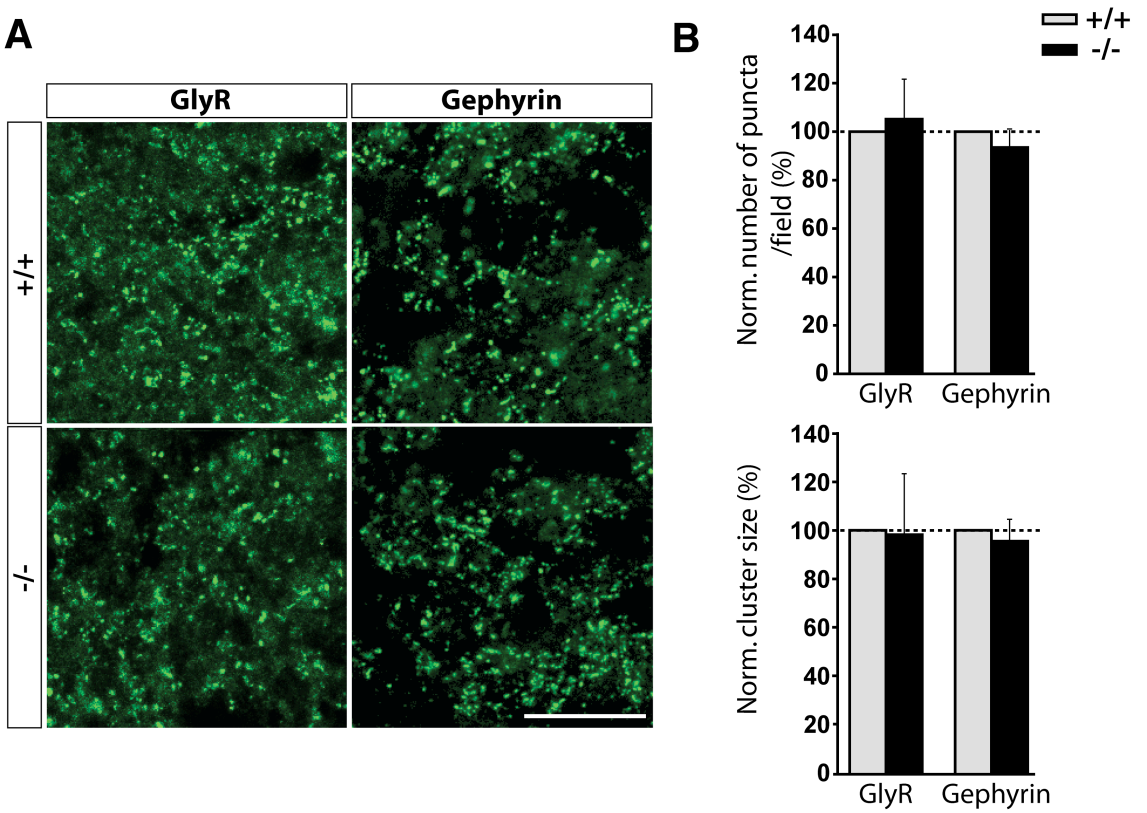

Fig. 4.15. GlyR distribution analysis in brainstem of +/+ and SdpI-/- mice. A. Brain stem-sections of adult +/+ and SdpI-/- mice were stained with the mAb4 and mAb7 antibodies to detect GlyR and gephyrin clusters, respectively. Scale bar: 20 μm**. B**. Quantification of the experiments shown in **A**. Number of GlyR and gephyrin puncta per optical field and average size of GlyR as well as gephyrin clusters were quantified with the ImageJ software. Shown are mean values ± SEM (n=5). No significant differences as compared to +/+ : p-value > 0.05.

4.1.6.3 GlyR distribution in rat spinal cord neurons after acute SdpI down-regulation

The results presented above indicate that SdpI and both splice variants of SdpII interact directly with the GlyRβ subunit (see 4.1.1.1). However, SdpI-/- neurons and mice did not show any changes in GlyR and gephyrin cluster densities and sizes. Alternative transport mechanisms or a redundant function of Sdps in GlyR trafficking might explain our negative results. Here, acute SdpI knock-down experiments were performed to investigate whether the function of SdpI might be compensated. To down-regulate SdpI in neurons, a sequence for the knock-down of SdpI by RNA interference, kindly provided by Dr. Britta Qualmann, was cloned into a second generation small-hairpin interference RNA vector (miR). Since standard lipid-mediated transfection methods function unefficiently in spinal cord neurons, a recombinant adeno-associated viral system was employed to reach a high infection rate. The SdpI-miR sequence was then cloned into a recombinant adeno-associated viral vector (rAAV). Additionally, myc-tagged SdpI resistant to SdpI-miR was also cloned into a rAAV vector in order to rescue SdpI expression (SdpI-siR). Then 6-7 DIV spinal cord neurons were infected with equivalent infectious units (i.u.) of rAAV viruses containing the SdpI-miR sequence (SdpI-miR-rAAV) or a control miR vector (cont-miR-rAAV). For the rescue experiment, the neurons were co-infected with two rAAV viruses encoding SdpI-miR-rAAV and SdpI-siR-rAAV, respectively. In our cultures, rAAV viruses showed an infection efficiency of ~50%. Cont-miR-rAAV and SdpI-miR-rAAV infected neurons were identified by direct observation due to GFP reporter gene expression encoded in the rAAV vector. SdpI-siR-rAAV infection was detected by myc staining.

In initial control experiments, neurons were harvested at 20-21 DIV, and their protein contents were analysed by Western blot. β3-Tubulin, analyzed to check for cell viability, showed a significant reduction upon SdpI-miR-rAAV infection as compared to cont-miR-rAAV infection (see Fig. 4.16.A). This reduction in β3-tubulin content was strictly increased upon co-infection of the SdpI-miR and SdpI-siR viruses, indicating that viral infection reduced the survival of neural or glial cells. We then determined SdpI protein concentrations as normalized to the β3-tubulin band to monitor SdpI downregulation. Western blotting with an anti-SdpI antibody revealed a ~60% reduction in SdpI protein content upon infection with the SdpI-miR-rAAV virus (39.0 ± 15.8 % of control) as compared to control-miR virus (Fig. 4.16.B). This indicates that the SdpI-miR sequence effectively down-regulates the expression of the SdpI protein. Additionally, when SdpI-siR was incubated in the presence of SdpI-mIR, Western blot analysis showed about 8-fold increase in SdpI expression (Fig. 4.16.A, right lane), indicating that SdpI-siR-rAAV induced the

overexpression of SdpI in spinal cord neurons in the presence of SdpI-miR-rAAV and thus allowed rescue of SdpI expression.

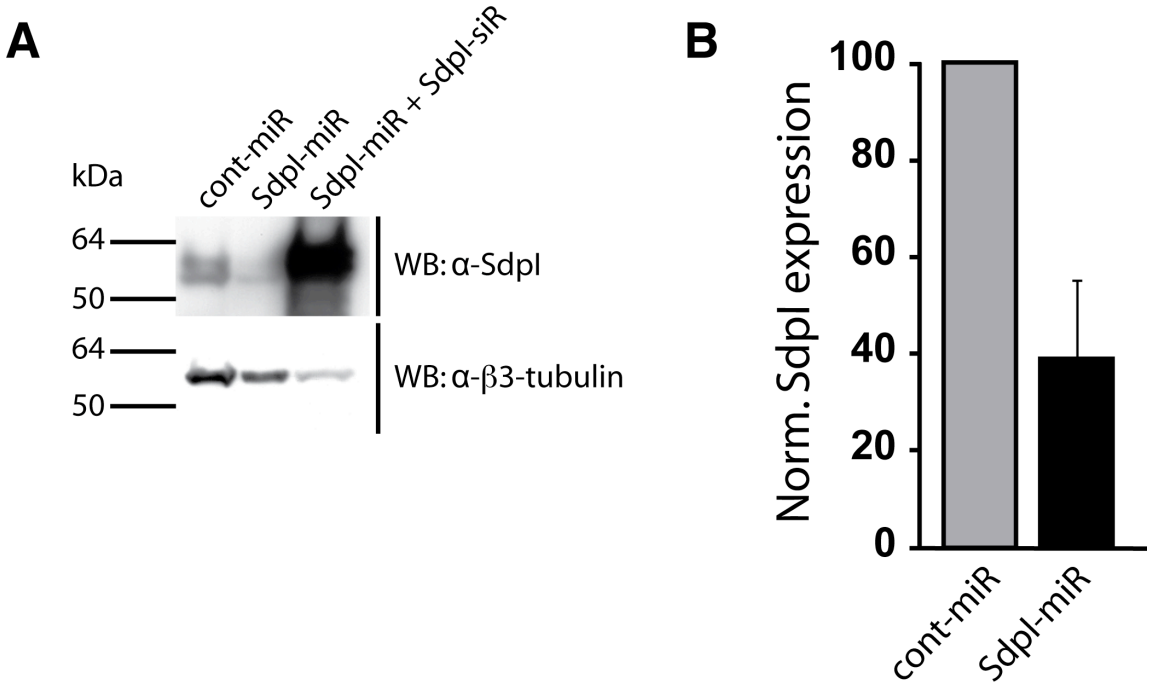

Fig. 4.16. Knock-down of SdpI in spinal cord neuron cultures. A. Spinal cord neurons were infected at DIV7 with control-miR, SdpI-miR, and SdpI-siR virus. DIV20 spinal cord neurons were harvested and homogenates were analyzed by Western blotting with anti-SdpI and anti-β3 tubulin antibodies. **B**. Quantification of band intensity of SdpI normalized to β3-tubulin expression in western blots of three independent experiments. SdpI band expression was significantly decreased in neurons infected with the SdpI-miR virus when compared to neurons infected with a control-miR virus ($p < 0.05$).

In order to investigate the effects of SdpI down-regulation on GlyR cluster distribution, spinal cord neurons were infected from DIV7 to DIV20 with cont-miR-rAAV, SdpI-miR-rAAV and SdpI-miR-rAAV + SdpI-siR-rAAV. Cont-miR-rAAV and SdpI-miR-rAAV infection was monitored by endogenous GFP expression. GlyR and SdpI-siR expression was detected with mAb4 and myc antibodies, which stained GlyR and myc-tagged SdpI-siR proteins respectively. Staining with the corresponding secondary antibodies Alexa-635-anti-mouse and Alexa-546-anti-rabbit allowed to monitor the expression of the three proteins. Fluorescences from the GFP, myc-546 and GlyR-635 channels were analysed as described in 4.1.6.2. Subsequently, GlyR cluster numbers and average sizes in cont-miR and SdpI-miR infected neurons were determined along 50 μm neurite (n=10) in the proximity of the soma of GFP-positive neurons. These analyses showed that upon SdpI down-regulation GlyR cluster numbers/50 μm were reduced from 35.9 ± 6.1 in control-miR

infected neurons to 16.9 ± 3 in SdpI-miR infected neurons (~50 % reduction, n=3, $p < 0.01$)(see Fig. 4.17). In the same neurons, GlyR mean cluster size dropped from 2.3 ± 0.1 μm^2 in cont-miR infected to 1.6 ± 0.3 μm^2 in SdpI-miR infected neurons (~30% reduction, n=3, $p < 0.05$)(see Fig. 4.17). In rescue experiments with doubly SdpI-miR-rAAV + SdpI-siR-rAAV infected neuronal cultures, GlyR clusters were examined in cells double-positive for GFP and myc expression. In these cells, GlyR cluster density rose from 48.0 ± 6.7% upon SdpI knock-down to 111.8 ± 23.6 % of control upon SdpI-siR co-expression (16.9 ± 3 immunoreactive puncta/50 μm in SdpI-miR vs. 37.2 ± 2.4 puncta in doubly SdpI-miR + SdpI-siR infected neurons; n=3, $p < 0.05$). Similarly, the reduction of GlyR mean cluster size to 69.5 ± 9.4 % of control observed upon SdpI down-regulation was fully rescued upon SdpI-siR overexpression to 125.9 ± 4.3 % of control (1.6 ± 0.3 μm^2 in SdpI-miR vs. 2.9 ± 0.1 μm^2 in double-infected neurons, respectively; n=3, $p < 0.05$).

Together these results indicate that the acute downregulation of SdpI impairs GlyR clustering at inhibitory synaptic sites. Furthermore, they also suggest that Sdps are implicated in a GlyR transport mechanism, which is not strictly SdpI-dependent, but may also use other Sdp isoforms or other trafficking proteins. Finally, our rescue experiments confirm that the reductions in GlyR number and mean cluster size observed upon SdpI down-regulation are indeed specific, i.e. SdpI-dependent.

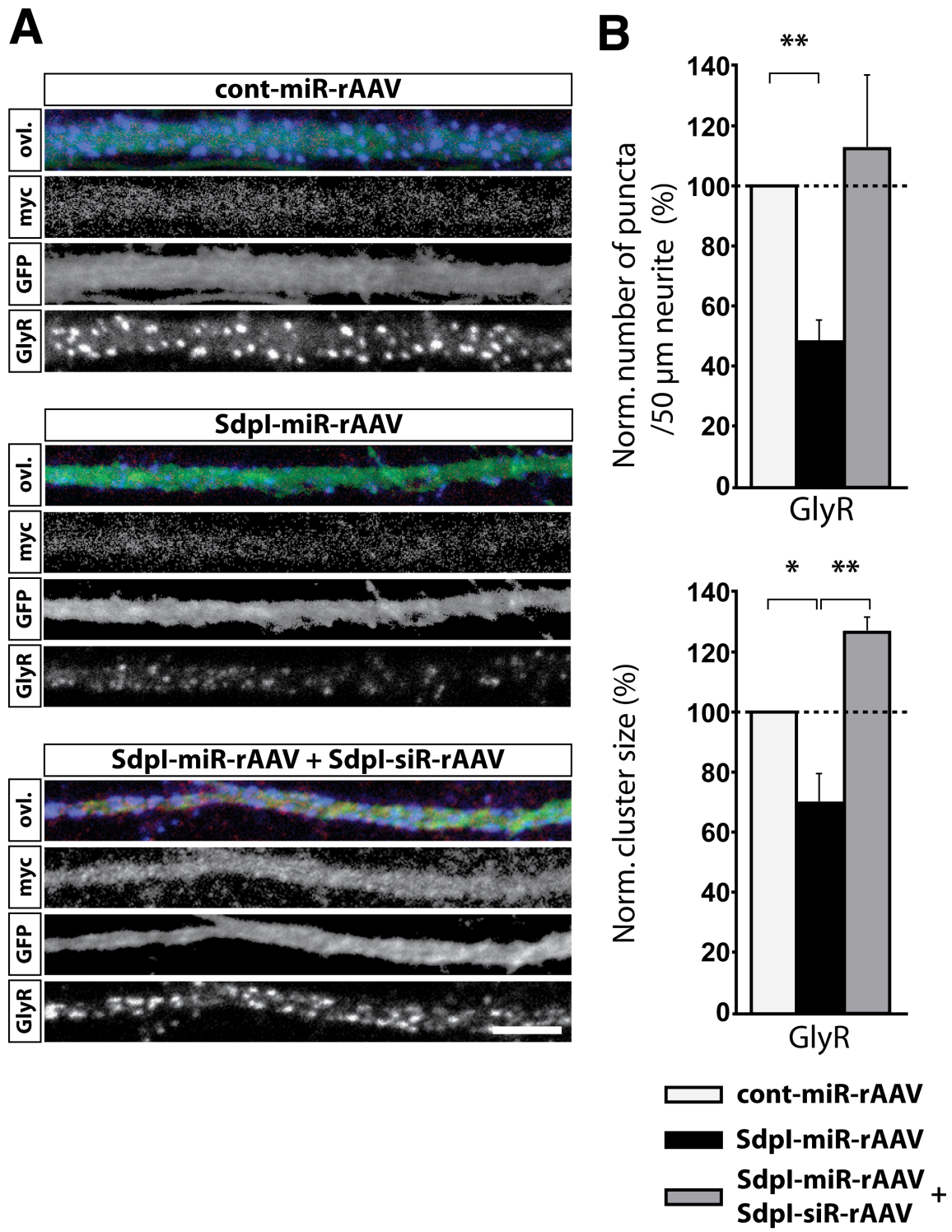

Fig. 4.17. SdpI knock-down reduces GlyR cluster and size. A. Rat spinal cord neurons were infected at DIV7 with cont-miR-rAAV, SdpI-miR-rAAV and double-infected with SdpI-miR-rAAV + SdpI-siR-rAAV. DIV20 neurons were fixed and stained with mAb4 and myc antibodies as well as the corresponding secondary antibodies, Alexa-635-anti-mouse and Alexa-546-anti-rabbit, to detect GlyR and SdpI-siR proteins. miR-rAAV infection induced GFP reporter gene expression. Scale bar: 5 μm. **B**. Quantification of the experiments shown in **A**. Number and average size of GlyR clusters per 50 μm neurite were determined. Values represent means ± SEM nomalized to control-miR-rAAV infection (n=3). Significant differences compared to control-miR-rAAV infected neurons: *, $p < 0.05$; **, $p < 0.01$

4.1.6.4 Effect of SdpI down-regulation on the synaptic localization of different inhibitory pre- and postsynaptic proteins

Our gephyrin/Sdp colocalization data had suggested that Sdps may contribute to gephyrin's association with the plasma membrane (see 4.1.3.2). To find out whether SdpI may contribute to gephyrin trafficking, both gephyrin and GlyR clusters were analyzed under the same SdpI-knockdown conditions as used above (see 4.1.6.3). To this end, spinal cord neurons infected at DIV7 with cont-miR or SdpI-miR were fixed at DIV20-21 and stained with mAb7 or mAb4a and the corresponding secondary Alexa-546-anti-mouse antibodies (Fig. 4.18.A). Images of the gephyrin and GlyR clusters in proximal neurites of GFP expressing neurons were collected and analyzed as detailed under 4.1.6.3. This disclosed a slight but not significant reduction in gephyrin cluster density of ~10% (89.5 ± 18.5 % of control) in neurons with SdpI down-regulation as compared to control neurons (n=3, each; $p > 0.05$). In contrast, GlyR cluster densities were again reduced by ~30% in the down-regulated neurons (67.8 ± 11.6 % of control; n=3, $p < 0.05$). The analysis of gephyrin cluster size showed a reduction to 72.8 ± 21.3 % of control in neurons with SdpI down (n=3, $p > 0.05$) (see Fig. 4.18.B). However, when mean GlyR cluster sizes were analyzed in cont-miR and SdpI-miR infected neurons, a highly significant reduction was found (55.7 ± 7.9 % of control; n=3, $p < 0.01$). In summary, SdpI knock-down induces highly significant changes in mean GlyR cluster numbers and sizes whereas mean gephyrin cluster numbers and sizes are only slightly but not significantly reduced. Thus, SdpI appears to be important for GlyR but not gephyrin synaptic distribution.

To investigate whereas changes in GlyR cluster number and size affect presynaptic differentiation, VIAAT staining was analyzed under SdpI knock-down conditions. Images of VIAAT fluorescence in proximal neurites from GFP expressing neurons were collected and analyzed as described above. This revealed no significant difference in densities of VIAAT immunoreactive terminals between SdpI-miR (96.8 ± 13.9 % of control; n=3, $p > 0.05$) and cont-miR infected neurons. In contrast, the mean size of VIAAT puncta was reduced to 73.8 ± 13 % of control upon SdpI down-regulation (Fig. 4.18.B). However this reduction was not significant (n=3; $p > 0.05$), indicating that SdpI depletion does not primarily disrupt inhibitory presynaptic function.

Previous studies have demonstrated that SdpI localizes near GAD67 in spinal cord neurons (4.1.5). In order to investigate whether SpdI function is restricted to GlyR clustering, $GABA_AR$ clusters were also examined under SdpI knock-down conditions. For the staining of $GABA_ARs$,

antibodies against the $GABA_AR\gamma2$ subunit were employed, and synaptic images were collected and evaluated as mentioned under 4.1.6.3. SdpI-miR infected neurons exhibited 23.0 ± 7.6 immunoreactive puncta per 50 μm neurite, and cont-miR infected neurons 35.5 ± 7.2 per 50 μm neurite (reduction to 62.8 ± 9.9 % of control; n=3, $p < 0.05$). $GABA_AR\gamma2$ clusters exhibited an average size of 2.6 ± 0.6 μm^2 in cont-miR and of 1.4 ± 0.2 μm^2 in SdpI-miR infected neurons (reduction to 56.6 ± 5.2 % of control; n=3, $p < 0.01$) (see Fig. 4.18.B). In conclusion, about 40% and ~45% reductions in $GABA_AR\gamma2$ mean cluster number and size were observed in neurons upon SdpI down-regulation. Thus, the loss of SdpI affects both GlyR and $GABA_AR$ synaptic localization.

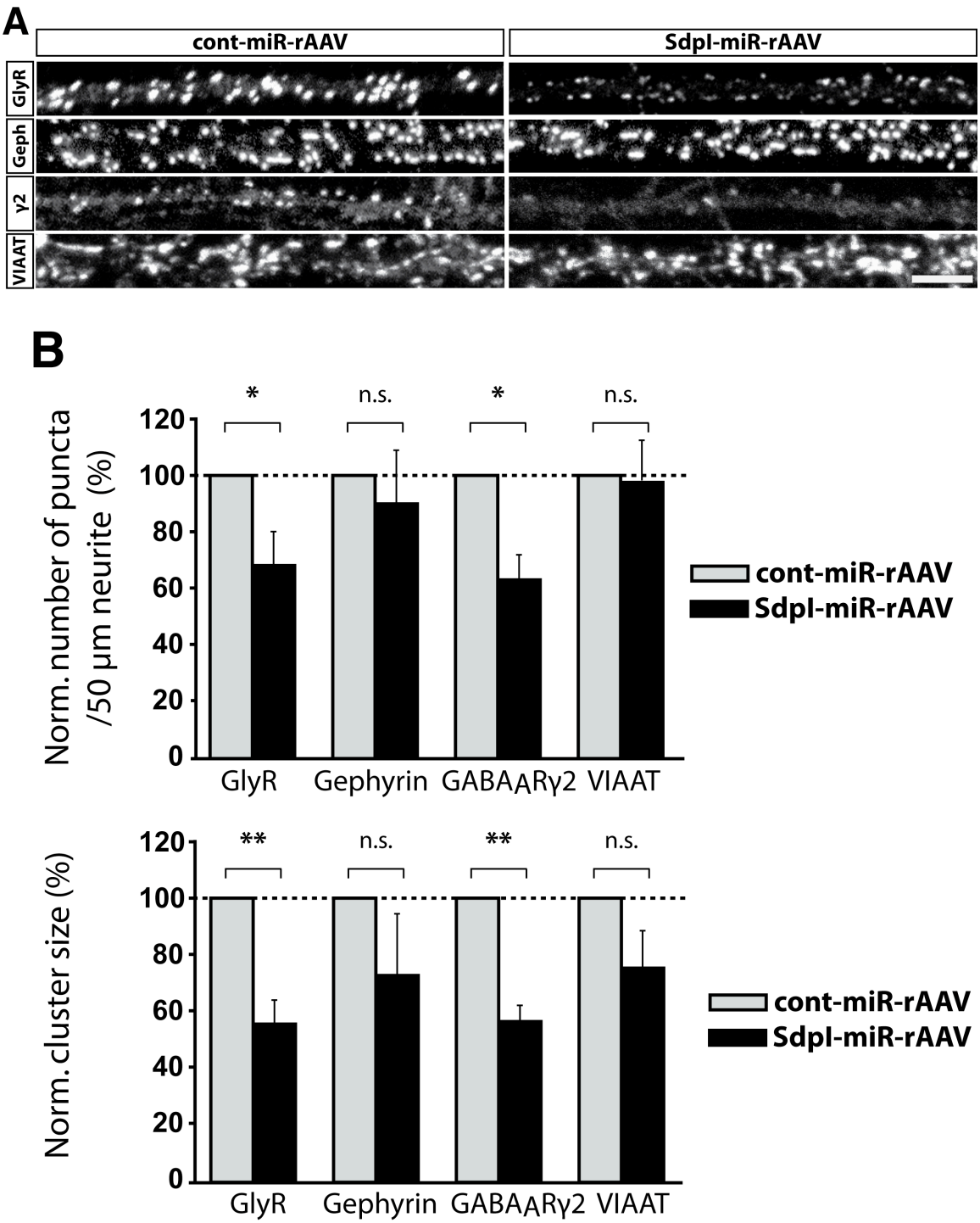

Fig. 4.18. SdpI knockdown affects inhibitory postsynaptic receptor clustering. A. Rat spinal cord neurons were infected at DIV7 with cont-miR-rAAV and SdpI-miR-rAAV. DIV20-21 neurons were fixed and stained with mAb4, mAb7, γ2 and VIAAT antibodies as well as the corresponding secondary antibodies, Alexa-546-anti-mouse or anti-rabbit, to detect GlyR, gephyrin, $GABA_AR\gamma2$, and the vesicular inhibitory aa tranporter. miR-rAAV infection induced GFP reporter gene expression. Scale bar: 5 μm. **B.** Quantification of the experiments shown in **A**. Numbers and average sizes of puncta per 50 μm neurite were determined with the ImageJ software. Values represent means ± SEM nomalized to control-miR-rAAV infection (n=3). Significant differences as compared to control-miR-rAAV infected neurons: *, $p < 0.05$; **, $p < 0.01$

4.2 Analysis of the interaction between vacuolar protein sorting 35 (Vps35) and the GlyRβ subunit

In addition to the proteomic screen in which SdpI was isolated (4.1), another screen was performed in an attempt to find other new binding partners for GlyRβ. In this screen, a GST fusion protein encompassing 49 amino acids (positions 378 to 426) of the intracellular loop between transmembrane domains 3 and 4 of the GlyRβ subunit ($GlyR\beta_{49}$) was utilized as bait for the isolation of binding proteins from a rat brain detergent extract. One of the protein bands found exhibited an apparent molecular weight of about 90 kDa and was identified by matrix-assisted laser desorption/ionisation-time of flight mass spectrometry (Maldi-ToF) analysis as Vps35 (I. Paarmann et al., unpublished data).

4.2.1 *In vitro* analysis of the interaction between Vps35, the GlyRβ subunit and gephyrin

As for SdpI (4.1.1), a GST pull-down assay was employed here in order to investigate the interactions between Vps35 and other putative binding proteins. Vps35 is part of the retromer complex and interacts with Vps29 (see introduction 2.4.2.1). Therefore a GST-tagged Vps29 construct was used as positive control for Vps35 binding in GST pull-down experiments. GST fusions of $GlyR\beta_{49}$, gephyrin, Vps29 and GST alone were incubated with a bacterial lysate containing the recombinant His_6-tagged Vps35 (His-Vps35). A His_6-tagged fragment of collybistin II (first 240 aa) served as a positive control for gephyrin binding (I.Paarmann, unpublished). Anti-His_6 Western blot analysis revealed a band of about 94 kDa, corresponding to the expected molecular weight of His-Vps35 that was found with the GST-fusion of Vps29 and the GST fusions of $GlyR\beta_{49}$ and gephyrin but was absent in the GST eluate (see Fig. 4.19). This result indicates that Vps35 interacts *in vitro* with the intracellular loop of the GlyRβ subunit and gephyrin.

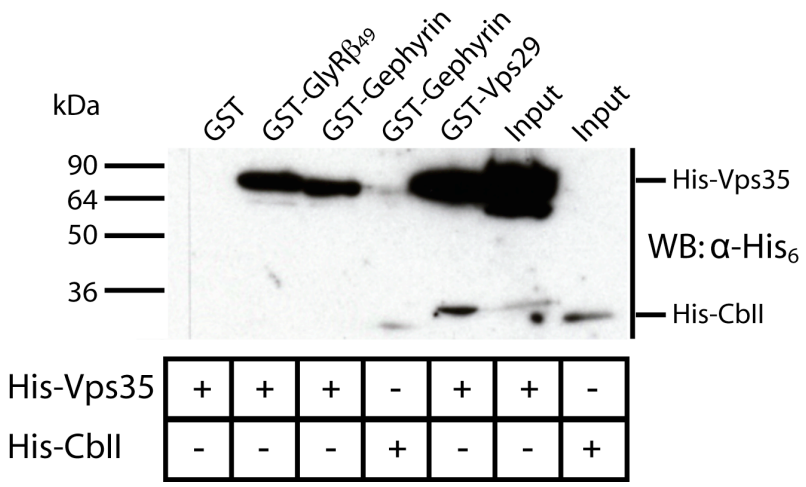

Fig. 4.19. Vps35 interacts with the GlyRβ loop and gephyrin *in vitro*. GST fusion proteins of GlyRβ_{49}, gephyrin, Vps29 and GST were incubated with bacterial lysate containing the recombinant His_6-tagged-Vps35. A corresponding bacterial lysate containing a His_6-tagged fragment of collybistin-II (His-CbII) was incubated with GST-gephyrin to confirm that the recombinant gephyrin protein was "active". Western blot and anti-His_6 immunodetection revealed a ~94 kDa protein band, corresponding to the molecular weight of His-Vps35, in the eluates from GlyRβ_{49}, gephyrin, Vps29 but not GST. A protein band of ~30 kDa, corresponding to the 240 aa fragment of collybistin-II, also bound to GST-gephyrin. Bands below 36 kDa in the GST-Vps29 and His-Vps35 Input lanes represent degradation products of Vps35 or unspecifically bound proteins.

4.2.2 Localization of Vps35 in the central nervous system

If the interaction between Vps35 and the GlyRβ subunit would occur in neurons, both proteins should show overlapping subcellular localizations. Here, the subcellular distribution of Vps35 was investigated by immunocytochemistry. Commercially available antibodies against Vps35 only worked in Western blot analysis, but failed to detect the native Vps35 protein *in situ* (data not shown). Therefore, an antibody suitable for the immunocytochemical and immunohistochemical detection of Vps35 was needed. Hence, polyclonal antibodies against Vps35 were generated in collaboration with the group of Dr. Jaroslav Blahos at the Academy of Sciences of the Czech Republic (Czech Republic).

4.2.2.1 Generation of polyclonal antibodies against Vps35

Full-length Vps35 was expressed as a His_6 fusion protein in *E.coli* BL21, purified on a Ni-NTA matrix under stringent conditions and dialysed as previously described under 3.3.7.2. The purified recombinant protein was employed as antigen for the immunization of four guinea pigs and two rabbits. After the third immunization, (see 3.3.10 for immunization protocol), antibody immunoreactivity was examined by Western blotting and immunocytochemistry.

4.2.2.2 Characterization of anti-Vps35 antibodies

4.2.2.2.1 Western blot analysis

First, the Vps35 antisera were tested for their specificity using Western blot analyses. This revealed that the antisera were able to recognize the recombinant Vps35 protein expressed in bacteria as well as the protein endogenously expressed in spinal cord neurons Moreover, putative cross-reactions of the antisera with another GST-tagged protein of the retromer complex, GST-Vps29, were investigated. Bacterial lysates containing GST fusion proteins of Vps35 and Vps29 and the original antigen (His_6-Vps35) were separated by SDS-PAGE and probed for antibody binding by Western blotting. From the six different sera examined, the rabbit anti-Vps35 antibodies in serum 08 (Vps35-Rb08) detected a band of about 118 kDa corresponding to the molecular weight of GST-Vps35 and a band of ~ 94 kDa corresponding to the apparent molecular weight of His_6-Vps35 (Fig. 4.20.A). No band was detected in the GST-Vps29 sample, indicating that the Vps35-Rb08 antibodies recognized the antigen used for immunization and also the bacterially expressed GST-Vps35 protein but did not cross-react with GST-Vps29 protein. The antibodies also bound to a protein of approximately 90 kDa in the spinal cord homogenate, which is consistent with the molecular weight of endogenous Vps35 (Fig. 4.20.B). Together, these results indicate that the Vps35-Rb08 antiserum specifically recognized the denatured Vps35 protein.

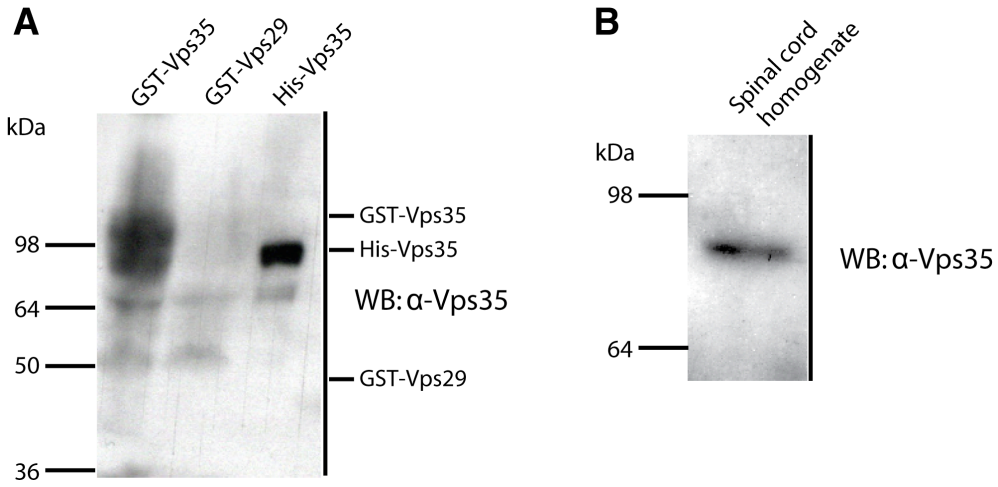

Fig. 4.20. Specificity test of a rabbit polyclonal Vps35 antiserum revealed by Western blot analysis. A. The following samples were separated by SDS-PAGE and tested for anti-Vps35 reactivity using the Vps35-Rb08 serum: GST-Vps35, GST-Vps29 and antigen (His-Vps35). **B**. Additionally, spinal cord homogenate was analysed as described in **A**. Western blots show that the antiserum recognized the antigen, GST-Vps35, but no GST-Vps29. Moreover, the Vps35 antiserum specifically recognized the endogenous Vps35 in spinal cord homogenate. Protein bands below 90 kDa correspond to weak unspecific reactivity of the Vps35-Rb08 antibodies.

4.2.2.2.2 Immunocytochemistry

After having demonstrated reactivity against denatured Vps35 protein by Western blot analysis, the ability of the Vps35 antisera to recognize the native protein in mammalian cells was examined. For this purpose, Vps35 antiserum-specificity was analyzed by means of immunocytochemical experiments. COS-7 cells were transfected with cDNAs encoding GFP-tagged Vps35 and GFP alone and fixed 24 h later. Cells were subsequently incubated with the Vps35 antisera and stained with Alexa-546 conjugated anti-rabbit antibodies following the standard protocol used for immunocytochemical staining (see 3.5.9). From the two rabbit sera tested, only the Vps35-Rb08 serum stained cells expressing GFP-tagged Vps35 (Fig. 4.21.A) but not cells expressing GFP alone (Fig. 4.21.B), indicating that the Vps35-Rb08 serum specifically recognizes Vps35 and does not cross-react with unspecific proteins in a native environment.

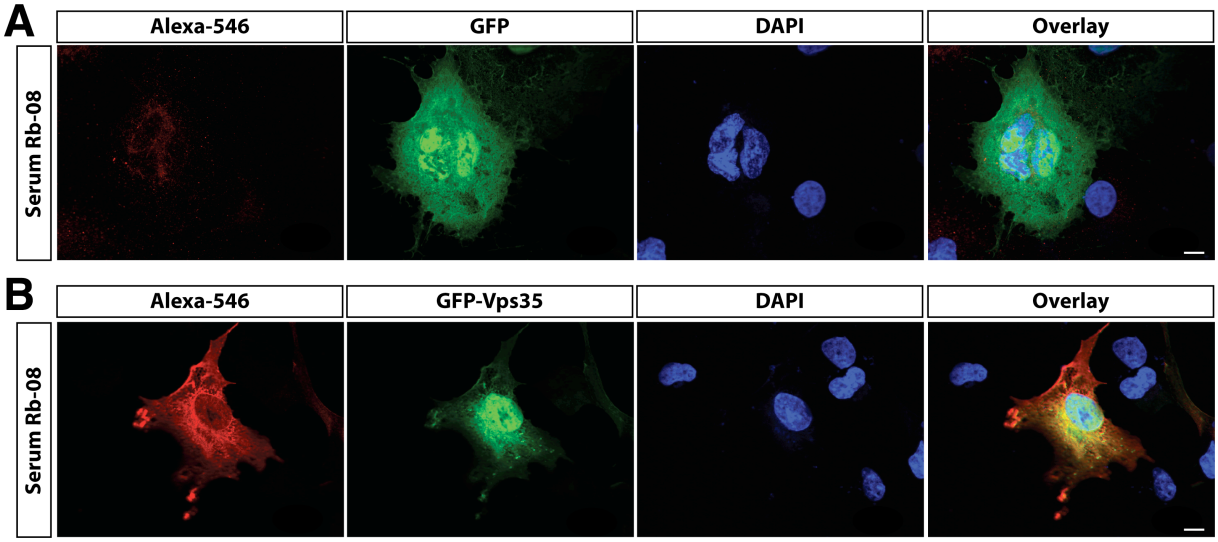

Fig. 4.21. Specificity of the Vps35 Rb-08 antiserum demonstrated by immunostaining of transfected COS-7 cells. COS-7 cells transfected with cDNAs encoding GFP (**A**) or GFP-tagged Vps35 (**B**) were stained with the Vps35-Rb08 antiserum and secondary Alexa-546-conjugated anti-rabbit antibodies. Cell nuclei were stained with DAPI. Note that the Vps35-Rb08 antiserum stained cells expressing GFP-Vps35 (overlay of the bottom panel), but not cells expressing GFP (no yellow signal in the overlay of the top panel). Scale bar: 10 μm.

4.2.2.3 Immunocytochemical analysis of the localization of Vps35 in spinal cord neuronal cultures

After the last immunization (see 3.3.10 for immunization protocol), specific antibodies were purified from the Vps35-Rb08 sera by means of antigen-affinity-chromatography as described under 3.3.11.

In order to test whether the purified Vps35 antibody recognizes specifically the native protein in neuronal cells, DIV20 spinal cord neuron cultures were fixed and stained with the anti-Vps35 antibody as primary and Alexa-546-anti-rabbit as secondary antibodies. Since there is no Vps35 -/- mouse available, as a negative control the antibody was pre-incubated in the presence of an excess of the GST-tagged Vps35 protein immobilized on a GSH matrix. This should cause specific antibody depletion and, hence reduce immunostaining. As a positive control, the same procedure was performed by pre-incubating the antibody solution in the presence of an excess of immobilized GST.

These experiments showed that the purified Vps35 antibody stained cultured spinal cord neurons in the presence of GST (see Fig. 4.22.B), whereas in the presence of GST-Vps35 the staining of neurons was prevented (see Fig. 4.22.A). Closer inspection of the staining pattern revealed that Vps35 immunoreactivity in cultured spinal cord neurons was enriched perisomatically and along neurites often in punctate structures (see Fig. 4.22.D); again, this staining was absent upon incubation with GST-Vps35 (see Fig. 4.22.C).

These results are consistent with the antisera results and show that the purified antibody specifically recognizes Vps35. Together, they provide strong evidence for Vps35 expression in spinal cord neurons, where Vps35 seems to be present both at somatic locations and in neuronal processes. Additionally, the punctate staining pattern is consistent with an association of Vps35 with transport vesicles. Double-stainings using anti-Vps35 and anti-GlyR antibodies could not be performed during the time available but may help to identify the subcellular structures, in which GlyRs and Vps35 are associated in spinal cord neurons.

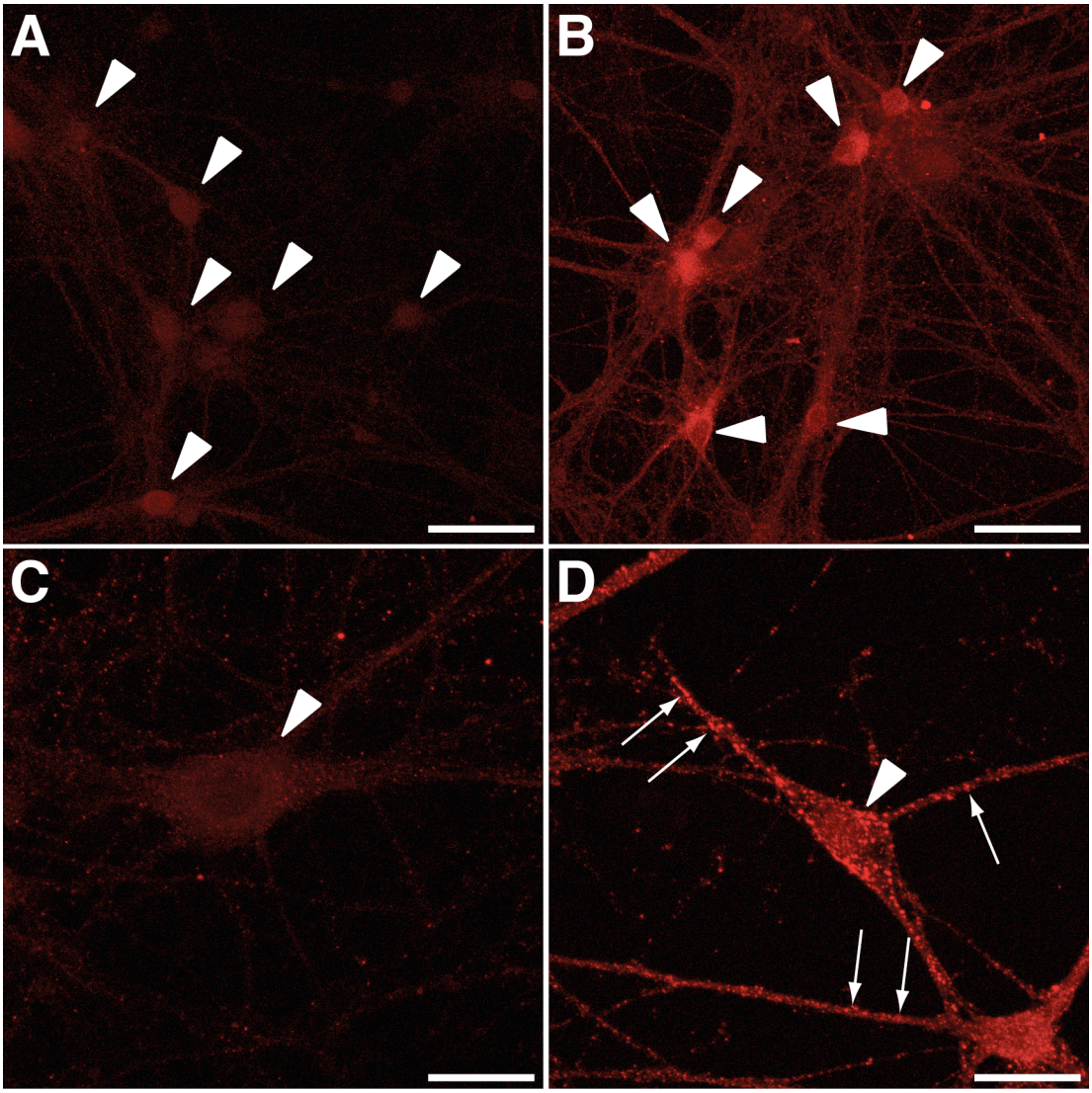

Fig. 4.22. Immunocytochemical analysis of Vps35 localization in rat spinal cord neurons. DIV20 rat spinal cord neuron cultures were fixed and stained with purified Vps35 antibody that had been pre-incubated with GST-Vps35 (**A** and **C**) or GST (**B** and **D**) protein immobilized on a GSH matrix. Bound antibody was visualized with Alexa-546 anti-rabbit secondary antibodies. Note that Vps35 antibody pre-incubated with GST, but not with GST-Vps35, stained neuronal cell bodies (arrowheads). Magnification shows the staining pattern of Vps35 in punctate structures in soma and along neurites (arrows) of neurons stained with Vps35 antibody pre-incubated with GST (**D**), but not with GST-Vps35 (**C**). Maximal projections were taken at 40X (**A** and **B**, scale bar: 50 μm) and 63X magnification (**C** and **D**, scale bar: 20 μm).

4.3 Analysis of the interaction between Neurobeachin and the GlyRβ subunit

In the proteomic screen used for the isolation of Vps35 from brain lysate (see 4.2), an additional protein band with a molecular weight of approx. 350 kDa had been identified by Maldi-ToF analysis as Neurobeachin (Nbea) (Paarmann, unpublished observation). Here, the significance of this proteomic result was examined by pull-down experiments and immunocytochemistry.

4.3.1 *In vitro* binding of Nbea to the GlyRβ subunit

As for SdpI (4.1.1) and Vps35 (4.2.1), a GST pull-down assay was employed in order to investigate the interactions between Nbea and the GlyRβ subunit. Since there was no construct available that encompassed the huge full-length Nbea coding sequence (> 8.8 kb; see Wang et al., 2000), three GFP-tagged fragments of the Nbea cDNA provided by the Kilimann group were employed (Fig. 4.23.A, see 3.1.13). These constructs, which together cover the entire Nbea open reading frame (Fig. 4.23.A), were transfected into HEK 293T cells, and protein expression was allowed for 24 h. The GFP-tagged Nbea-fragments were normally expressed and localized to the cytosol of HEK 293T cells (Fig. 4.23.B). Anti-GFP Western blot analysis of HEK 293T cell homogenates confirmed that the recombinant NbeaBCD protein matched the expected molecular weights of 131 kDa, indicating a proper expression of this fragment. In contrast, recombinantly expressed NbeaA and NbeaEFG proteins were detected at molecular weights of ~ 110 kDa and ~ 131 kDa, e.g. below the expected sizes of 130 kDa and 154 kDa, respectively, suggesting partial cleavage of the polypeptides (see Fig. 4.23.C). Additionally, the band intensity of the NbeaEFG fragment was reduced as compared to the band intensities of the NbeaA and NbeaBCD fragments, indicating that the GFP-NbeaEFG protein is less efficiently expressed in HEK 293T cells than NbeaA-GFP and GFP-NbeaBCD (see Fig. 4.23.C).

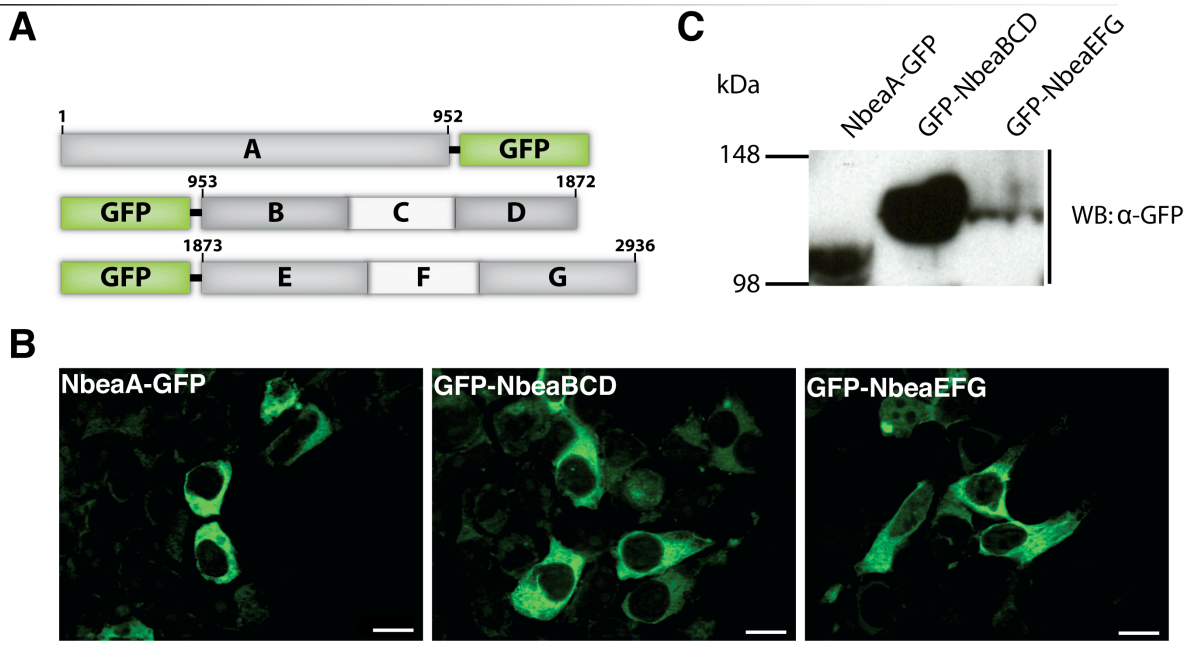

Fig. 4.23. Expression of three Nbea fragments. A. Schematic representation of GFP-tagged Nbea fragments. Numbers indicate the amino acid positions at the N- and C-termini of the respective Nbea fragments. **B**. Transfected HEK 293T cells express the different GFP-tagged Nbea fragments. Note the cytosolic distribution of all GFP-tagged proteins. Scale bar: 10 μm. **C**. Anti-GFP Western blot analysis of transfected HEK 293T detergent extracts shows the band sizes of the recombinant GFP-Nbea proteins and a reduced expression of GFP-NbeaEFG as compared to GFP-NbeaBCD or NbeaA-GFP.

In pull-down experiments, detergent extracts of HEK 293T cells expressing the three different Nbea fragments were incubated with either the GST-tagged GlyRβ_{49} loop construct (GST-GlyRβ_{49}) or GST as a negative control. As a positive control for GlyRβ_{49} binding, GFP-gephyrin was also expressed in HEK 293T cells. Following SDS-PAGE, anti-GFP Western blot analysis revealed that prominent bands corresponding to the molecular weight of GFP-gephyrin, GFP-NbeaBCD and GFP-NbeaEFG were present in the GST-GlyRβ_{49} pull-downs, but absent or only weakly seen in the GST control lanes. These results suggest that, similar to gephyrin, Nbea interacts with GlyRβ_{49} *in vitro* through its BCD and EFG domains, whereas the A domain of Nbea is not required for this interaction (Fig. 4.24).

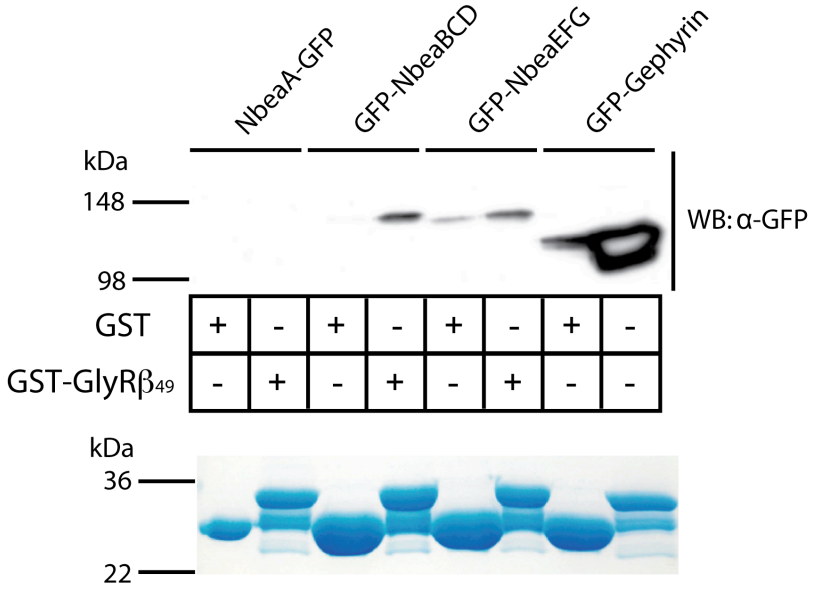

Fig. 4.24 *In vitro* interaction between Nbea fragments and the GlyRβ loop. GST fusion proteins of GlyRβ_{49} and GST were incubated with HEK 293T detergent extracts containing GFP-tagged Nbea fragments. GFP-gephyrin was used as a positive control for GlyRβ_{49}-binding. The top panel shows the anti-GFP Western blot analysis, in which GFP-Nbea BCD, GFP-NbeaEFG and GFP-gephyrin bands co-precipitated with GST-GlyRβ_{49} but not or only little with GST. GST-protein loads are shown in the Coomassie stained gel below. Double bands for GST-GlyRβ_{49} result from partial cleavage between GST and the fused GlyRβ_{49} sequence.

4.3.2 Subcellular localization of Nbea in neurons.

An *in vivo* interaction of Nbea with the GlyR requires that both proteins are present in the same neuronal compartments. In order to investigate Nbea distribution and localization at excitatory and inhibitory synapses, double immunolabeling experiments were performed with cultured hippocampal and spinal cord neurons. As a first approach to investigate Nbea distribution, DIV14 hippocampal neurons were stained with a Nbea antibody provided by Dr. M. W. Kilimann (Wang et al., 2000). Nbea immunoreactivity was predominant in the soma and sparse along the neuronal processes. The presence of Nbea near trans-Golgi membranes was confirmed by double immunofluorescence, in which hippocampal neurons where co-stained with Nbea and a trans-Golgi network marker (TGN38). Fluorescence analysis revealed a clear colocalization of Nbea with the TGN38 in the cell bodies and along neurites (Fig. 4.25), indicating that Nbea is located near the trans-Golgi network in the soma and along neuronal processes.

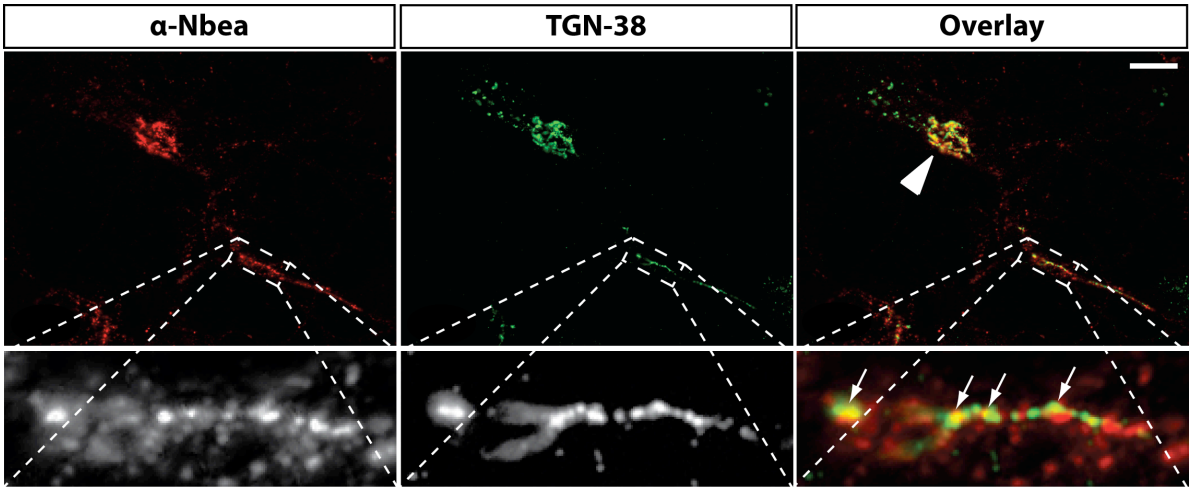

Fig. 4.25. Neurobeachin is found at the trans-Golgi network in primary hippocampal neurons. DIV14 hippocampal neurons were fixed and stained with the Nbea antibody and for the TGN38 marker. Nbea immunoreactivity largely colocalized with the TGN-marker as indicated in the overlay in yellow (right panel). Magnification shows the colocalization of Nbea and TGN38 along a neurite. The arrowhead points to a signal overlapping in the neuronal cell bodies, and arrows in the magnification point to signals overlapping along neuronal processes. Scale bar: 10 μm.

Subsequently, in order to examine Nbea localization at synapses, double immunostainings were performed in DIV20-22 spinal cord cultures with the Nbea antibody and antibodies against several inhibitory presynaptic (VIAAT, GAD67) and postsynaptic (gephyrin, GlyR), marker proteins as well as an excitatory postsynaptic (PSD95) marker (Fig. 4.26.A). As observed in hippocampal neurons, Nbea staining was present predominantly in neuronal cell bodies and along neuronal processes forming intensely stained punctate structures. These enrichments in Nbea immunoreactivity partially colocalized with the different synaptic marker proteins stained along neurites of spinal cord neurons.

The quantification of colocalizing puncta was performed as previously described under 4.1.5. Fluorescence analysis revealed no significant difference between the colocalization of presynaptic and postsynaptic as well between excitatory and inhibitory presynaptic markers with Nbea immunoreactive puncta. The percentage of puncta of each synaptic marker co-localizing with or being apposed to Nbea puncta was 17.8 ± 3.9% for PSD95, 22.4 ± 8.5% for VIAAT, 16.5 ± 6.5% for GAD67, 18.6 ± 3.5 for GlyR and 16.4 ± 3.5% for gephyrin (n=3, $p > 0.05$). These results agree with a previous report showing a localization of Nbea near postsynaptic membranes (Wang et al., 2000). They also indicate that Nbea is located synaptically and additionally suggest that Nbea is not preferentially found at specific synapses but is equally present at excitatory and inhibitory synapses (Fig. 4.26.B, $p > 0.05$).

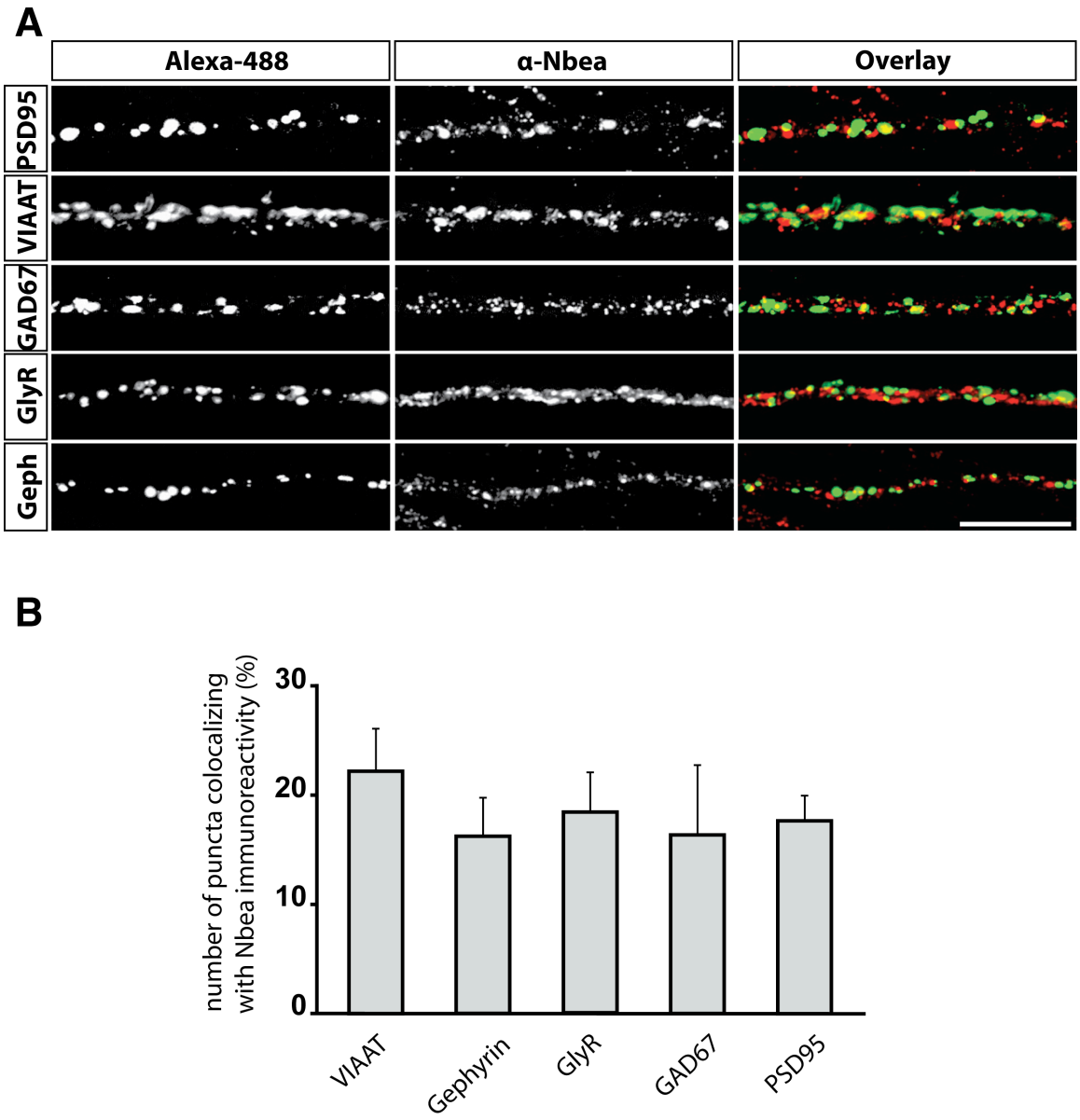

Fig. 4.26. Localization of Nbea in processes of spinal cord neurons. A. Spinal cord neurons were fixed and co-stained with Nbea antibody and several inhibitory (gephyrin, glyR, VIAAT, GAD67) and excitatory (PSD95) synaptic markers at DIV20-22. Note the yellow signal indicating clear co-localization of Nbea immunoreactive punctate structures with all the synaptic markers used (overlays). Scale bar, 10 μm **B**. Quantification of the experiment shown in **A**. Percentage of puncta of each synaptic marker colocalizing with Nbea. Values represent means ± SEM (n=3). No significant differences as compared to Nbea colocalization with VIAAT was found for all markers examined: $p > 0.05$.

5 DISCUSSION

The GlyR mediates inhibitory neurotransmission in spinal cord and brain stem. Fast and efficient inhibitory neurotransmission takes place due to GlyR and $GABA_AR$ clustering at inhibitory postsynaptic specializations. GlyRs localize to synaptic sites by virtue of their interaction with gephyrin mediated by the GlyRβ subunit. So far gephyrin was the only protein identified as binding partner of GlyRβ. Other proteins that may play a role in the synaptic localization and function of GlyRs had not been discovered. In this thesis, the interactions of three proteins found to bind the GlyRβ subunit were investigated. These proteins had been identified by affinity purification and subsequent MALDI-TOF analysis as SdpI, Vps35 and Nbea (I. Paarmann, unpublished data).

Sdp proteins contain F-BAR and SH3 domains, which are involved in membrane tubulation and protein-protein interactions, respectively. Sdps were proposed to interconnect actin polymerization and membrane remodelling. Vps35 is a component of the retromer complex that is involved in the retrieval of receptors from endosomes to the TGN and in receptor recycling to the plasma membrane. Nbea is a A-kinase anchoring protein known to be localized at the TGN and to be involved in the trafficking of synaptic membrane proteins. In this thesis, I investigated the interaction between these proteins and the GlyRβ subunit as well as their function in GlyR localization at synaptic sites. The *in vitro* results presented here demonstrate that SdpI and SdpII, Vps35 and Nbea bind directly to the GlyRβ intracellular loop, and that SdpI and Vps35 also interact with the GlyR scaffolding protein gephyrin. Deletion mapping, peptide competition and point mutation analysis indicate that the interaction of SdpI with the GlyRβ loop is SH3-domain dependent. Immunocytochemical analyses show that the SdpI and Nbea proteins are localized at inhibitory synapses whereas Vps35 distributes along the neurites of spinal cord neurons. SdpI down-regulation studies suggest that SdpI is involved in proper clustering of GlyRs at synaptic sites.

5.1 Sdp proteins

5.1.1 The SH3 domain of SdpI is required for interaction with GlyRβ

In co-immunoprecipitation experiments using the fraction of a spinal cord homogenate containing small membrane organelles, we obtained evidence for an association of SdpI with GlyR-containing cytoplasmic vesicles. Co-expression experiments in COS-7 cells revealed that the GlyRβ subunit interacts with SdpI as well as both isoforms of SdpII in mammalian cells; this confirms that the GlyRβ subunit is responsible for Sdp binding to the GlyR. GST-pulldown experiments confirmed that the interaction of SdpI and SdpII with the GlyRβ loop is a direct one. The further delineation of the Sdp binding site through deletion, peptide competition and point mutation approaches presented here indicates that the Sdp-GlyRβ loop interaction is specific and SH3 domain-ligand dependent (see 4.1). SH3 domains are highly conserved among all Sdp isoforms (Moddregger et al., 2000). This explains why both SdpI and SdpII bind to GlyRβ and also suggests a possible interaction between SdpIII and this GlyR subunit.

The Sdp binding region in the GlyRβ loop contains a class I R/KxxPxxP proline-rich motif i.e. one of the classical SH3 domain recognition sequences (Li, 2005). The KKxxPxxP motif is highly conserved in the GlyRβ subunits of rat, human, chick and zebrafish, suggesting that SH3 domain dependent interactions of Sdps with GlyRβ might occur in all vertebrates. Proline-rich motifs are widely distributed in the proteomes of prokaryotes and eukaryotes, and hundreds of SH3 domain-containing proteins can be found in the human proteome (Rubin et al., 2000). However, some SH3 domains display specificity for selected proline-rich motifs. This specificity relies on basic residues such as arginine and lysine, which provide extra binding energy through electrostatic interactions and additionally orient the ligand within the binding groove of the SH3 domain (Li, 2005). The results presented here demonstrate the importance of proline and lysine residues in the KKxxPxxP motif for SdpI-GlyRβ binding (see 4.1.1). A similar motif has been already shown to underlie SdpI-dynamin binding (Angonno et al., 2007). In the proline-rich motif of dynamin, arginine residues instead of lysine residues provide the positive charges required for binding to the SH3 domain of Sdp, and the ligand motif is unusually extended. The dephosphorylation of serine residues within the proline-rich motif has been found to constitute a key regulatory element in the phosphorylation-dependent interaction between SdpI and dynaminI (Angonno et al., 2007). Since the proline-rich motif in the GlyRβ loop does not contain serine residues, binding of SdpI to GlyR should not be phosphorylation-dependent.

SH3 ligands such as proline-rich motifs have been identified in both the α and β subunits of the GlyR (Lynch et al., 2004). Notably, GlyRα and β subunits contain different classes of proline-rich motifs in their intracellular loops. Class-III proline-rich motifs, with the standard sequence RxxK, are present at different positions in GlyRα and β subunits near the N-terminus of the TMD3-4 loop. The TMD3-4 loops harbour in the GlyRβ α1 and α2 subunits additional proline-rich motifs near their C-termini; however, these correspond to class-II proline-rich motifs (PxxPx[K/R])(Fig. 5.1). Moreover, the GlyRβ subunit contains a class-I proline-rich consensus sequence ([R/K]xxPxxP) close to the N-terminal loop sequence (Fig. 5.1). These different classes of proline-rich motifs might be important in determining the specific interactions of different GlyR subunits with SH3 domain-containing proteins like SdpI.

```
GlyRbeta human        438- GKPIEVNNGLGKSQAKNNKKPPPAKPVIPTAAKRIDLYAR -478
GlyRbeta mouse        437- YGKPIEVNNGLGKPQAKNKKPPPAKPVIPTAAKRIDLYAR -477
GlyRalpha1 human      388- VKGANNSNTTNPPPAPSKSPEEMRKLFIQRAKKIDKISR -428
GlyRalpha1 mouse      388- VKGANNNNTTTNPPPAPSKSPEEMRKLFIQRAKKIDKISR -428
GlyRalpha2 mouse      383- KDGTAVKATPANPLPQPPKDADAIKKKFVDRAKRIDTISR -423
GlyRalpha3 mouse      393- DGVVPKGPNHAVQVMPKSPDEMRKVFIDRAKKIDTISR -433
```

Fig. 5.1. Proline-rich motifs in the intracellular loops of several GlyR subunits. Proline-rich sequences in the intracellular loops of several GlyRα- and β-subunits are highlighted. Shown are the last 40 aa of each intracellular loop preceding TMD4. Aa numbering starts at the signal peptide of every GlyR subunit (Uniprot database). GlyRα- and β-subunits contain proline-rich sequences of different classes. Underlined are proline-rich sequences of class I (red), and class II (blue) as well as undefined (black) proline-rich motifs.

SH3 recognition domains have been postulated to serve as interaction sites involved in GlyR trafficking or cytoskeletal attachment (Lynch et al., 2004). The results presented in this thesis provide the first evidence for a function of the GlyRβ-SH3 binding motif (SBM) in Sdp-mediated GlyR trafficking. Since the TMD3-TMD4 intracellular loops of several GlyRα-subunits also comprise SBMs, GlyRα subunits may mediate other trafficking events through SH3 interactions.

5.1.2 SdpI is a gephyrin binding protein

Several cytoskeletal and cytosolic proteins such as tubulin, collybistin, mena/vasodilator-stimulated phosphoprotein (VASP) and profilin have been found to interact with gephyrin (Kirsch et al., 1991; Kins et al., 2000; Giesemann et al., 2003). Here, apart from binding to the GlyRβ subunit, SdpI is shown to also bind gephyrin (see 4.1.3). Upon heterologous co-expression in a mammalian cell line, SdpI colocalized with the aggregates formed by full-length gephyrin. *In vitro*

pull-down experiments provided evidence for SdpI binding at the linker region of gephyrin. In agreement with this result, gephyrin sequence analysis revealed the presence of proline-rich motifs in the linker region of gephyrin (see Table 4). However, further deletion and point mutation experiments are required to confirm that the interaction of SdpI with gephyrin is mediated by the recognition of these proline-rich motifs by the SdpI-SH3 domain.

Co-expression of collybistin II with gephyrin in a heterologous expression system leads to the redistribution of gephyrin into submembraneous microclusters that colocalize with collybistin II (Kins et al., 2000; Harvey et al., 2004). Interestingly, Sdp co-expression similarly induced a plasma membrane association of gephyrin in COS-7 cells (see Fig. 4.9). This redistribution of gephyrin resembles that observed in mammalian cells upon co-expression of collybistin II. SdpI and collybistin II activate N-WASP directly or through Cdc42 activation, respectively (Reid et al., 1999; Dharmalingam et al., 2007). However, a recent study has excluded a role of Cdc42 in collybistin-induced gephyrin microcluster formation (Reddy-Alla et al., 2010). By analogy, the activation of N-WASP and the actin polymerization induced by SdpI might be dispensable for gephyrin redistribution in COS-7 cells. Notably, the redistribution pattern of gephyrin to the plasma membrane induced by Sdp is different from that of gephyrin microcluster formation induced by collybistin II. This could be due to differences in the membrane binding activities of Sdp and collybistin II. Domain deletion and point mutation studies with colllybistin II indicate that PH domain binding to phosphatidylinositol 3-phosphate (PI3P) is required for the targeting of gephyrin into membrane-associated microclusters (Harvey et al., 2004; Kalscheuer et al., 2009; Reddy-Alla et al., 2010). In the case of SdpI, its F-BAR domain is responsible for the recruitment of SdpI to the plasma membrane, due to its ability to bind phosphatidylserine-containing membranes (Dharmalingam et al., 2007). Therefore, differences in lipid binding between collybistin II and SdpI may underlie the different gephyrin redistribution patterns observed upon co-expression of these proteins. Further deletion and point mutation studies should clarify whether membrane binding of Sdps through the F-BAR domain is required for gephyrin redistribution in mammalian cells.

5.1.3 The GlyR, gephyrin and SdpI: Mutually exclusive gephyrin/SdpI binding to the GlyR or a ternary complex?

Gephyrin binds to the GlyRβ loop through an 18 aa long hydrophobic motif called gephyrin binding motif (GBM) (Meyer et al., 1995). Our mapping and point mutation analyses of the SdpI binding region in the GlyRβ subunit indicate that SdpI binds to a proline-rich motif, which is

located 16 aa away from the GBM (Fig. 4.2 and Fig. 4.3). Therefore, simultaneous binding of gephyrin and SdpI to the GlyRβ loop could be possible. However, our protein competition assays showed that gephyrin's E-domain interferes with SdpI binding to the GlyRβ loop (see Fig. 4.11). This could be due to steric hindrance caused by the higher affinity of gephyrin binding to the GlyRβ subunit. Our results suggest that gephyrin and SdpI are mutually exclusive binding partners of the GlyRβ subunit.

Hetero-pentameric GlyRs contain three GlyRβ subunits (Grundzinska et al., 2005). Gephyrin interacts with GlyRβ at postsynaptic inhibitory synapses and intracellularly during motor protein driven transport (Maas et al., 2006 and 2009). At synaptic sites, gephyrin forms a hexagonal lattice through dimerization of the E-domain and trimerization of the G-domain (Sola et al., 2001 and 2004). A structural model for the binding of GlyRs to gephyrin trimers has suggested that the three GlyRβ subunits of a single receptor might bind the three E-domains of a gephyrin trimer in the submembraneous scaffold (Sola et al., 2004). However, the number of GlyRβ subunits occupied by gephyrin during intracelllular transport or lateral diffusion of the receptor in the plasma membrane is still unclear. Furthermore, gephyrin-free trafficking and diffusion of GlyRs occurs in gephyrin-deficient (Feng et al., 1998) and probably also wildtype mice. An analysis of the diffusion properties of a GlyRα1 chimera containing the gephyrin binding site of the GlyRβ subunit in the presence of gephyrin variants able and unable to trimerize has suggested that the amount of gephyrin bound to the GlyR is small (Ehrensperger et al., 2007). Additionally, this study reported multiple association states between GlyRs and gephyrin and also estimated that about 40% of the extrasynaptic GlyR chimeras are associated with gephyrin. Taking into account previous studies and the *in vitro* results of our protein competition experiments (see 4.1.4) which show that, in the presence of gephyrin's E-domain, SdpI is not able to bind the GlyRβ loop, we propose a model for GlyR/gephyrin/SdpI binding during synaptic and extrasynaptic transport. At synaptic sites, GlyRs are localized postsynaptically and do not bind SdpI due to high-affinity binding of gephyrin, which occupies all three subunits. SdpI might accumulate adjacent to postsynaptic scaffolds due to low-affinity binding to gephyrin or might be located extrasynaptically due to interactions with other proteins of the endocytotic and recycling pathway. When heteropentameric GlyRs have to be transported, two models of GlyR/gephyrin/SdpI complex formation might be considered. According to the first model, GlyRs might be transported as ternary complexes which bind simultaneously gephyrin trimers and SdpI through their interactions with different GlyRβ subunits (Fig. 5.2.a). The second model proposes that GlyRs are transported either as gephyrin-bound complexes or as gephyrin-free complexes.

Gephyrin-bound GlyRs might have all three β subunits interacting with a gephyrin trimer, whereas gephyrin-free GlyRs might have all three β subunits complexed to SdpI (see Fig. 5.2.b). Thus sorting to different transport pathways may be accomplished through mutually exclusive binding to either gephyrin or SdpI. Since gephyrin was present in the protein samples of our first pull-down experiments employed to isolate SdpI from brain lysate (I. Paarmann, data not shown), it seems rather plausible that GlyRs, gephyrin and SdpI may be associated in a ternary complex. In the work presented here, immunoprecipitation of GlyR subunits from a rat spinal cord homogenate could be achieved using specific SdpI antibodies (see 4.1.6.1). Further analysis of gephyrin co-immunoprecipitation employing SdpI antibodies or SdpI co-immunoprecipitation with gephyrin or GlyR antibodies from tissue extracts might help to disclose whether a ternary complex composed of gephyrin-Sdp-GlyR proteins may be formed *in vivo*.

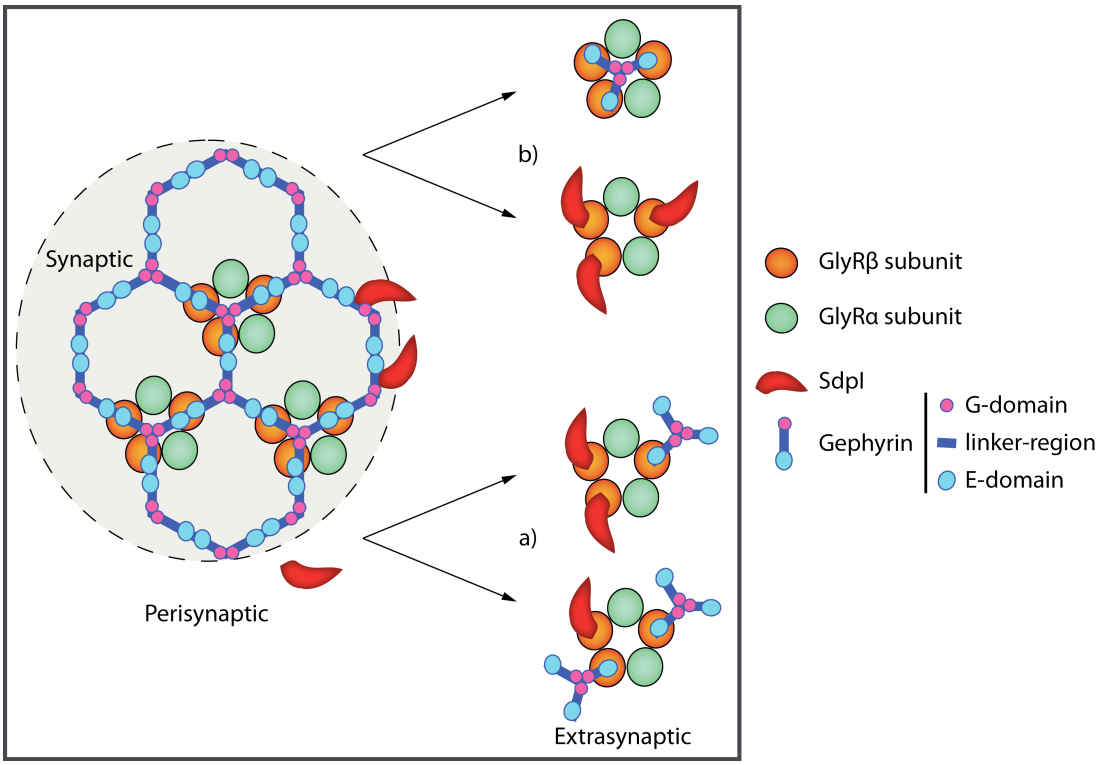

Fig. 5.2. Proposed models for the interaction of GlyRs with gephyrin and SdpI at synaptic and extrasynaptic sites. Heteropentameric GlyRs at synaptic sites bind gephyrin´s E-domains of the submembraneous hexagonal scaffold. High-affinity binding of gephyrin to GlyRβ subunits inhibits SdpI binding to the GlyR at synaptic sites. Thus, SdpI might localize perisynaptically or might distribute at the periphery of inhibitory postsynaptic scaffolds through its binding to gephyrin. GlyRs at extrasynaptic sites might recruit SdpI. In a first model (**a**), gephyrin binds as trimer to one or two GlyRβ subunits, allowing additional unoccupied GlyRβ subunits to bind SdpI. Thus, GlyR binds simultaneously gephyrin and SdpI and each β subunit interacts either with gephyrin or with SdpI. In a second model (**b**), GlyRs to be transported can be classified into two pools: gephyrin-bound or gephyrin-free GlyRs. In the gephyrin-bound GlyR pool, the three GlyRβ subunits of the pentameric receptor bind the three E-domains of a gephyrin trimer. In the gephyrin-free GlyR pool, all three GlyRβ subunits bind SdpI. Thus, binding to either gephyrin or SdpI might determine the pathway into which GlyRs are sorted.

5.1.4 Localization of Sdp protein family members at inhibitory synapses

In the central nervous system, SdpI has been found at excitatory pre- and postsynaptic structures in the rat hippocampus and presynaptically at reticulospinal synapses in lamprey (Qualmann et al., 2009; Perez-Otaño et al., 2006; Andersson et al., 2008). However, the ocurrence of SdpI at inhibitory synapses had not been reported. In agreement with SdpI mRNA detection in mouse spinal cord (Allen spinal cord atlas http://mousespinal.brain-map.org/), here the presence of Sdp protein in cultured rat spinal cord neurons could be demonstrated (see 4.1.5). SdpI immunoreactivity in cultured spinal cord neurons was found at the periphery of cell bodies and as intense punctate staining along neurites. This staining pattern of SdpI in spinal cord neurons resembled the distribution of SdpI-immunoreactivity in cultured cortical neurons (Qualmann et al., 1999), suggesting that SdpI distribution might be similar in neurons from different areas of the CNS. Quantification of the GlyR, gephyrin and VIAAT immunoreactive-spots colocalizing with SdpI at early stages (DIV11-13) showed that SdpI colocalized with a small fraction of the GlyR clusters, but more prominently with VIAAT and gephyrin puncta. This suggests two distribution patterns of SdpI at inhibitory synapses: a GlyR-independent SdpI distribution at synaptic sites and a GlyR-dependent SdpI distribution (see Fig. 4.12). Spinal cord neurons of later stages (DIV20-22) present a higher density of GlyR clusters as compared to young neurons, consistent with the developmental maturation of glycinergic synapses. However, the number of SdpI-immunoreactive puncta colocalizing with GlyR-immunoreactive spots at DIV20-22 was only slightly higher that at DIV11-13, indicating that SdpI association with synaptic and non-synaptic GlyR does not change significantly during development. Additionally, in agreement with a continuous localization of SdpI at synaptic sites, the colocalization rates of SdpI with VIAAT and gephyrin did not change or decreased only slightly during development (see 4.1.5).

Gephyrin clusters can be GABAergic, glycinergic or mixed GABA-glycinergic (Colin et al., 1998). The results obtained here on the colocalization of SdpI-immunoreactivity with GlyR clusters and GAD67-terminals suggest that SdpI is concentrated at both glycinergic and GABAergic synapses (see 4.1.5). Additionally, our colocalization analysis revealed similar extents of apposition between SdpI and PSD95 as well as gephyrin immunoreactive sites, suggesting an accumulation of SdpI at both excitatory and inhibitory synapses in mature spinal cord neurons. Our results are in agreement with previous studies demonstrating that SdpI is localized at the

postsynaptic density (PSD) and at perisynaptic sites of glutamatergic synapses (Perez-Otaño et al, 2006). On the same line, quantification of SdpI colocalization with inhibitory pre- and postsynaptic markers did not reveal a preferential enrichment of SdpI at specific synaptic structures. Presently, robust data that confirm the pre- and/or postsynaptic distribution of SdpI at GABAergic and glycinergic synapses are lacking. Therefore, high-resolution imaging techniques, like STED microscopy and immunogold electron microscopy, should be used to provide further insight into the role of SdpI at inhibitory synapses.

5.1.5 Sdp is involved in GlyR and $GABA_AR$ clustering

The broad expression pattern of SdpI in the central nervous system, its localization at inhibitory and excitatory synapses as well as its ability to interact with many different proteins involved in endocytosis, recycling, neurotansmitter responses and actin polymerization indicate that SdpI is a multifunctional player in the central nervous system. At lamprey reticulospinal synapses, SdpI has been implicated in vesicle formation following intense stimulation of presynaptic terminals (Andersson et al., 2008). Studies at the neuromuscular junctions of *D. melanogaster* indicate that Sdps act postsynaptically in the formation of the subsynaptic reticulum and exclude a function in vesicle endocytosis at the presynapse (Kumar et al., 2008 and 2009). Together these data suggest a broad spectrum of functions for Sdps, which is different depending on the synaptic system that is analyzed. In hippocampal neurons, SdpI has been found to mediate the endocytosis-dependent removal of NR3 containing NMDA receptors (NMDARs) from excitatory synapses. Interference with SdpI-NR3 interactions led to an increase in the cluster size of NR3 containing NMDARs (Perez-Otaño et al., 2006). The reduction in GlyR cluster size and number observed here in SdpI knock-down experiments argue against a similar function of SdpI in GlyR trafficking (see 4.1.6.3). SdpI binds to NR3 containing NMDARs through their NPF repeats and has been proposed to serve as linker between NMDARs and the endocytic machinery (Perez-Otaño et al., 2006). The results presented here demonstrate that the GlyRβ-Sdp interaction is SH3 domain-dependent. The difference in the SdpI mediated interactions with these receptors correlates with the different functions of SdpI at NMDARs and GlyRs. In agreement with this, the binding of NR3 and GlyRβ subunits to Sdps differs in that NR3 binding is restricted to SdpI and GlyRβ interacts with both SdpI and SdpII. This suggests a Sdp-mediated trafficking process of higher complexity for the GlyR.

Disruption of SdpI function by antibody microinjection leads to an impairment in synaptic vesicle recycling under intense stimulation (Andersson et al., 2008). Notably, the clustering of GlyRs is

activity-dependent (Kirsch and Betz, 1998; Maas et al., 2009), and a loss of synaptic vesicle recycling implies a subsequent disruption of neurotransmitter release. The depletion experiments performed here show that the number of VIAAT clusters is not significantly affected by SdpI down-regulation (Fig. 4.18). This result is in agreement with previous publications showing that SdpI inactivation induces a reduction in vesicle number at presynaptic sites, but no change in presynapse morphology (Andersson et al., 2008). Furthermore, the slight but insignificant change in VIAAT distribution found upon SdpI down-regulation suggests that SdpI is not implicated in inhibitory presynaptic maturation. Therefore, changes in GlyR cluster distribution induced by SdpI knock-down may not be attributed to presynaptic dysfunction.

In spinal cord neurons, GlyRs cluster at glycinergic synapses, but about 30% of the GlyRs share postsynaptic localizations with $GABA_A$Rs at mixed glycinergic/GABAergic synapses (Dumoulin et al., 2000). Additionally, SH3 ligand binding sites at inhibitory postsynaptic proteins are not restricted to GlyRβ but also present on GlyRα subunits, gephyrin, neuroligin-2 and $GABA_A$ but not $GABA_C$ receptor proteins (see Table 4). The SdpI depletion results presented here (see 4.1.6) revealed similar reductions in cluster number and size for heteropentameric GlyRs and γ2-subunit containing $GABA_A$Rs, suggesting that SdpI participates in a trafficking process shared by both types of inhibitory postsynaptic receptors. This is consistent with different $GABA_A$R subunits containing different types of SH3 ligand binding motifs in their TMD3-4 intracellular loops (see Table 4). Future studies will show whether $GABA_A$R subunits bind Sdp directly through SH3-proline-rich motifs mediated interactions.

The SdpI depletion results presented in this thesis showed a reduction of ca. 40% in cluster number, and of about 45% in cluster size for both GlyRs and $GABA_A$Rs. The remaining 60% and 55% of synaptic GlyR and γ2 containing $GABA_A$R clusters might reflect residual SdpI expression due to incomplete knock-down but also could be due to redundant functions of SdpII and SdpIII or even compensation by Sdp-independent protein transportation pathways. On the same line, our analysis of GlyR and gephyrin distribution in the brain stem of SdpI -/- mice demonstrates that SdpI-deficiency does not affect GlyR and gephyrin clustering at inhibitory synapses, in agreement with the results obtained on spinal cord cultures of SdpI -/- mice (see 4.1.6.2). Moreover, the absence of a GlyR cluster phenotype in SdpI -/- mice correlates with the lack of neuromotor symptoms in these mice (Koch et al., submitted). However, in our SdpI depletion experiments we saw a decrease in the densities of γ2 subunit containing $GABA_A$R clusters in spinal cord neurons. Assuming that SdpI would similarly contribute to inhibitory receptor trafficking in forebrain regions, the epileptic seizures that SdpI -/- mice present under stress

conditions (Koch et al., submitted) might be explained. As discussed above, the absence of a clear effect on GlyR distribution might be due to compensatory effects of SdpII and SdpIII in brainstem and spinal cord. The generation of constitutive and conditional triple SdpI/SdpII/SdpIII -/- mice and the specific knockdown of all Sdps in neurons should allow to clarify the roles of these proteins in neurotransmitter receptor trafficking.

Protein	Species	Motif 1	Motif 2	Motif 3	Motif 4
$GABA_A\alpha1$	Rat	-	1*+ 1*	1*+ 2*	1*
$GABA_A\alpha2$	Rat	-	-	-	1
$GABA_A\alpha3$	Rat	1*	1*	1*	0
$GABA_A\alpha4$	Rat	1*	-	2*+ 3*	-
$GABA_A\alpha5$	Rat	-	-	1	-
$GABA_A\alpha6$	Rat	-	-	1 + 4*	-
$GABA_A\beta1$	Rat	-	-	3	-
$GABA_A\beta2$	Rat	-	-	1	-
$GABA_A\beta3$	Rat	-	-	1	-
$GABA_A\gamma1$	Rat	-	-	-	-
$GABA_A\gamma2$	Rat	-	1* + 1*	2* + 1*	1*
$GABA_A\gamma3$	Rat	-	-	2	-
$GABA_A\delta$	Rat	-	-	2	-
$GABA_A\varepsilon$	Rat	-	-	-	-
$GABA_A\pi$	Rat	-	-	-	-
$GABA_A\Theta$	Rat	-	-	1	-
Gephyrin	Rat	-	-	3* + 1	-
Neuroligin-2	Rat	-	-	1 + 1 + 9*	-

Table 4. Putative SH3 ligand binding motifs in inhibitory postsynaptic proteins. Predictions by the eukaryotic linear motifs (ELM) program. Standard sequences for SH3 ligand binding motifs are: 1- [RKY]xxPxxP, 2- PxxPx[KR], 3- xxx[PV]xxP, 4- KPxx[QK]xxxx. *: Overlapping. Sequences analyzed are: the large intracellular loop of $GABA_AR$ subunits, linker regions of gephyrin and the C-terminal region of Neuroligin 2. No putative intracellular SH3 ligand binding motifs were found in $GABA_CR$ subunits (from del Pino et al., in preparation).

5.1.6 A role of SdpI in gephyrin clustering?

A co-transport of GlyRs and gephyrin to and from synaptic sites is thought mediated by microtubule-associated motor proteins, namely kinesin and dynein in the anterograde and retrograde directions, respectively (Maas et al., 2006 and 2009). Here, the SdpI depletion experiments resulted in a reduction of about 45% of the synaptic GlyRs but only about 30% of the gephyrin cluster size as well as a reduction of ~30% in synaptic GlyR cluster density, whereas the density of gephyrin clusters was only marginally reduced (10%) (see 4.1.6.3). Due to the modest effect of SdpI depletion on gephyrin cluster distribution, it remains unclear whether SdpI participates actively in any gephyrin transport mechanism or is just a secondary effect of the loss of synaptic GlyRs and $GABA_A$Rs.

Studies on conditionally and constitutively collybistin-deficient mice found a loss in synaptic gephyrin and $GABA_A$R cluster densities in particular regions of the CNS, e.g. in the stratum radiatum and stratum oriens of the hippocampus, the cerebellum, the amygdala, etc; however, no effect on glycinergic synapses was observed (Papadopoulos et al., 2007 and 2008). Here, brain stem sections from +/+ and SdpI-/- (Koch et al., submitted) mice did not show any significant difference in gephyrin cluster distribution (see 4.1.6.2). These results do not support a role of SdpI in gephyrin oligomerization and clustering at glycinergic and GABAergic synapses in brain stem and spinal cord. However, similarly to what was observed by Papadopoulos and colleagues, a detailed analysis of gephyrin distribution in several regions of the SdpI-/- brain might clarify whether SdpI is required for gephyrin clustering at a subset of GABAergic or glycinergic synapses in specific regions of the CNS.

5.1.7 Possible roles of SdpI in GlyR trafficking: potential sites of action

The results presented in this thesis show that SdpI depletion leads to a reduction in the cluster size and number of inhibitory postsynaptic receptors but has no significant effect on gephyrin cluster distribution. As possible mechanistic explanations of how SdpI may function in GlyR trafficking, three different models may be considered:

Model 1: SdpI mediates gephyrin-independent ER/TGN exit of αβ heteropentameric GlyRs

A prerequisite for GlyR exit from the ER is the assembly of GlyRα and GlyRβ subunits into pentameric receptors (Griffon et al., 1999). Similarly, $GABA_AR$ subunits need to assemble at proper stoichiometries to allow ER exit. Previous studies have identified two cytosolic proteins, PIC1 and BIG1, which bind $GABA_AR$ subunits and promote the translocation of fully assembled receptors from the ER and TGN to the plasma membrane (Charych et al., 2004; Saliba et al., 2008). Additionally, complex formation of SdpII with dynamin II has been demonstrated to be important for transport vesicle formation from the TGN in heterologous expression systems (Kessels et al., 2006). For synaptic receptor clustering, the insertion of receptors into the plama membrane and thus their availability for recruitment to postsynaptic scaffolds is a prerequisite of synapse formation. However it is still unclear whether newly synthesized GlyRs are recruited after directional insertion near postsynaptic sites in addition to being captured by lateral diffusion from extrasynaptic insertion sites. It has been reported that the GlyR α1 subunit, which forms heteropentameric receptors with the GlyRβ subunit, is extrasynaptically inserted at the cell soma and in the proximal regions of dendrites (Rosenberg et al., 2001). Also, exocytosis of $GABA_ARs$ has been shown to occur exclusively at extrasynaptic sites (Thomas et al., 2005; Bogdanov et al., 2006). GlyRs are thought to be co-transported with gephyrin (Mass et al., 2006 and 2009), but GlyR and $GABA_AR$ surface expression proceeds in gephyrin-deficient mice (Feng et al., 1998; Kneussel et al., 1999). Therefore, for insertion into the plasma membrane GlyRs can use gephyrin-independent trafficking mechanisms. We hence propose in a first model that Sdp-dynamin complex formation is required for transport vesicle formation in the TGN of neurons, and that GlyRs and $GABA_ARs$ are inserted at extrasynaptic sites followed by lateral diffusion to synaptic sites. Accordingly, the partial loss of inhibitory postsynaptic receptors from synaptic sites seen upon SdpI depletion may be induced by an impairment of GlyR and $GABA_AR$ exit from the TGN to the plasma membrane. In this model, SdpI would act in a gephyrin-independent manner as regulator of assembled GlyR trafficking. SdpI would allow properly assembled GlyRs

to enter budding vesicles formed at the TGN for delivery to the plasma membrane and facilitate vesicle formation through binding to dynamin. Vesicles generated form the TGN would fuse at extrasynaptic sites with the plasma membrane, and the inserted GlyRs would diffuse laterally until gephyrin scaffolds trap them. In the absence of SdpI, extrasynaptic insertion of GlyR into the plasma membrane would be impaired, and consequently the number of GlyRs available for trapping at synaptic sites would be reduced (Fig. 5.3).

Model 2. SdpI mediates anterograde trafficking of αβ heteropentameric GlyRs

Time-lapse imaging has revealed a somatodendritic anterograde co-transport of gephyrin and GlyR along microtubules in hippocampal neurons, which requires the interaction of gephyrin with kinesin (Maas et al., 2009). Here, an interaction of SdpI with the GlyRβ subunit but also with gephyrin was demonstrated. Maas et al. (2006) have shown that GlyR and gephyrin interact in the neuronal membrane fraction containing cytosolic vesicles. Using the same membrane fraction from spinal cord tissue, an interaction of SdpI with GlyR was found here (see 4.1.6.1). Moreover, our *in vitro* results suggest that binding of the gephyrin E-domain to the GlyRβ loop impairs the interaction with SdpI. Therefore, assuming that SdpI and gephyrin can bind simultaneously the GlyR through interactions with different GlyRβ subunits, a role of SdpI in the anterograde transport of GlyR containing vesicles appears feasible. The loss of inhibitory postsynaptic receptors at synaptic sites found upon SdpI depletion may then be due to an impairment of GlyR anterograde transport along microtubules. According to this second model, SdpI would act as an adaptor protein that binds both gephyrin and the β subunit of heteropentameric GlyRs at transport steps preceding gephyrin oligomerization at postsynaptic sites. Hence, SdpI would be required for ternary complex formation and facilitate the binding of gephyrin to GlyRs during somatodendritic anterograde, but not retrograde, transport. Down-regulation of SdpI would reduce GlyR-gephyrin complex formation in cytoplasmic vesicles and thereby decrease the amount of surface GlyR available for postsynaptic clustering. Additionally, a loss of SdpI might lead to misrouting of GlyRs to other trafficking pathways (see Fig. 5.3).

Model 3: SdpI is involved in synaptic GlyR recycling

At glutamatergic synapses, endocytic zones have been identified at stable positions adjacent to the postsynaptic densities (PSDs) (Blanpied et al., 2002; Racz et al., 2004). Follow-up studies revealed that these endocytic zones are essential for the recycling of alpha-amino-3-hydroxy-5-

methyl-4-isoxazolepropionic acid (AMPA) receptors during basal transmission and synaptic potentiation (Petrini et al., 2009). The PSD-adjacent positioning of endocytic zones is very important and depends on a direct interaction between the large GTPase dynamin III and the postsynaptic scaffold complex containing the Homer and Shank proteins (Lu et al., 2004). Presently, there is no evidence supporting the existence of endocytic zones at inhibitory synapses. However, recycling of $GABA_A$Rs from internal pools has been reported to occur in heterologous expression systems and also in neurons (Kittler et al., 2000; van Rinjnsoever et al., 2005). Furthermore, the recycling of $GABA_A$Rs in neurons is regulated through interactions between $GABA_A$Rβ subunits and the Huntingtin-associated protein 1 (HAP1) and between the $GABA_A$Rγ2 subunits and the calcium-modulating cycophilin ligand (CAML) (Kittler et al., 2004; Yuan et al., 2008). The huntingtin protein itself has been suggested to be an integral component of the HAP1-KIF5 complex and to be involved in the trafficking of $GABA_A$R containing vesicles, since a mutant huntingtin, polyQ-huntingtin, disrupts $GABA_A$R surface accumulation (Twelvetrees et al., 2010). On the other hand, different lines of evidence support a participation of SdpI in the endocytosis and recycling of membrane proteins. SdpI is required for presynaptic activity-dependent vesicle recycling, which depends on SdpI-dynamin-N-WASP complex-formation (Andersson et al., 2005), and for transferrin receptor recycling, which is SdpI-EHD complex-dependent (Braun et al., 2005). Additionally, SdpI binds through its SH3 domain to the huntingtin protein (Modregger et al., 2002). Therefore, assuming that GlyRs undergo the same recycling processes like $GABA_A$Rs, the reduced GlyR clustering seen upon SdpI down-regulation can be explained by disruption of GlyR recycling. Accordingly, SdpI would be implicated in the recruitment of $\alpha\beta$ GlyRs to the endocytic zones and thus facilitate delivery of the receptor to a recycling pool. SdpI depletion would imply that GlyRs are not recruited to endocytic zones. As a result, GlyRs would further diffuse from synaptic to extrasynaptic sites where they are not efficiently recycled, and hence the number of perisynaptic GlyRs available for trapping at synaptic gephyrin scaffolds would be reduced, resulting in a decrease of synaptic GlyR cluster size. Alternatively, SdpI might target endocytosed GlyRs to the recycling pool. This could prevent GlyR degradation and facilitate receptor recycling to the plasma surface. In this scheme, down-regulation of SdpI would result in the lack of a signal supporting GlyR sorting during the recycling process and allow for misssorting of GlyRs to other trafficking pathways (see Fig. 5.3). As a consequence, again the number of surface GlyRs would decrease, and GlyR cluster size would be reduced.

It remains unclear in which of these presumptive mechanisms SdpI is actually participating. Biotinylation experiments would be required to clarify whether the number of GlyRs at the cell surface is reduced in the absence of SdpI. In addition, high-resolution imaging techniques should shed light on the SdpI-dependent trafficking mechanism that controls the intracellular pools and plasma membrane concentrations of αβ GlyRs, such us live-cell single particle tracking with the quantum dot method as well as metabolic labelling based on fluorescently-tagged amino acid incorporation into proteins. These methods should be useful for identifying the specific trafficking mechanisms, in which Sdps are involved.

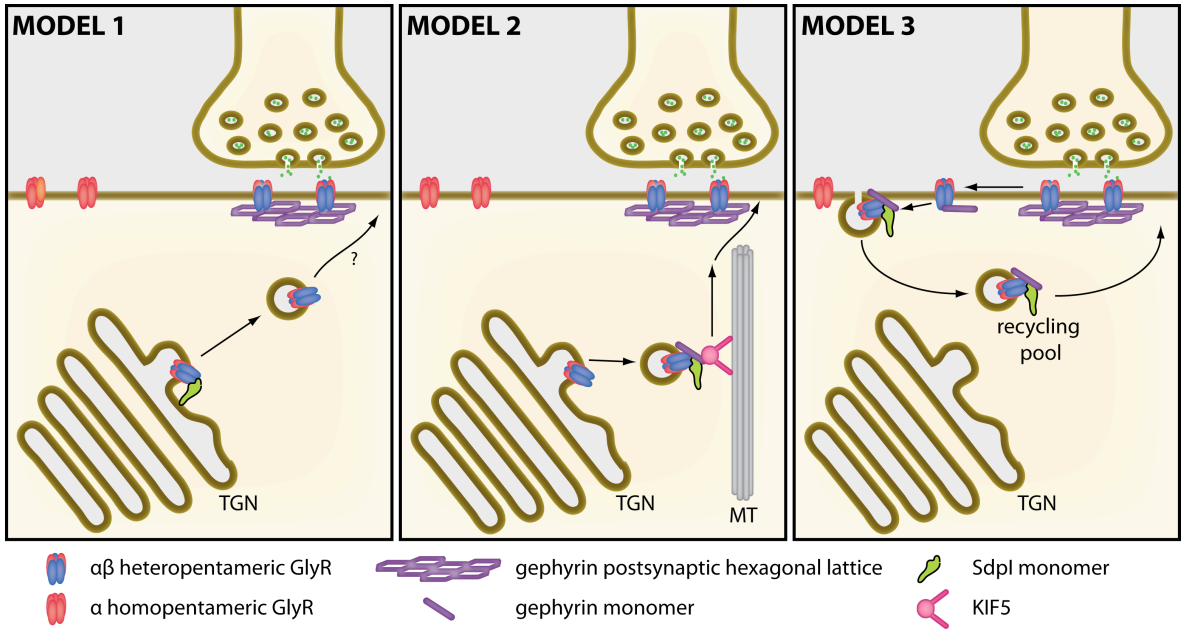

Fig. 5.3. Possible sites of SdpI function in GlyR trafficking. Model 1: ER/TGN exit of heteropentameric GlyRs. After synthesis and assembly in the ER, GlyRs undergo post-translational modifications at the Golgi apparatus. SdpI might recruit heteropentameric GlyRs to budding vesicles in the TGN, thus regulating their sorting to somatodendritic extrasynaptic sites in the plasma membrane. From these extrasynaptic sites, GlyRs diffuse laterally in the plasma membrane and get trapped at gephyrin scaffolds formed at synaptic sites. **Model 2: Anterograde trafficking of GlyR-gephyrin complexes.** GlyRs are co-transported with gephyrin along microtubules through the binding of gephyrin to kinesin 5 (Maas et al., 2009). SdpI might be required in this process for the sorting of GlyRs to the anterograde trafficking pathway by binding simultaneously heteropentameric GlyRs and gephyrin. **Model 3: Synaptic recycling of heteropentameric GlyRs.** Similarly as for the recycling of synaptic $GABA_A$Rs, GlyRs might undergo a recycling process, which involves their endocytosis to a subsynaptic intracellular pool and reinsertion into the plasma membrane. SdpI might be implicated in this recycling process, either by recruiting GlyRs diffusing out of synaptic sites to endocytic zones or by stabilizing the endocytosed GlyRs in the subsynaptic pool by inhibiting their degradation and inducing their sorting to the plasma membrane. In models 2 and 3, gephyrin is depicted as monomer at some stages. This has only been done to make the models as simple as possible. Presumably, intracellular gephyrin is trimeric.

5.2 Vps35

5.2.1 Vps35 interacts with the GlyRβ subunit and gephyrin

The retromer complex drives the retrieval of receptors in yeast, plants and mammals (Seaman et al., 1998; Bonifacino and Hurley, 2008). A broad spectrum of receptor types is sorted by the retromer complex for internalization or recycling, e.g. wingless, the ion transporter DMT1, the cation-independent mannose-6-phosphate receptor, the polymeric immunoglobulin receptor, etc. (Vergés et al., 2004; Arighi et al., 2004; Belenkaya et al., 2008; Tabuchi et al., 2010). Vps35 plays a central role in the receptor retrieving function of the retromer, because it is the subunit responsible for the interaction with the cytoplasmic tails of the receptors (Nothwehr et al., 2000). Here, the GlyRβ subunit was shown to bind Vps35. *In vitro* studies demonstrated that Vps35 interacts directly with 49 aa of the GlyRβ-intracellular loop (see 4.2.1). Furthermore, these studies also revealed that gephyrin binds directly to Vps35 *in vitro* (see 4.2.1). However, the domains and binding motifs driving the Vps35-GlyRβ and Vps35-gephyrin interactions remain to be elucidated.

Previous studies have shown that different Vps35 mutant alleles exhibit cargo-specific defects in membrane protein retrieval, demonstrating that distinct motifs in the sequence of yeast Vps35 govern binding to cytosolic domains of different cargo proteins (Nothwehr et al., 1999). Thus, it appears conceivable that different binding motifs of Vps35 bind independently to the GlyR and gephyrin. *In vitro* competition assays using an immoilized GST-Vps35 construct and the GlyRβ loop and gephyrin as binding proteins might help to clarify this question. It should however, be noted that consensus sequences for the general retrieval of receptors by the retromer complex have not been identified. Short hydrophobic sequence motifs, such as WLM and FLV, in the cytosolic tails of the cation-independent mannose-6-phosphate receptor and sortilin, respectively, have been found to serve as crucial binding sites for cargo recognition (Seaman 2007). Similarly, in the cytosolic tail of dipeptidyl aminopeptidase A the sequence FxFxD was found to be required for its interaction with Vps35 (Nothwehr et al., 2000). Common features of the yeast and mammalian binding motifs are hydrophobicity and the presence of aromatic residues (Bonifacino and Hurley, 2008). Inspection of the GlyRβ loop and gephyrin sequences confirmed that none of the Vps35 recognition motifs identified so far is present in these proteins. Notably, the 49 aa of the GlyRβ loop displaying Vps35 binding comprise one aromatic residue F400, which is highly conserved in mouse, rat, human and zebrafish (see Fig. 5.4.A). Thus, this

residue might form part of the Vps35 recognition motif. Additionally, the F400 residue is known to be involved in gephyrin binding (Meyer et al., 1995). Assuming that Vps35 interacts with the F400 residue, this would imply an overlap of the Vps35 and gephyrin binding sequences, and hence mutually exclusive binding of these proteins to the GlyRβ subunit.

In gephyrin, a phenylalanine repeat sequence FQFIL resembling the FxFxD motif in dipeptidyl aminopeptidase A and a short sequence motif FPV reminiscent of the FLV recognition motif of sortilin are highly conserved in the gephyrin–E- and G-domains, respectively, of mammals, chicken and gephyrin isoform 1 from zebrafish (see Fig. 5.4.B). An additional short sequence motif FVV in the G-domain is conserved in mammals and chicken (see Fig. 5.4.B). These sequences contain hydrophobic residues such as phenylalanines that might be hidden in the domains and not accessible from the surface. However, the gephyrin crystal structure shows that the phenylalanine repeat in the E-domain and the FPV sequence, but not the FVV sequence, of the G-domain are exposed in the folded protein even after E-domain dimerization and G-domain trimerization. The substitution of the phenylalanine residues in these motifs of both gephyrin and the GlyRβ loop might disclose a putative consensus motif important for Vps35 recognition, such as the phenylalanine repeats FxF or the highly hydrophobic motifs FϕV (ϕ stands for an hydrophobic residue). Clearly, further studies are required to uncover the binding motifs for retromer-specific retrieval of synaptic receptors.

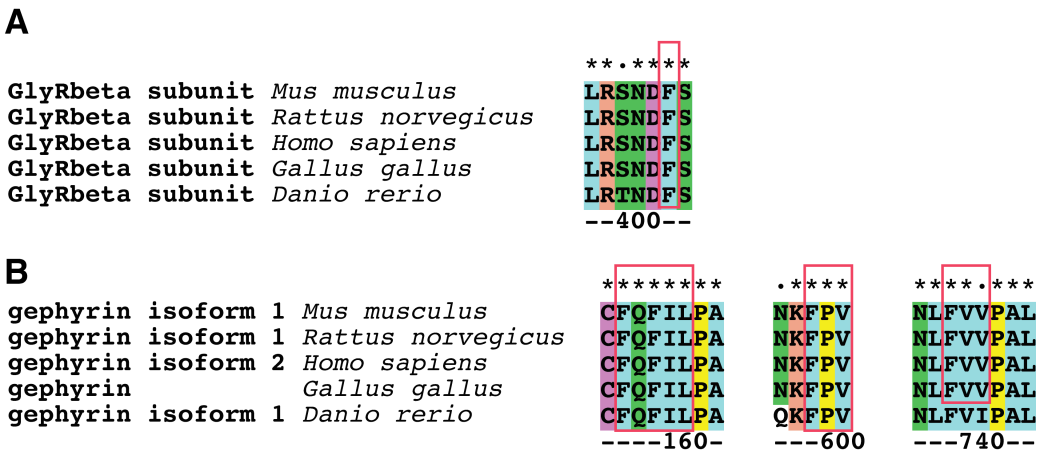

Fig. 5.4. Putative Vps35 binding sites in the GlyRβ loop and gephyrin. A. Multiple alignments of the protein sequences from aa 418 to 422 of the GlyRβ intracellular loops from different species. The phenylalanine residue in the 49 aa construct used for the pull-down of Vps35 by the GlyRβ loop is boxed in red. This residue is proposed to be required for Vps35 binding. **B.** Multiple alignments of gephyrin fragments from different species. The fragments depicted correspond to the aa sequences: 155 to 162, 596 to 600 and 736 to 743. Phenylalanine-containing sequences, thought to constitute putative binding sequences for Vps35 are boxed in red. Asterisks indicate conserved aa in all species. Dots indicate aa conserved in mammals and chicken.

5.2.2 Role of Vps35 in GlyR trafficking?

The retromer was first described in yeast as a complex mediating retrieval of Vps10p, the carboxypeptidase Y vacuolar protein receptor (Seaman et al., 1998). Two members of the Vps10 family of receptors, SorLA and sortilin, have been identified as interacting partners of the retromer complex in the mammalian CNS (Small et al., 2005, Rogaeva et al., 2007). Here, the GlyRβ subunit was found to be a new binding partner of Vps35 (see 4.2) suggesting that the GlyR is the third receptor known to associate with the retromer complex in neurons. Since Vps35 binds directly not only to the GlyRβ loop but also to gephyrin (see 4.2.1), the possible existence of ternary Vps35/GlyR/gephyrin complexes will have to be examined in neurons.

Several studies have demonstrated that the retromer complex is required for the sorting of membrane receptors for acid hydrolases to lysosomes, transcytosis of the polymeric immunoglobulin receptor 8, Wnt gradient formation, recycling of the iron transporter DMT1 and processing of the amyloid precursor protein in neuronal and non-neuronal cells (Arighi et al., 2004; Vergés et al., 2004; Coudreuse et al., 2006; Muhammad et al., 2008; Tabuchi et al., 2010). This is consistent with the retromer complex functioning in a general transport pathway that is essential for the retrieval or recycling of transmembrane proteins. Our demonstration that the GlyRβ subunit binds directly to Vps35 provides the first evidence for a role of the retromer complex in the retrieval or recycling of synaptic receptors. We also found by using Western blotting that Vps35 is expressed in spinal cord tissue, and by immunocytochemistry that Vps35 is present in the soma and along processes of cultured spinal cord neurons. These findings support the concept of retromer-mediated transport of GlyRs in the spinal cord. Future experiments should show whether Vps35 binding is restricted to GlyRs or also occurs with other inhibitory receptors, such as $GABA_A$Rs or the excitatory NMDARs and AMPARs.

The generation of Vps26 -/- mice has shown that mice homozygous for the inactive Vps26 allele present gross developmental abnormalities and are not viable (Lee et al., 1992). Moreover, analysis of the heterozygous animals has revealed that reduced protein levels of Vps26 cause a secondary reduction of Vps35, leading to retromer deficiency. Behavioural studies performed in the heterozygous Vps26 -/- mice indicate that retromer-deficient animals have a defect in hippocampus-dependent memory formation but no motor, sensory or motivational deficits. The investigation of inhibitory receptor distribution in these retromer-deficient mice should help to

disclose a putative role of the retromer in synaptic receptor trafficking and elucidate the roles of the retromer complex in synaptic receptor clustering and neurotransmission.

Expression of the Vps35 gene in the grey matter of mouse spinal cord is documented by *in situ* hybridization data in the Allen Brain Atlas (http://mousespinal.brain-map.org/gene/detail/Vps35.html). The immunocytochemical work performed here proves the presence of Vps35 protein in neuritic processes of spinal cord neurons. Future analyses of the subcellular localization of Vps35 by electron microscopy might clarify whether the retromer complex is synaptic or perisynaptically localized, next to postsynaptic structures or in subsynaptic vesicles. Similarly, histological studies might establish the expression pattern of this protein in the CNS and resolve whether the involvement of the retromer complex in synaptic receptor trafficking is brain region-dependent.

5.3 Nbea

5.3.1 Nbea interacts with the GlyRβ subunit

Nbea was initially identified as a neuron specific A-kinase anchoring protein (AKAP) (Wang et al., 2000). Nbea interacts with the type II regulatory subunit of protein kinase A (PKA), which has been the unique interaction partner known so far. In this thesis, the GlyRβ subunit was identified as a binding partner of Nbea, which binds to 49 aa, from position 378 to 426, of the GlyRβ intracellular loop. However, the Nbea domain responsible for the binding to the GlyRβ subunit could not be mapped during the time available. The *in vitro* results presented here show that both the NbeaBCD and NbeaEFG fragments interact with the GlyRβloop. This suggests the presence of multiple binding sites for GlyRβ binding in Nbea. Future mapping experiments should reveal whether the interaction of Nbea with the GlyR depends on single domain-ligand recognition or involves the interaction of multiple domains of Nbea with the GlyRβloop.

Investigation of the interaction of Nbea with PKA has revealed that a short sequence of 19 aa in the NbeaB domain is responsible for binding to the type II regulatory subunit of PKA (Wang et al., 2000). NbeaB as well as NbeaD domains share low similarity with the Nbea isoform BGL which might explain the specific Nbea-PKA interaction in neurons. Similarly, the NbeaB and NbeaD domains might be the regions implicated in specific Nbea-GlyRβ loop interaction. Further analysis of a putative interaction between BGL and the GlyRβ loop should help to disclose whether the GlyRβ interaction with BEACH domain-containing proteins is restricted to Nbea.

5.3.2 Synaptic localization of Nbea

The distribution of Nbea in the CNS had been investigated previously by immunocytochemistry both at the light and electron microscopic level in forebrain regions such as the hippocampus (Wang et al, 2000). Additionally, the expression of the Nbea gene has been analyzed in the mouse brain by *in situ* hybridization (http://mouse.brain-map.org/brain/Nbeal2.html?ispopup=1). However, the presence of Nbea protein in spinal cord had not been studied. Here, the antibody employed in immunocytochemical studies by Wang et al. was used to investigate the localization of Nbea in spinal cord neurons. Nbea expression was demonstrated by Western blotting (data not shown) and immunocytochemistry (see 4.3.2) in spinal cord neurons. Additionally,

examination of the staining pattern revealed that Nbea is found in the neuronal somata and along neurites in hippocampal as well as spinal cord neurons (see 4.3.2).

The immuno-electron microscopic analysis performed by Wang et al. (2000) has revealed Nbea near the TGN in rat cerebellar neurons. In agreement with this, colocalization experiments using antibodies specific for Nbea and the TGN-marker TGN38 showed that Nbea displays a near TGN localization in the soma and along neuronal processes of hippocampal neurons (see 4.3.2). In addition to being present near the TGN, Nbea immunoreactivity has been also reported previously at subpopulations of synapses near postsynaptic plasma membranes (Wang et al., 2000). However, a preferential association of Nbea with excitatory or inhibitory synapses had not been examined. This work shows for the first time that Nbea staining is apposed to both excitatory and inhibitory synaptic markers (see 4.3.2), indicating that Nbea does not display a preferential localization at distinct synapses. Consistent with this result, recent electrophysiological studies performed in the Nbea -/- mice have shown that excitatory as well as inhibitory postsynaptic currents are impaired (Medrinah et al., 2009), suggesting a role of Nbea at both types of synapses.

5.3.3 A role of Nbea in GlyR trafficking?

Nbea is a member of the BEACH domain family of proteins. Homologs of this family such as the lysosomal trafficking regulator (LYST) have been proposed to mediate the subcellular targeting of membrane proteins (Nagle et al., 1996; Faigle et al 1998). Nbea -/- mice show reduced levels of a subset of synaptic proteins and reduced numbers of synaptic contacts (Medrinah et al., 2009). This suggests a general role of Nbea in synapse formation and function. The results presented here revealed a direct interaction of Nbea with the GlyRβ subunit, and colocalization immunocytochemistry supports an accumulation of Nbea at inhibitory synapses (see 4.3). Together these results are in agreement with a synaptic function of Nbea, which involves direct interactions with membrane receptors. However, the analysis of GlyR contents by Western blotting showed that receptor levels are not affected upon Nbea knockout (Medrinah et al., 2009). This indicates that Nbea is not involved in GlyR degradation pathways. Whether Nbea is indeed involved in GlyR trafficking pathways needs further investigation, in particular a careful analysis of receptor surface expression. So far, functions of Nbea in the trafficking of different types of inhibitory and excitatory receptors remain speculative.

6 BIBLIOGRAPHY

Akagi, H., Hirai, K. & Hishinuma, F. (1991). *Functional properties of strychnine-sensitive glycine receptors expressed in Xenopus oocytes injected with a single mRNA*. Neurosci Res. 11, 28-40.

Akagi, H., Hirai, K. & Hishinuma, F. (1991). *Cloning of a glycine receptor subtype expressed in rat brain and spinal cord during a specific period of neuronal development*. FEBS Lett. 281, 160-166.

Andersson, F., Jakobsson, J., Lšw, P., Shupliakov, O. & Brodin, L. (2008). *Perturbation of syndapin/PACSIN impairs synaptic vesicle recycling evoked by intense stimulation*. J Neurosci. 28, 3925-3933.

Anggono, V. & Robinson, P.J. (2007). *Syndapin I and endophilin I bind overlapping proline-rich regions of dynamin I: role in synaptic vesicle endocytosis*. J Neurochem. 102, 931-943.

Anggono, V., Smillie, K.J., Graham, M.E., Valova, V.A., Cousin, M.A. & Robinson, P.J. (2006). *Syndapin I is the phosphorylation-regulated dynamin I partner in synaptic vesicle endocytosis*. Nat Neurosci. 9, 752-760.

Arighi, C.N., Hartnell, L.M., Aguilar, R.C., Haft, C.R. & Bonifacino, J.S. (2004). *Role of the mammalian retromer in sorting of the cation-independent mannose 6-phosphate receptor*. J Cell Biol. 165, 123-133.

Baer, K., Waldvogel, H.J., During, M.J., Snell, R.G., Faull, R.L.M. & Rees, M.I. (2003). *Association of gephyrin and glycine receptors in the human brainstem and spinal cord: an immunohistochemical analysis*. Neuroscience. 122, 773-784.

Baer, K., Waldvogel, H.J., Faull, R.L.M. & Rees, M.I. (2009). *Localization of glycine receptors in the human forebrain, brainstem, and cervical spinal cord: an immunohistochemical review*. Front Mol Neurosci. 2, 25.

Barber, A.J., Pepper, D.S. & Jamieson, G.A. (1971). *A comparison of methods for platelet lysis and the isolation of platelet membranes*. Thromb Diath Haemorrh. 26, 38-57.

Barrett, S., Beck, J.C., Bernier, R., Bisson, E., Braun, T.A., Casavant, T.L., Childress, D., Folstein, S.E., Garcia, M., Gardiner, M.B., Gilman, S., Haines, J.L., Hopkins, K., Landa, R., Meyer, N.H., Mullane, J.A., Nishimura, D.Y., Palmer, P., Piven, J., Purdy, J., Santangelo, S.L., Searby, C., Sheffield, V., Singleton, J. & Slager, S. (1999). *An autosomal genomic screen for autism. Collaborative linkage study of autism*. Am J Med Genet. 88, 609-615.

Becker, C.M., Hoch, W. & Betz, H. (1988). *Glycine receptor heterogeneity in rat spinal cord during postnatal development*. EMBO J. 7, 3717-3726.

Belenkaya, T.Y., Wu, Y., Tang, X., Zhou, B., Cheng, L., Sharma, Y.V., Yan, D., Selva, E.M. & Lin, X. (2008). *The retromer complex influences Wnt secretion by recycling wntless from endosomes to the trans-Golgi network*. Dev Cell. 14, 120-131.

Betz, H. (1991). *Glycine receptors: heterogeneous and widespread in the mammalian brain*. Trends Neurosci. 14, 458-461.

Betz, H., Kuhse, J., Schmieden, V., Malosio, M.L., Langosch, D., Prior, P., Schmitt, B. & Kirsch, J. (1991). *How to build a glycinergic postsynaptic membrane*. J Cell Sci Suppl. 15, 23-25.

Blanpied, T.A., Scott, D.B. & Ehlers, M.D. (2002). *Dynamics and regulation of clathrin coats at specialized endocytic zones of dendrites and spines*. Neuron. 36, 435-449.

Bloch, R.J. & Froehner, S.C. (1987). *The relationship of the postsynaptic 43K protein to acetylcholine receptors in receptor clusters isolated from cultured rat myotubes*. J Cell Biol. 104, 645-654.

Bogdanov, Y., Michels, G., Armstrong-Gold, C., Haydon, P.G., Lindstrom, J., Pangalos, M. & Moss, S.J. (2006). *Synaptic GABAA receptors are directly recruited from their extrasynaptic counterparts*. EMBO J. 25, 4381-4389.

Bonifacino, J.S. & Hurley, J.H. (2008). *Retromer*. Curr Opin Cell Biol. 20, 427-436.

Bormann, J., Rundstršm, N., Betz, H. & Langosch, D. (1993). *Residues within transmembrane segment M2 determine chloride conductance of glycine receptor homo- and hetero-oligomers*. EMBO J. 12, 3729-3737.

Braulke, T. & Bonifacino, J.S. (2009). *Sorting of lysosomal proteins*. Biochim Biophys Acta. 1793, 605-614.

Braun, A., Pinyol, R., Dahlhaus, R., Koch, D., Fonarev, P., Grant, B.D., Kessels, M.M. & Qualmann, B. (2005). *EHD proteins associate with syndapin I and II and such interactions play a crucial role in endosomal recycling*. Mol Biol Cell. 16, 3642-3658.

Burgess, A., Mornon, J.-P., de Saint-Basile, G. & Callebaut, I. (2009). *A concanavalin A-like lectin domain in the CHS1/LYST protein, shared by members of the BEACH family*. Bioinformatics. 25, 1219-1222.

Carlton, J.G., Bujny, M.V., Peter, B.J., Oorschot, V.M.J., Rutherford, A., Arkell, R.S., Klumperman, J., McMahon, H.T. & Cullen, P.J. (2005). *Sorting nexin-2 is associated with tubular elements of the early endosome, but is not essential for retromer-mediated endosome-to-TGN transport*. J Cell Sci. 118, 4527-4539.

Castermans, D., Wilquet, V., Parthoens, E., Huysmans, C., Steyaert, J., Swinnen, L., Fryns, J.-P., de Ven, W.V. & Devriendt, K. (2003). *The neurobeachin gene is disrupted by a translocation in a patient with idiopathic autism*. J Med Genet. 40, 352-356.

Charych, E.I., Yu, W., Miralles, C.P., Serwanski, D.R., Li, X., Rubio, M. & Blas, A.L.D. (2004). *The brefeldin A-inhibited GDP/GTP exchange factor 2, a protein involved in vesicular trafficking, interacts with the beta subunits of the GABA receptors*. J Neurochem. 90, 173-189.

Chattipakorn, S.C. & McMahon, L.L. (2002). *Pharmacological characterization of glycine-gated chloride currents recorded in rat hippocampal slices*. J Neurophysiol. 87, 1515-1525.

Clayton, E.L., Anggono, V., Smillie, K.J., Chau, N., Robinson, P.J. & Cousin, M.A. (2009). *The phospho-dependent dynamin-syndapin interaction triggers activity-dependent bulk endocytosis of synaptic vesicles*. J Neurosci. 29, 7706-7717.

Colin, I., Rostaing, P., Augustin, A. & Triller, A. (1998). *Localization of components of glycinergic synapses during rat spinal cord development*. J Comp Neurol. 398, 359-372.

Cooper, A.A. & Stevens, T.H. (1996). *Vps10p cycles between the late-Golgi and prevacuolar compartments in its function as the sorting receptor for multiple yeast vacuolar hydrolases*. J Cell Biol. 133, 529-541.

Cremona, O., Paolo, G.D., Wenk, M.R., LŸthi, A., Kim, W.T., Takei, K., Daniell, L., Nemoto, Y., Shears, S.B., Flavell, R.A., McCormick, D.A. & Camilli, P.D. (1999). *Essential role of phosphoinositide metabolism in synaptic vesicle recycling*. Cell. 99, 179-188.

Dahan, M., LŽvi, S., Luccardini, C., Rostaing, P., Riveau, B. & Triller, A. (2003). *Diffusion dynamics of glycine receptors revealed by single-quantum dot tracking*. Science. 302, 442-445.

Devignot, V., de Carvalho, L.P., Bregestovski, P. & Goblet, C. (2003). *A novel glycine receptor alpha Z1 subunit variant in the zebrafish brain*. Neuroscience. 122, 449-457.

Dharmalingam, E., Haeckel, A., Pinyol, R., Schwintzer, L., Koch, D., Kessels, M.M. & Qualmann, B. (2009). *F-BAR proteins of the syndapin family shape the plasma membrane and are crucial for neuromorphogenesis*. J Neurosci. 29, 13315-13327.

Dumoulin, A., LŽvi, S., Riveau, B., Gasnier, B. & Triller, A. (2000). *Formation of mixed glycine and GABAergic synapses in cultured spinal cord neurons*. Eur J Neurosci. 12, 3883-3892.

Dumoulin, A., Triller, A. & DieudonnŽ, S. (2001). *IPSC kinetics at identified GABAergic and mixed GABAergic and glycinergic synapses onto cerebellar Golgi cells*. J Neurosci. 21, 6045-6057.

Dumoulin, A., Triller, A. & Kneussel, M. (2009). *Cellular transport and membrane dynamics of the glycine receptor*. Front Mol Neurosci. 2, 28.

Edeling, M.A., Sanker, S., Shima, T., Umasankar, P.K., Hšning, S., Kim, H.Y., Davidson, L.A., Watkins, S.C., Tsang, M., Owen, D.J. & Traub, L.M. (2009). *Structural requirements for PACSIN/Syndapin operation during zebrafish embryonic notochord development*. PLoS One. 4, e8150.

Faigle, W., Raposo, G., Tenza, D., Pinet, V., Vogt, A.B., Kropshofer, H., Fischer, A., de Saint-Basile, G. & Amigorena, S. (1998). *Deficient peptide loading and MHC class II endosomal sorting in a human genetic immunodeficiency disease: the Chediak-Higashi syndrome*. J Cell Biol. 141, 1121-1134.

Feng, G., Tintrup, H., Kirsch, J., Nichol, M.C., Kuhse, J., Betz, H. & Sanes, J.R. (1998). *Dual requirement for gephyrin in glycine receptor clustering and molybdoenzyme activity*. Science. 282, 1321-1324.

Feng, S., Chen, J.K., Yu, H., Simon, J.A. & Schreiber, S.L. (1994). *Two binding orientations for peptides to the Src SH3 domain: development of a general model for SH3-ligand interactions*. Science. 266, 1241-1247.

Ferguson, S.M., Brasnjo, G., Hayashi, M., Wšlfel, M., Collesi, C., Giovedi, S., Raimondi, A., Gong, L.-W., Ariel, P., Paradise, S., O'toole, E., Flavell, R., Cremona, O., Miesenbšck, G., Ryan, T.A. & Camilli, P.D. (2007). *A selective activity-dependent requirement for dynamin 1 in synaptic vesicle endocytosis*. Science. 316, 570-574.

Frost, A., Perera, R., Roux, A., Spasov, K., Destaing, O., Egelman, E.H., Camilli, P.D. & Unger, V.M. (2008). *Structural basis of membrane invagination by F-BAR domains*. Cell. 132, 807-817.

Fuhrmann, J.C., Kins, S., Rostaing, P., Far, O.E., Kirsch, J., Sheng, M., Triller, A., Betz, H. & Kneussel, M. (2002). *Gephyrin interacts with Dynein light chains 1 and 2, components of motor protein complexes*. J Neurosci. 22, 5393-5402.

Fuji, K., Shimada, T., Takahashi, H., Tamura, K., Koumoto, Y., Utsumi, S., Nishizawa, K., Maruyama, N. & Hara-Nishimura, I. (2007). *Arabidopsis vacuolar sorting mutants (green fluorescent seed) can be identified efficiently by secretion of vacuole-targeted green fluorescent protein in their seeds*. Plant Cell. 19, 597-609.

Fujita, M., Sato, K., Sato, M., Inoue, T., Kozuka, T. & Tohyama, M. (1991). *Regional distribution of the cells expressing glycine receptor beta subunit mRNA in the rat brain*. Brain Res. 560, 23-37.

Gallop, J.L. & McMahon, H.T. (2005). *BAR domains and membrane curvature: bringing your curves to the BAR*. Biochem Soc Symp., 223-231.

Giesemann, T., Schwarz, G., Nawrotzki, R., Berhšrster, K., Rothkegel, M., SchlŸter, K., Schrader, N., Schindelin, H., Mendel, R.R., Kirsch, J. & Jockusch, B.M. (2003). *Complex formation between the postsynaptic scaffolding protein gephyrin, profilin, and Mena: a possible link to the microfilament system*. J Neurosci. 23, 8330-8339.

Gokool, S., Tattersall, D. & Seaman, M.N.J. (2007). *EHD1 interacts with retromer to stabilize SNX1 tubules and facilitate endosome-to-Golgi retrieval*. Traffic. 8, 1873-1886.

Green, W.N. & Millar, N.S. (1995). *Ion-channel assembly*. Trends Neurosci. 18, 280-287.

Grenningloh, G., Pribilla, I., Prior, P., Multhaup, G., Beyreuther, K., Taleb, O. & Betz, H. (1990). *Cloning and expression of the 58 kd beta subunit of the inhibitory glycine receptor*. Neuron. 4, 963-970.

Grenningloh, G., Rienitz, A., Schmitt, B., Methfessel, C., Zensen, M., Beyreuther, K., Gundelfinger, E.D. & Betz, H.

(1987). *The strychnine-binding subunit of the glycine receptor shows homology with nicotinic acetylcholine receptors*. Nature. 328, 215-220.

Grenningloh, G., Schmieden, V., Schofield, P.R., Seeburg, P.H., Siddique, T., Mohandas, T.K., Becker, C.M. & Betz, H. (1990). *Alpha subunit variants of the human glycine receptor: primary structures, functional expression and chromosomal localization of the corresponding genes*. EMBO J. 9, 771-776.

Griffin, C.T., Trejo, J. & Magnuson, T. (2005). *Genetic evidence for a mammalian retromer complex containing sorting nexins 1 and 2*. Proc Natl Acad Sci U S A. 102, 15173-15177.

Griffon, N., BŸttner, C., Nicke, A., Kuhse, J., Schmalzing, G. & Betz, H. (1999). *Molecular determinants of glycine receptor subunit assembly*. EMBO J. 18, 4711-4721.

Grudzinska, J., Schemm, R., Haeger, S., Nicke, A., Schmalzing, G., Betz, H. & Laube, B. (2005). *The beta subunit determines the ligand binding properties of synaptic glycine receptors*. Neuron. 45, 727-739.

Haeger, S., Kuzmin, D., Detro-Dassen, S., Lang, N., Kilb, M., Tsetlin, V., Betz, H., Laube, B. & Schmalzing, G. (2010). *An intramembrane aromatic network determines pentameric assembly of Cys-loop receptors*. Nat Struct Mol Biol. 17, 90-98.

Halbach, A., Mšrgelin, M., Baumgarten, M., Milbrandt, M., Paulsson, M. & Plomann, M. (2007). *PACSIN 1 forms tetramers via its N-terminal F-BAR domain*. FEBS J. 274, 773-782.

Harvey, K., Duguid, I.C., Alldred, M.J., Beatty, S.E., Ward, H., Keep, N.H., Lingenfelter, S.E., Pearce, B.R., Lundgren, J., Owen, M.J., Smart, T.G., LŸscher, B., Rees, M.I. & Harvey, R.J. (2004). *The GDP-GTP exchange factor collybistin: an essential determinant of neuronal gephyrin clustering*. J Neurosci. 24, 5816-5826.

Harvey, R.J., Schmieden, V., Holst, A.V., Laube, B., Rohrer, H. & Betz, H. (2000). *Glycine receptors containing the alpha4 subunit in the embryonic sympathetic nervous system, spinal cord and male genital ridge*. Eur J Neurosci. 12, 994-1001.

Henne, W.M., Boucrot, E., Meinecke, M., Evergren, E., Vallis, Y., Mittal, R. & McMahon, H.T. (2010). *FCHo Proteins Are Nucleators of Clathrin-Mediated Endocytosis*. Science.

Henne, W.M., Kent, H.M., Ford, M.G.J., Hegde, B.G., Daumke, O., Butler, P.J.G., Mittal, R., Langen, R., Evans, P.R. & McMahon, H.T. (2007). *Structure and analysis of FCHo2 F-BAR domain: a dimerizing and membrane recruitment module that effects membrane curvature*. Structure. 15, 839-852.

Hevers, W. & LŸddens, H. (1998). *The diversity of GABAA receptors. Pharmacological and electrophysiological properties of GABAA channel subtypes*. Mol Neurobiol. 18, 35-86.

Hierro, A., Rojas, A.L., Rojas, R., Murthy, N., Effantin, G., Kajava, A.V., Steven, A.C., Bonifacino, J.S. & Hurley, J.H. (2007). *Functional architecture of the retromer cargo-recognition complex*. Nature. 449, 1063-1067.

Hilfiker, S., Pieribone, V.A., Czernik, A.J., Kao, H.T., Augustine, G.J. & Greengard, P. (1999). *Synapsins as regulators of neurotransmitter release*. Philos Trans R Soc Lond B Biol Sci. 354, 269-279.

Hoflack, B., Fujimoto, K. & Kornfeld, S. (1987). *The interaction of phosphorylated oligosaccharides and lysosomal enzymes with bovine liver cation-dependent mannose 6-phosphate receptor*. J Biol Chem. 262, 123-129.

Horazdovsky, B.F., Davies, B.A., Seaman, M.N., McLaughlin, S.A., Yoon, S. & Emr, S.D. (1997). *A sorting nexin-1 homologue, Vps5p, forms a complex with Vps17p and is required for recycling the vacuolar protein-sorting receptor*. Mol Biol Cell. 8, 1529-1541.

Itoh, T., Erdmann, K.S., Roux, A., Habermann, B., Werner, H. & Camilli, P.D. (2005). *Dynamin and the actin cytoskeleton cooperatively regulate plasma membrane invagination by BAR and F-BAR proteins*. Dev Cell. 9, 791-804.

Jeong, H.-J., Jang, I.-S., Moorhouse, A.J. & Akaike, N. (2003). *Activation of presynaptic glycine receptors facilitates glycine release from presynaptic terminals synapsing onto rat spinal sacral dorsal commissural nucleus neurons*. J Physiol. 550, 373-383.

Jogl, G., Shen, Y., Gebauer, D., Li, J., Wiegmann, K., Kashkar, H., Kršnke, M. & Tong, L. (2002). *Crystal structure of the BEACH domain reveals an unusual fold and extensive association with a novel PH domain*. EMBO J. 21, 4785-4795.

Johnson, K.F., Chan, W. & Kornfeld, S. (1990). *Cation-dependent mannose 6-phosphate receptor contains two internalization signals in its cytoplasmic domain*. Proc Natl Acad Sci U S A. 87, 10010-10014.

Jonas, P., Bischofberger, J. & SandkŸhler, J. (1998). *Corelease of two fast neurotransmitters at a central synapse*. Science. 281, 419-424.

Kaelin, W.G., Krek, W., Sellers, W.R., DeCaprio, J.A., Ajchenbaum, F., Fuchs, C.S., Chittenden, T., Li, Y., Farnham, P.J. & Blanar, M.A. (1992). *Expression cloning of a cDNA encoding a retinoblastoma-binding protein with E2F-like properties*. Cell. 70, 351-364.

Kalscheuer, V.M., Musante, L., Fang, C., Hoffmann, K., Fuchs, C., Carta, E., Deas, E., Venkateswarlu, K., Menzel, C., Ullmann, R., Tommerup, N., Dalprˆ, L., Tzschach, A., Selicorni, A., LŸscher, B., Ropers, H.-H., Harvey, K. & Harvey, R.J. (2009). *A balanced chromosomal translocation disrupting ARHGEF9 is associated with epilepsy, anxiety, aggression, and mental retardation*. Hum Mutat. 30, 61-68.

Kessels, M.M., Dong, J., Leibig, W., Westermann, P. & Qualmann, B. (2006). *Complexes of syndapin II with dynamin II promote vesicle formation at the trans-Golgi network*. J Cell Sci. 119, 1504-1516.

Kessels, M.M. & Qualmann, B. (2006). *Syndapin oligomers interconnect the machineries for endocytic vesicle formation and actin polymerization*. J Biol Chem. 281, 13285-13299.

Kessels, M.M. & Qualmann, B. (2004). *The syndapin protein family: linking membrane trafficking with the cytoskeleton*. J Cell Sci. 117, 3077-3086.

Kessels, M.M. & Qualmann, B. (2002). *Syndapins integrate N-WASP in receptor-mediated endocytosis*. EMBO J. 21, 6083-6094.

Kins, S., Betz, H. & Kirsch, J. (2000). *Collybistin, a newly identified brain-specific GEF, induces submembrane clustering of gephyrin*. Nat Neurosci. 3, 22-29.

Kirsch, J. & Betz, H. (1998). *Glycine-receptor activation is required for receptor clustering in spinal neurons*. Nature. 392, 717-720.

Kirsch, J. & Betz, H. (1995). *The postsynaptic localization of the glycine receptor-associated protein gephyrin is regulated by the cytoskeleton*. J Neurosci. 15, 4148-4156.

Kirsch, J. & Betz, H. (1993). *Widespread expression of gephyrin, a putative glycine receptor-tubulin linker protein, in rat brain*. Brain Res. 621, 301-310.

Kirsch, J., Kuhse, J. & Betz, H. (1995). *Targeting of glycine receptor subunits to gephyrin-rich domains in transfected human embryonic kidney cells*. Mol Cell Neurosci. 6, 450-461.

Kirsch, J., Langosch, D., Prior, P., Littauer, U.Z., Schmitt, B. & Betz, H. (1991). *The 93-kDa glycine receptor-associated protein binds to tubulin*. J Biol Chem. 266, 22242-22245.

Kirsch, J., Wolters, I., Triller, A. & Betz, H. (1993). *Gephyrin antisense oligonucleotides prevent glycine receptor clustering in spinal neurons*. Nature. 366, 745-748.

Kittler, J.T., Thomas, P., Tretter, V., Bogdanov, Y.D., Haucke, V., Smart, T.G. & Moss, S.J. (2004). *Huntingtin-*

associated protein 1 regulates inhibitory synaptic transmission by modulating gamma-aminobutyric acid type A receptor membrane trafficking. Proc Natl Acad Sci U S A. 101, 12736-12741.

Kleckner, N.W. & Dingledine, R. (1988). *Requirement for glycine in activation of NMDA-receptors expressed in Xenopus oocytes*. Science. 241, 835-837.

Kotak, V.C., Korada, S., Schwartz, I.R. & Sanes, D.H. (1998). *A developmental shift from GABAergic to glycinergic transmission in the central auditory system*. J Neurosci. 18, 4646-4655.

Kubota, H., Alle, H., Betz, H. & Geiger, J.R.P. (2010). *Presynaptic glycine receptors on hippocampal mossy fibers*. Biochem Biophys Res Commun. 393, 587-591.

Kuhse, J., Kuryatov, A., Maulet, Y., Malosio, M.L., Schmieden, V. & Betz, H. (1991). *Alternative splicing generates two isoforms of the alpha 2 subunit of the inhibitory glycine receptor*. FEBS Lett. 283, 73-77.

Kuhse, J., Laube, B., Magalei, D. & Betz, H. (1993). *Assembly of the inhibitory glycine receptor: identification of amino acid sequence motifs governing subunit stoichiometry*. Neuron. 11, 1049-1056.

Kuhse, J., Schmieden, V. & Betz, H. (1990). *Identification and functional expression of a novel ligand binding subunit of the inhibitory glycine receptor*. J Biol Chem. 265, 22317-22320.

Kumar, V., Alla, S.R., Krishnan, K.S. & Ramaswami, M. (2009). *Syndapin is dispensable for synaptic vesicle endocytosis at the Drosophila larval neuromuscular junction*. Mol Cell Neurosci. 40, 234-241.

Kumar, V., Fricke, R., Bhar, D., Reddy-Alla, S., Krishnan, K.S., Bogdan, S. & Ramaswami, M. (2009). *Syndapin promotes formation of a postsynaptic membrane system in Drosophila*. Mol Biol Cell. 20, 2254-2264.

Langosch, D., Thomas, L. & Betz, H. (1988). *Conserved quaternary structure of ligand-gated ion channels: the postsynaptic glycine receptor is a pentamer*. Proc Natl Acad Sci U S A. 85, 7394-7398.

Lee, E.-A., Cho, J.-H., Choi, I.-S., Nakamura, M., Park, H.-M., Lee, J.-J., Lee, M.-G., Choi, B.-J. & Jang, I.-S. (2009). *Presynaptic glycine receptors facilitate spontaneous glutamate release onto hilar neurons in the rat hippocampus*. J Neurochem. 109, 275-286.

Lee, J.J., Radice, G., Perkins, C.P. & Costantini, F. (1992). *Identification and characterization of a novel, evolutionarily conserved gene disrupted by the murine H beta 58 embryonic lethal transgene insertion*. Development. 115, 277-288.

Li, S.S.-C. (2005). *Specificity and versatility of SH3 and other proline-recognition domains: structural basis and implications for cellular signal transduction*. Biochem J. 390, 641-653.

Lopez, L.A. & Sheetz, M.P. (1993). *Steric inhibition of cytoplasmic dynein and kinesin motility by MAP2*. Cell Motil Cytoskeleton. 24, 1-16.

Lozanne, A.D. (2003). *The role of BEACH proteins in Dictyostelium*. Traffic. 4, 6-12.

Lu, J., Helton, T.D., Blanpied, T.A., R‡cz, B., Newpher, T.M., Weinberg, R.J. & Ehlers, M.D. (2007). *Postsynaptic positioning of endocytic zones and AMPA receptor cycling by physical coupling of dynamin-3 to Homer*. Neuron. 55, 874-889.

Lynch, J.W. (2004). *Molecular structure and function of the glycine receptor chloride channel*. Physiol Rev. 84, 1051-1095.

Maas, C., Belgardt, D., Lee, H.K., Heisler, F.F., Lappe-Siefke, C., Magiera, M.M., van Dijk, J., Hausrat, T.J., Janke, C. & Kneussel, M. (2009). *Synaptic activation modifies microtubules underlying transport of postsynaptic cargo*. Proc Natl Acad Sci U S A. 106, 8731-8736.

Maas, C., Tagnaouti, N., Loebrich, S., Behrend, B., Lappe-Siefke, C. & Kneussel, M. (2006). *Neuronal cotransport of glycine receptor and the scaffold protein gephyrin*. J Cell Biol. 172, 441-451.

Malosio, M.L., Grenningloh, G., Kuhse, J., Schmieden, V., Schmitt, B., Prior, P. & Betz, H. (1991). *Alternative splicing generates two variants of the alpha 1 subunit of the inhibitory glycine receptor*. J Biol Chem. 266, 2048-2053.

Malosio, M.L., Marquze-Pouey, B., Kuhse, J. & Betz, H. (1991). *Widespread expression of glycine receptor subunit mRNAs in the adult and developing rat brain*. EMBO J. 10, 2401-2409.

Mari, M., Bujny, M.V., Zeuschner, D., Geerts, W.J.C., Griffith, J., Petersen, C.M., Cullen, P.J., Klumperman, J. & Geuze, H.J. (2008). *SNX1 defines an early endosomal recycling exit for sortilin and mannose 6-phosphate receptors*. Traffic. 9, 380-393.

von Massow, A., Mandelkow, E.M. & Mandelkow, E. (1989). *Interaction between kinesin, microtubules, and microtubule-associated protein 2*. Cell Motil Cytoskeleton. 14, 562-571.

Matzenbach, B., Maulet, Y., Sefton, L., Courtier, B., Avner, P., GuŽnet, J.L. & Betz, H. (1994). *Structural analysis of mouse glycine receptor alpha subunit genes. Identification and chromosomal localization of a novel variant*. J Biol Chem. 269, 2607-2612.

Medrihan, L., Rohlmann, A., Fairless, R., Andrae, J., Dšring, M., Missler, M., Zhang, W. & Kilimann, M.W. (2009). *Neurobeachin, a protein implicated in membrane protein traffic and autism, is required for the formation and functioning of central synapses*. J Physiol. 587, 5095-5106.

Meier, J., Vannier, C., SergŽ, A., Triller, A. & Choquet, D. (2001). *Fast and reversible trapping of surface glycine receptors by gephyrin*. Nat Neurosci. 4, 253-260.

Meyer, G., Kirsch, J., Betz, H. & Langosch, D. (1995). *Identification of a gephyrin binding motif on the glycine receptor beta subunit*. Neuron. 15, 563-572.

Milani, N., MŸlhardt, C., Weber, R.G., Lichter, P., Kioschis, P., Poustka, A. & Becker, C.M. (1998). *The human glycine receptor beta subunit gene (GLRB): structure, refined chromosomal localization, and population polymorphism*. Genomics. 50, 341-345.

Modregger, J., DiProspero, N.A., Charles, V., Tagle, D.A. & Plomann, M. (2002). *PACSIN 1 interacts with huntingtin and is absent from synaptic varicosities in presymptomatic Huntington's disease brains*. Hum Mol Genet. 11, 2547-2558.

Muhammad, A., Flores, I., Zhang, H., Yu, R., Staniszewski, A., Planel, E., Herman, M., Ho, L., Kreber, R., Honig, L.S., Ganetzky, B., Duff, K., Arancio, O. & Small, S.A. (2008). *Retromer deficiency observed in Alzheimer's disease causes hippocampal dysfunction, neurodegeneration, and Abeta accumulation*. Proc Natl Acad Sci U S A. 105, 7327-7332.

Mϕrkve, S.H. & Hartveit, E. (2009). *Properties of glycine receptors underlying synaptic currents in presynaptic axon terminals of rod bipolar cells in the rat retina*. J Physiol. 587, 3813-3830.

Nagle, D.L., Karim, M.A., Woolf, E.A., Holmgren, L., Bork, P., Misumi, D.J., McGrail, S.H., Dussault, B.J., Perou, C.M., Boissy, R.E., Duyk, G.M., Spritz, R.A. & Moore, K.J. (1996). *Identification and mutation analysis of the complete gene for Chediak-Higashi syndrome*. Nat Genet. 14, 307-311.

Neer, E.J., Schmidt, C.J., Nambudripad, R. & Smith, T.F. (1994). *The ancient regulatory-protein family of WD-repeat proteins*. Nature. 371, 297-300.

Nielsen, M.S., Gustafsen, C., Madsen, P., Nyengaard, J.R., Hermey, G., Bakke, O., Mari, M., Schu, P., Pohlmann, R., Dennes, A. & Petersen, C.M. (2007). *Sorting by the cytoplasmic domain of the amyloid precursor protein binding receptor SorLA*. Mol Cell Biol. 27, 6842-6851.

Niethammer, M., Kim, E. & Sheng, M. (1996). *Interaction between the C terminus of NMDA receptor subunits and multiple members of the PSD-95 family of membrane-associated guanylate kinases*. J Neurosci. 16, 2157-2163.

Nikolic, Z., Laube, B., Weber, R.G., Lichter, P., Kioschis, P., Poustka, A., MŸlhardt, C. & Becker, C.M. (1998). *The human glycine receptor subunit alpha3. Glra3 gene structure, chromosomal localization, and functional characterization of alternative transcripts*. J Biol Chem. 273, 19708-19714.

Nishimura, A., Morita, M., Nishimura, Y. & Sugino, Y. (1990). *A rapid and highly efficient method for preparation of competent Escherichia coli cells*. Nucleic Acids Res. 18, 6169.

Nothwehr, S.F., Ha, S.A. & Bruinsma, P. (2000). *Sorting of yeast membrane proteins into an endosome-to-Golgi pathway involves direct interaction of their cytosolic domains with Vps35p*. J Cell Biol. 151, 297-310.

O'Brien, R.J., Lau, L.F. & Huganir, R.L. (1998). *Molecular mechanisms of glutamate receptor clustering at excitatory synapses*. Curr Opin Neurobiol. 8, 364-369.

Oertel, J., Villmann, C., Kettenmann, H., Kirchhoff, F. & Becker, C.-M. (2007). *A novel glycine receptor beta subunit splice variant predicts an unorthodox transmembrane topology. Assembly into heteromeric receptor complexes*. J Biol Chem. 282, 2798-2807.

Okada, H., Zhang, W., Peterhoff, C., Hwang, J.C., Nixon, R.A., Ryu, S.H. & Kim, T.-W. (2010). *Proteomic identification of sorting nexin 6 as a negative regulator of BACE1-mediated APP processing*. FASEB J

Paarmann, I., Schmitt, B., Meyer, B., Karas, M., & Betz, H. (2006). *Mass spectrometric análisis if glycine receptor-associated gephyrin splice variants*. J Bioll. Chem. 281, 34918-25.

Papadopoulos, T., Eulenburg, V., Reddy-Alla, S., Mansuy, I.M., Li, Y. & Betz, H. (2008). *Collybistin is required for both the formation and maintenance of GABAergic postsynapses in the hippocampus*. Mol Cell Neurosci. 39, 161-169.

Papadopoulos, T., Korte, M., Eulenburg, V., Kubota, H., Retiounskaia, M., Harvey, R.J., Harvey, K., O'Sullivan, G.A., Laube, B., HŸlsmann, S., Geiger, J.R.P. & Betz, H. (2007). *Impaired GABAergic transmission and altered hippocampal synaptic plasticity in collybistin-deficient mice*. EMBO J. 26, 3888-3899.

Paravicini, G., Horazdovsky, B.F. & Emr, S.D. (1992). *Alternative pathways for the sorting of soluble vacuolar proteins in yeast: a vps35 null mutant missorts and secretes only a subset of vacuolar hydrolases*. Mol Biol Cell. 3, 415-427.

Petrini, E.M., Lu, J., Cognet, L., Lounis, B., Ehlers, M.D. & Choquet, D. (2009). *Endocytic trafficking and recycling maintain a pool of mobile surface AMPA receptors required for synaptic potentiation*. Neuron. 63, 92-105.

Pfeiffer, F., Graham, D. & Betz, H. (1982). *Purification by affinity chromatography of the glycine receptor of rat spinal cord*. J Biol Chem. 257, 9389-9393.

Phillips, W.D., Maimone, M.M. & Merlie, J.P. (1991). *Mutagenesis of the 43-kD postsynaptic protein defines domains involved in plasma membrane targeting and AChR clustering*. J Cell Biol. 115, 1713-1723.

Plomann, M., Lange, R., Vopper, G., Cremer, H., Heinlein, U.A., Scheff, S., Baldwin, S.A., Leitges, M., Cramer, M., Paulsson, M. & Barthels, D. (1998). *PACSIN, a brain protein that is upregulated upon differentiation into neuronal cells*. Eur J Biochem. 256, 201-211.

van den Pol, A.N. & Gorcs, T. (1988). *Glycine and glycine receptor immunoreactivity in brain and spinal cord*. J Neurosci. 8, 472-492.

Popoff, V., Mardones, G.A., Bai, S.-K., Chambon, V., Tenza, D., Burgos, P.V., Shi, A., Benaroch, P., UrbŽ, S., Lamaze, C., Grant, B.D., Raposo, G. & Johannes, L. (2009). *Analysis of articulation between clathrin and retromer in retrograde sorting on early endosomes*. Traffic. 10, 1868-1880.

Popoff, V., Mardones, G.A., Tenza, D., Rojas, R., Lamaze, C., Bonifacino, J.S., Raposo, G. & Johannes, L. (2007). *The retromer complex and clathrin define an early endosomal retrograde exit site*. J Cell Sci. 120, 2022-2031.

Port, F., Kuster, M., Herr, P., Furger, E., BŠnziger, C., Hausmann, G. & Basler, K. (2008). *Wingless secretion promotes and requires retromer-dependent cycling of Wntless*. Nat Cell Biol. 10, 178-185.

Pribilla, I., Takagi, T., Langosch, D., Bormann, J. & Betz, H. (1992). *The atypical M2 segment of the beta subunit confers picrotoxinin resistance to inhibitory glycine receptor channels*. EMBO J. 11, 4305-4311.

Prior, P., Schmitt, B., Grenningloh, G., Pribilla, I., Multhaup, G., Beyreuther, K., Maulet, Y., Werner, P., Langosch, D. & Kirsch, J. (1992). *Primary structure and alternative splice variants of gephyrin, a putative glycine receptor-tubulin linker protein*. Neuron. 8, 1161-1170.

Pérez-Otaño, I., Luján, R., Tavalin, S.J., Plomann, M., Modregger, J., Liu, X.-B., Jones, E.G., Heinemann, S.F., Lo, D.C. & Ehlers, M.D. (2006). *Endocytosis and synaptic removal of NR3A-containing NMDA receptors by PACSIN1/syndapin1*. Nat Neurosci. 9, 611-621.

Qualmann, B. & Kelly, R.B. (2000). *Syndapin isoforms participate in receptor-mediated endocytosis and actin organization*. J Cell Biol. 148, 1047-1062.

Qualmann, B., Kessels, M.M. & Kelly, R.B. (2000). *Molecular links between endocytosis and the actin cytoskeleton*. J Cell Biol. 150, F111-F116.

Qualmann, B., Roos, J., DiGregorio, P.J. & Kelly, R.B. (1999). *Syndapin I, a synaptic dynamin-binding protein that associates with the neural Wiskott-Aldrich syndrome protein*. Mol Biol Cell. 10, 501-513.

Ramarao, M.K., Bianchetta, M.J., Lanken, J. & Cohen, J.B. (2001). *Role of rapsyn tetratricopeptide repeat and coiled-coil domains in self-association and nicotinic acetylcholine receptor clustering*. J Biol Chem. 276, 7475-7483.

Reddy-Alla, S., Schmitt, B., Birkenfeld, J., Eulenburg, V., Dutertre, S., Bšhringer, C., Gštz, M., Betz, H. & Papadopoulos, T. (2010). *PH-domain-driven targeting of collybistin but not Cdc42 activation is required for synaptic gephyrin clustering*. Eur J Neurosci. 31, 1173-1184.

Reid, T., Bathoorn, A., Ahmadian, M.R. & Collard, J.G. (1999). *Identification and characterization of hPEM-2, a guanine nucleotide exchange factor specific for Cdc42*. J Biol Chem. 274, 33587-33593.

van Rijnsoever, C., Sidler, C. & Fritschy, J.-M. (2005). *Internalized GABA-receptor subunits are transferred to an intracellular pool associated with the postsynaptic density*. Eur J Neurosci. 21, 327-338.

Rojas, R., Kametaka, S., Haft, C.R. & Bonifacino, J.S. (2007). *Interchangeable but essential functions of SNX1 and SNX2 in the association of retromer with endosomes and the trafficking of mannose 6-phosphate receptors*. Mol Cell Biol. 27, 1112-1124.

Rojas, R., van Vlijmen, T., Mardones, G.A., Prabhu, Y., Rojas, A.L., Mohammed, S., Heck, A.J.R., Raposo, G., van der Sluijs, P. & Bonifacino, J.S. (2008). *Regulation of retromer recruitment to endosomes by sequential action of Rab5 and Rab7*. J Cell Biol. 183, 513-526.

Rosenberg, M., Meier, J., Triller, A. & Vannier, C. (2001). *Dynamics of glycine receptor insertion in the neuronal plasma membrane*. J Neurosci. 21, 5036-5044.

Rubin, G.M., Yandell, M.D., Wortman, J.R., Miklos, G.L.G., Nelson, C.R., Hariharan, I.K., Fortini, M.E., Li, P.W., Apweiler, R., Fleischmann, W., Cherry, J.M., Henikoff, S., Skupski, M.P., Misra, S., Ashburner, M., Birney, E., Boguski, M.S., Brody, T., Brokstein, P., Celniker, S.E., Chervitz, S.A., Coates, D., Cravchik, A., Gabrielian, A., Galle, R.F., Gelbart, W.M., George, R.A., Goldstein, L.S., Gong, F., Guan, P., Harris, N.L., Hay, B.A., Hoskins, R.A., Li, J., Li, Z., Hynes, R.O., Jones, S.J., Kuehl, P.M., Lemaitre, B., Littleton, J.T., Morrison, D.K., Mungall, C.,

O'Farrell, P.H., Pickeral, O.K., Shue, C., Vosshall, L.B., Zhang, J., Zhao, Q., Zheng, X.H. & Lewis, S. (2000). *Comparative genomics of the eukaryotes*. Science. 287, 2204-2215.

Rácz, B., Blanpied, T.A., Ehlers, M.D. & Weinberg, R.J. (2004). *Lateral organization of endocytic machinery in dendritic spines*. Nat Neurosci. 7, 917-918.

Saiyed, T., Paarmann, I., Schmitt, B., Haeger, S., Sola, M., Schmalzing, G., Weissenhorn, W. & Betz, H. (2007). *Molecular basis of gephyrin clustering at inhibitory synapses: role of G- and E-domain interactions*. J Biol Chem. 282, 5625-5632.

Saliba, R.S., Pangalos, M. & Moss, S.J. (2008). *The ubiquitin-like protein Plic-1 enhances the membrane insertion of GABAA receptors by increasing their stability within the endoplasmic reticulum*. J Biol Chem. 283, 18538-18544.

Sanger, F., Nicklen, S. & Coulson, A.R. (1977). *DNA sequencing with chain-terminating inhibitors*. Proc Natl Acad Sci U S A. 74, 5463-5467.

Savelyeva, L., Sagulenko, E., Schmitt, J.G. & Schwab, M. (2006). *The neurobeachin gene spans the common fragile site FRA13A*. Hum Genet. 118, 551-558.

Schmieden, V., Grenningloh, G., Schofield, P.R. & Betz, H. (1989). *Functional expression in Xenopus oocytes of the strychnine binding 48 kd subunit of the glycine receptor*. EMBO J. 8, 695-700.

Schmitt, B., Knaus, P., Becker, C.M. & Betz, H. (1987). *The Mr 93,000 polypeptide of the postsynaptic glycine receptor complex is a peripheral membrane protein*. Biochemistry. 26, 805-811.

Schrader, N., Kim, E.Y., Winking, J., Paulukat, J., Schindelin, H. & Schwarz, G. (2004). *Biochemical characterization of the high affinity binding between the glycine receptor and gephyrin*. J Biol Chem. 279, 18733-18741.

Schršder, S., Hoch, W., Becker, C.M., Grenningloh, G. & Betz, H. (1991). *Mapping of antigenic epitopes on the alpha 1 subunit of the inhibitory glycine receptor*. Biochemistry. 30, 42-47.

Seaman, M.N., Marcusson, E.G., Cereghino, J.L. & Emr, S.D. (1997). *Endosome to Golgi retrieval of the vacuolar protein sorting receptor, Vps10p, requires the function of the VPS29, VPS30, and VPS35 gene products*. J Cell Biol. 137, 79-92.

Seaman, M.N., McCaffery, J.M. & Emr, S.D. (1998). *A membrane coat complex essential for endosome-to-Golgi retrograde transport in yeast*. J Cell Biol. 142, 665-681.

Seaman, M.N.J. (2008). *Endosome protein sorting: motifs and machinery*. Cell Mol Life Sci. 65, 2842-2858.

Seaman, M.N.J. (2007). *Identification of a novel conserved sorting motif required for retromer-mediated endosome-to-TGN retrieval*. J Cell Sci. 120, 2378-2389.

Seaman, M.N.J. (2004). *Cargo-selective endosomal sorting for retrieval to the Golgi requires retromer*. J Cell Biol. 165, 111-122.

Seaman, M.N.J., Harbour, M.E., Tattersall, D., Read, E. & Bright, N. (2009). *Membrane recruitment of the cargo-selective retromer subcomplex is catalysed by the small GTPase Rab7 and inhibited by the Rab-GAP TBC1D5*. J Cell Sci. 122, 2371-2382.

Sever, S., Damke, H. & Schmid, S.L. (2000). *Dynamin:GTP controls the formation of constricted coated pits, the rate limiting step in clathrin-mediated endocytosis*. J Cell Biol. 150, 1137-1148.

Shi, H., Rojas, R., Bonifacino, J.S. & Hurley, J.H. (2006). *The retromer subunit Vps26 has an arrestin fold and binds Vps35 through its C-terminal domain*. Nat Struct Mol Biol. 13, 540-548.

Shimada, A., Niwa, H., Tsujita, K., Suetsugu, S., Nitta, K., Hanawa-Suetsugu, K., Akasaka, R., Nishino, Y.,

Toyama, M., Chen, L., Liu, Z.-J., Wang, B.-C., Yamamoto, M., Terada, T., Miyazawa, A., Tanaka, A., Sugano, S., Shirouzu, M., Nagayama, K., Takenawa, T. & Yokoyama, S. (2007). *Curved EFC/F-BAR-domain dimers are joined end to end into a filament for membrane invagination in endocytosis*. Cell. 129, 761-772.

Shimada, T., Koumoto, Y., Li, L., Yamazaki, M., Kondo, M., Nishimura, M. & Hara-Nishimura, I. (2006). *AtVPS29, a putative component of a retromer complex, is required for the efficient sorting of seed storage proteins*. Plant Cell Physiol. 47, 1187-1194.

Small, S.A., Kent, K., Pierce, A., Leung, C., Kang, M.S., Okada, H., Honig, L., Vonsattel, J.-P. & Kim, T.-W. (2005). *Model-guided microarray implicates the retromer complex in Alzheimer's disease*. Ann Neurol. 58, 909-919.

Sola, M., Bavro, V.N., Timmins, J., Franz, T., Ricard-Blum, S., Schoehn, G., Ruigrok, R.W.H., Paarmann, I., Saiyed, T., O'Sullivan, G.A., Schmitt, B., Betz, H. & Weissenhorn, W. (2004). *Structural basis of dynamic glycine receptor clustering by gephyrin*. EMBO J. 23, 2510-2519.

Sparks, A.B., Hoffman, N.G., McConnell, S.J., Fowlkes, D.M. & Kay, B.K. (1996). *Cloning of ligand targets: systematic isolation of SH3 domain-containing proteins*. Nat Biotechnol. 14, 741-744.

Sparks, A.B., Rider, J.E., Hoffman, N.G., Fowlkes, D.M., Quillam, L.A. & Kay, B.K. (1996). *Distinct ligand preferences of Src homology 3 domains from Src, Yes, Abl, Cortactin, p53bp2, PLCgamma, Crk, and Grb2*. Proc Natl Acad Sci U S A. 93, 1540-1544.

Stil, A., Liabeuf, S., Jean-Xavier, C., Brocard, C., Viemari, J.-C. & Vinay, L. (2009). *Developmental up-regulation of the potassium-chloride cotransporter type 2 in the rat lumbar spinal cord*. Neuroscience. 164, 809-821.

Stradal, T.E.B. & Scita, G. (2006). *Protein complexes regulating Arp2/3-mediated actin assembly*. Curr Opin Cell Biol. 18, 4-10.

Su, Y., Balice-Gordon, R.J., Hess, D.M., Landsman, D.S., Minarcik, J., Golden, J., Hurwitz, I., Liebhaber, S.A. & Cooke, N.E. (2004). *Neurobeachin is essential for neuromuscular synaptic transmission*. J Neurosci. 24, 3627-3636.

Sumoy, L., Pluvinet, R., Andreu, N., Estivill, X. & Escarceller, M. (2001). *PACSIN 3 is a novel SH3 domain cytoplasmic adapter protein of the pacsin-syndapin-FAP52 gene family*. Gene. 262, 199-205.

Tabuchi, M., Yanatori, I., Kawai, Y. & Kishi, F. (2010). *Retromer-mediated direct sorting is required for proper endosomal recycling of the mammalian iron transporter DMT1*. J Cell Sci. 123, 756-766.

Tapia, J.C. & Aguayo, L.G. (1998). *Changes in the properties of developing glycine receptors in cultured mouse spinal neurons*. Synapse. 28, 185-194.

Thomas, P., Mortensen, M., Hosie, A.M. & Smart, T.G. (2005). *Dynamic mobility of functional GABAA receptors at inhibitory synapses*. Nat Neurosci. 8, 889-897.

Triller, A., Cluzeaud, F., Pfeiffer, F., Betz, H. & Korn, H. (1985). *Distribution of glycine receptors at central synapses: an immunoelectron microscopy study*. J Cell Biol. 101, 683-688.

Twelvetrees, A.E., Yuen, E.Y., Arancibia-Carcamo, I.L., MacAskill, A.F., Rostaing, P., Lumb, M.J., Humbert, S., Triller, A., Saudou, F., Yan, Z. & Kittler, J.T. (2010). *Delivery of GABAARs to synapses is mediated by HAP1-KIF5 and disrupted by mutant huntingtin*. Neuron. 65, 53-65.

Utskarpen, A., Slagsvold, H.H., Dyve, A.B., SkŒnland, S.S. & Sandvig, K. (2007). *SNX1 and SNX2 mediate retrograde transport of Shiga toxin*. Biochem Biophys Res Commun. 358, 566-570.

Vergés, M., Luton, F., Gruber, C., Tiemann, F., Reinders, L.G., Huang, L., Burlingame, A.L., Haft, C.R. & Mostov, K.E. (2004). *The mammalian retromer regulates transcytosis of the polymeric immunoglobulin receptor*. Nat Cell Biol. 6, 763-769.

Waldvogel, H.J., Baer, K., Allen, K.L., Rees, M.I. & Faull, R.L.M. (2007). *Glycine receptors in the striatum, globus pallidus, and substantia nigra of the human brain: an immunohistochemical study*. J Comp Neurol. 502, 1012-1029.

Wang, Q., Navarro, M.V.A.S., Peng, G., Molinelli, E., Goh, S.L., Judson, B.L., Rajashankar, K.R. & Sondermann, H. (2009). *Molecular mechanism of membrane constriction and tubulation mediated by the F-BAR protein Pacsin/Syndapin*. Proc Natl Acad Sci U S A. 106, 12700-12705.

Wang, X., Herberg, F.W., Laue, M.M., Wullner, C., Hu, B., Petrasch-Parwez, E. & Kilimann, M.W. (2000). *Neurobeachin: A protein kinase A-anchoring, beige/Chediak-higashi protein homolog implicated in neuronal membrane traffic*. J Neurosci. 20, 8551-8565.

Wasiak, S., Quinn, C.C., Ritter, B., de Heuvel, E., Baranes, D., Plomann, M. & McPherson, P.S. (2001). *The Ras/Rac guanine nucleotide exchange factor mammalian Son-of-sevenless interacts with PACSIN 1/syndapin I, a regulator of endocytosis and the actin cytoskeleton*. J Biol Chem. 276, 26622-26628.

Wassmer, T., Attar, N., Bujny, M.V., Oakley, J., Traer, C.J. & Cullen, P.J. (2007). *A loss-of-function screen reveals SNX5 and SNX6 as potential components of the mammalian retromer*. J Cell Sci. 120, 45-54.

Worby, C.A. & Dixon, J.E. (2002). *Sorting out the cellular functions of sorting nexins*. Nat Rev Mol Cell Biol. 3, 919-931.

Wässle, H., Koulen, P., BrandstŠtter, J.H., Fletcher, E.L. & Becker, C.M. (1998). *Glycine and GABA receptors in the mammalian retina*. Vision Res. 38, 1411-1430.

Yuan, X., Yao, J., Norris, D., Tran, D.D., Bram, R.J., Chen, G. & Luscher, B. (2008). *Calcium-modulating cyclophilin ligand regulates membrane trafficking of postsynaptic GABA(A) receptors*. Mol Cell Neurosci. 38, 277-289.

Zusammenfassung

An chemischen Synapsen findet die Reizweiterleitung durch präsynaptische Neurotransmitterausschüttung in den synaptischen Spalt statt, wo durch Rezeptoren in der postsynaptischen Plasmamembran aktiviert werden. Glyzin und γ-Aminobuttersäure (GABA) sind die häufigsten inhibitorischen Neurotransmitter im Zentralnervensystem der Säuger. Sie aktivieren Glyzinrezeptoren (GlyR) und Typ A GABA-Rezeptoren ($GABA_AR$), ligandengesteuerte Chloridkanäle, an inhibitorischen Synapsen. Eine schnelle synaptische Reizweiterleitung erfordert, dass diese Rezeptoren an der Postsynapse in räumlich präzise angeordneten Clustern gegenüber der präsynaptischen Endigung organisiert sind. An inhibitorischen Synapsen werden diese Cluster von Glyzin- und $GABA_A$-Rezeptoren in der postsynaptischen Plasmamembran durch das Gerüstprotein Gephyrin verankert.

GlyR bestehen aus α- und β-Untereinheiten, die entweder α-Homopentamere oder $\alpha_2\beta_3$-Heteropentamere bilden. Gephyrin verankert heteropentamere GlyR an postsynaptischen Endigungen durch die direkte Bindung an die große intrazelluläre Schleife (Loop) zwischen den Transmembrandomänen 3 und 4 der GlyRβ-Untereinheit (GlyRβ-Loop). GlyR können zusammen mit Gephyrin auch extrasynaptisch gefunden werden. Diese GlyR-Gephyrin-Komplexe werden sowohl in anterograder als auch in retrograder Richtung entlang von Mikrotubuli durch die Interaktion von Gephyrin mit den Transportproteinen Kinesin-5 beziehungsweise Dynein transportiert. Zusätzlich können GlyR lateral in der Plasmamembran diffundieren. Diese Diffusionsdynamik kann durch synaptisches oder extrasynaptisches Gephyrin beeinflusst werden, was die Bildung von GlyR-Gephyrin-Komplexen durch laterale Diffusion in der Plasmamembran nahelegt.

Gephyrin ist bislang der einzige beschriebene Bindungspartner der GlyRβ-Untereinheit. Um tiefere Einblicke in die molekulare Organisation inhibitorischer glyzinerger Postsynapsen zu bekommen, wurden affinitätschromatographisch aus Rattenhirn drei weitere Bindungspartner für den GlyRβ-Loop isoliert und über Massenspektrometrie identifiziert: synaptisches Dynamin-bindendes Protein (Sdp) I, vakuoläres Sortierungsprotein 35 (Vps35) und Neurobeachin (Nbea). In dieser Arbeit wurden die Interaktionen dieser Proteine mit GlyRβ genauer analysiert und charakterisiert.

Die Sdp-Proteinfamilie besteht aus drei Isoformen (Sdp I, II, III) und zwei Spleißvarianten von SdpII (SdpII-S und –L). Das Sdp-Protein besitzt eine F-BAR- und eine SH3-Domäne und ist in die Endozytose und das Recycling von Vesikeln involviert. Die F-BAR-Domäne ist an der Induktion und Stabilisierung von Membranwölbungen beteiligt, wohingegen die SH3-Domäne mit Prolin-reichen Domänen (PRD) verschiedener zytosolischer Proteine wie z.B. Dynamin und dem neuronalen Wiskott-Aldrich Syndrom-Protein interagiert. In Hippocampusneuronen spielt SdpI außerdem eine Rolle in der Endozytose und beim Entfernen von NR3A-Untereinheiten-enthaltenden N-Methyl-D-aspartat-Rezeptoren von der Synapse.

In immunzytochemischen Experimente wurde beobachtet, dass sowohl SdpI als auch beide SdpII-Spleißvarianten mit der GlyRβ-Untereinheit in COS7-Zellen kolokalisieren. Bindungsexperimente mit bakteriell exprimierten Glutathion-S-Transferase (GST)-Fusionsproteinen und His_6-markierten Proteinen bestätigten, dass SdpI und beide Spleißvarianten von SdpII mit dem GlyRβ-Loop *in vitro* interagieren. Über die Generierung von verschiedenen Deletionskonstrukten konnte die SdpI-Bindungsstelle auf 22 Aminosäuren eingeengt werden. Peptid-Kompetitionsexperimente bestätigten die Spezifität der Interaktion zwischen SdpI und dem GlyRβ-Loop.

Durch die Analyse von Punktmutationen konnte eine Prolin-reiche Sequenz als SdpI-Bindungsstelle der GlyRβ-Untereinheit identifiziert werden. Da die Bindungsstellen für Gephyrin und SdpI sehr dicht beieinander im GlyRβ-Loop liegen, wurde der Einfluss der Gephyrin- auf die SdpI-Bindung an den GlyRβ-Loop untersucht. In Protein-Kompetitionsstudien wurde bestätigt, dass die E-Domäne von Gephyrin mit dem GlyRβ-Loop um die SdpI-Bindung konkurriert. Darüber hinaus wurde eine mögliche Interaktion zwischen SdpI und Gephyrin untersucht. Bindungsexperimente in Säugerzellen zeigten, dass SdpI und beide SdpII-Spleißvarianten mit Gephyrin interagieren.

Außerdem wurde eine mögliche Funktion von SdpI in der Regulation der Verteilung synaptischer GlyR untersucht. Dabei wurde eine partielle Kolokalisation von SdpI mit verschiedenen inhibitorischen und exzitatorischen synaptischen Markern in kultivierten Rückenmarksneuronen detektiert. Die Anzahl der SdpI-immunreaktiven Puncta, die mit inhibitorischen und exzitatorischen synaptischen Markern kolokalisierte, war ähnlich groß, was demonstriert, dass SdpI an beiden Synapsentypen vorhanden ist.

Bei Ko-Immunpräzipitationsexperimenten mit SdpI-spezifischen Antikörpern wurde eine endogene SdpI-GlyR Assoziation in der vesikulär-angereicherten Fraktion aus

Rückenmarksgewebe der Ratte beobachtet. Dennoch zeigten Studien SdpI-defizienter Mäuse, dass die GlyR-Verteilung sowohl in kultivierten Rückenmarksneuronen als auch im Hirnstamm beim Fehlen von SdpI nicht signifikant verändert ist. Wegen möglicher kompensatorischer Effekte durch die beiden weiteren Sdp-Isoformen und andere Proteintransportwege in diesen Experimenten wurden zusätzlich SdpI-Knockdown Experimente durchgeführt. In der Tat führte der rAAV-Virus-vermittelte Knockdown von SdpI mit SdpI-spezifischer shRNA in kultivierten Rückenmarksneuronen von Ratten zu einer klaren Reduktion der Dichte und Größe von GlyR-Clustern. Durch die Überexpression shRNA-resistenter SdpI-Proteine konnte die ursprüngliche Anzahl und Größe der GlyR-Cluster wiederhergestellt werden. Weitere immunzytochemische Analysen zur Verteilung von Gephyrin, der $GABA_AR\gamma2$-Untereinheit und des vesikulären inhibitorischen Aminosäuretransporters unter SdpI-Knockdown Bedingungen zeigten zusätzlich, dass die Anzahl und die Größe von $GABA_AR\gamma2$-Untereinheiten-beinhaltenden $GABA_AR$ Clustern signifikant reduziert war. Diese Ergebnisse weisen auf eine mögliche Rolle von SdpI im intrazellulären Transport inhibitorischer Neurotransmitterrezeptoren hin. Weiterhin könnte SdpI notwendig für die synaptische Clusterbildung von $GABA_AR\gamma2$-Untereinheiten-beinhaltenden $GABA_AR$ in Rückenmarks- und Hirnstammneuronen sein.

Die Übermittlung von verschiedenen Rezeptortypen vom Endosom zum Golgi-Apparat wird in allen eukaryontischen Zellen von Hefe bis zu den Säugern vom sogenannten Retromerkomplex vermittelt. Dieser Retromerkomplex besteht aus zwei Unterkomplexen, dem die Fracht erkennenden Unterkomplex aus Vps35, Vps29 und Vps26, und dem Sortin-Nexin-Komplex, der in Hefe aus Vps5p und Vps17p aufgebaut ist. Vps35 ist innerhalb des Retromerkomplexes für die Erkennung der zytoplasmatischen Aminosäuresequenzen der zu transportierenden Rezeptoren zuständig. In dieser Arbeit wurde über GST-Pulldowns nachgewiesen, dass Vps35 *in vitro* mit dem GlyRβ-Loop und Gephyrin interagiert. Um die Verteilung von Vps35 im ZNS untersuchen zu können, wurden spezifische polyklonale Antikörper gegen Vps35 hergestellt und charakterisiert. Mit diesen Antikörpern konnte Vps35 im Soma und entlang der Neuriten von Rückenmarksneuronen detektiert werden, was auf eine mögliche Interaktion zwischen Vps35 und GlyR unter physiologischen Bedingungen hindeutet.

Nbea ist ein Proteinkinase A-bindendes neuronales Protein mit einer BEACH-(Beige and Chediak Higashi Syndrome) Domäne, das in den neuronalen Membrantransport impliziert ist. Interaktionsstudien mit GST-Pulldowns zeigten, dass zwei Fragmente von Nbea an den GlyRβ-Loop binden. Immunzytochemische Experimente bestätigten die somatische und synaptische Lokalisation von Nbea in Primärkulturen von Rückenmarksneuronen. Außerdem wurde eine teilweise Kolokalisation von Nbea mit inhibitorischen synaptischen Markern gefunden, was ein Indiz für eine mögliche Interaktion zwischen Nbea und dem GlyR an inhibitorischen Synapsen in Rückenmark und Hirnstamm ist.

Zusammenfassend kann gesagt werden, dass SdpI, SdpII, Vps35 und Nbea als neue Bindungspartner der GlyRβ-Untereinheit identifiziert und näher charakterisiert werden konnten. Zusätzlich konnte gezeigt werden, dass SdpI, SdpII und Vps35 ebenfalls mit dem Gerüstprotein Gephyrin interagieren. Immunzytochemische Experimente weisen darauf hin, dass SdpI und Nbea an inhibitorischen und exzitatorischen Synapsen lokalisiert sind. Über die Etablierung eines Antikörpers gegen Vps35 konnte dessen Lokalisation im Soma und entlang der Neuriten von Rückenmarksneuronen demonstriert werden. Die Charakterisierung der Interaktion zwischen SdpI und der GlyRβ-Untereinheit ergab, dass die SH3-Domäne von SdpI mit einer Prolin-reichen Sequenz der GlyRβ−Untereinheit interagiert. Die SdpI-Knockdown Ergebnisse sind ein starker Hinweis auf eine Rolle von SdpI in der Clusterbildung von GlyR- und $GABA_AR\gamma2$-Untereinheiten beinhaltenden $GABA_AR$-Komplexen an inhibitorischen Synapsen. Die Ergebnisse dieser Arbeit liefern erste Hinweise auf die Funktion und Regulation des GlyR an inhibitorischen Synapsen durch diese neu identifizierten Interaktionspartner. Spätere Analysen könnten die exakte Funktion dieser Proteine sowohl im intrazellulären Transport als auch in der GlyR-Clusterbildung aufdecken.

Erklärung

Die anfänglichen Mapping und GST-Pulldown Experimente von SdpI wurden von Dr. I. Paarmann in der Abteilung Neurochemie des Max-Planck-Instituts für Hirnforschung durchgeführt (siehe Seiten 58 und 59).

Ich erkläre hiermit, dass ich diese Doktorarbeit selbständig verfasst und keine anderen als die angegebenen Quellen und Hilfsmittel verwendet habe.

Frankfurt am Main, den…….. _____

Isabel del Pino Pariente